Pile Run Initiation in Transitional Soils

A Risk Assessment Framework for Dropfall Events for Offshore Foundation Piles in Silty Soils

Otto Robert Schultze

Delft University of Technology

TU Delft

Pile Run Initiation in Transitional Soils

A Risk Assessment Framework for Dropfall Events for Offshore Foundation Piles in Silty Soils

by

Otto Robert Schultze

to obtain the degree of Master of Science
at the Delft University of Technology,
to be defended publicly on Friday 10th of October at 14:00.

Student number:	4897986	
Project duration:	Februari, 2025 – September, 2025	
Faculty:	Faculty of Civil Engineering	
Company:	Heerema Marine Contractors	
Thesis committee:	Prof.dr. A. Metrikine,	TU Delft, Chairman & Examiner
	Dr. M. Cabrera	TU Delft, Supervisor & Examiner
	Dr. K. Duffy	TU Delft, Supervisor
	Dr. S. Maghsoodi,	Heerema MC, Supervisor
	Ir. T. Kamphuis,	Heerema MC, Supervisor

Cover: Pin pile installation by the DCV Aegir for the Changhua project, Taiwan.

TU Delft

MARINE CONTRACTORS

Preface

The 'pile run' topic was first introduced during the lectures of Soil Structure Interaction given by Vagelis Kementzetzidis. I finished this course of my master Civil Engineering with a 5.8, so I knew that there was more than enough wisdom to obtain on offshore foundations. If it was this lecture or my nurture that brought me to offshore foundation engineering remains the question. With my dad graduating on 'Franki trekpalen', the link could easily be made that my choice for large open-ended steel piles is not an accident. In Dutch is the conclusion on this question quite easy: 'De appel valt niet ver van de boom.'

The first meeting with Teun Karnebeek and Soheib Maghsoodi from Heerema MC felt like a match. The straight forward communication and clear expectations are new to a academic student coming from the TU Delft. A lot of different topics were talked about in great detail. What happened as a result? There was no reaction for weeks. Another company offered me a job as a graduate intern, and that's when I called Heerema. One week later, everything was signed and sealed, but there was still a lot to deliver.

The thesis started in February with three supervisors: Prof. Dr. Andrei Metrikine from the Faculty of Civil Engineering and Geosciences, Dr. Soheib Maghsoodi from foundation development Heerema MC and Ir. Thijs Kamphuis from wind development Heerema MC. Up to my opinion a very diverse group, but according to the TU Delft regulations not diverse enough. It started with researching the soil fundamentals and modelling SRDs. At the kick of meeting I presented my SRD knowledge and a plan to improve them. The only comment from Andrei was: "Nice presentation but I do not believe in the SRD models". This turned the black and white soil mechanics into a gray ocean. *The only thing I know is that I know nothing* (Plato). This is a bit shocking as I tend to have the feeling that I know quite something if you ask the people around me.

Although I felt like a first year student with his face in the mud, the thesis preparation was signed and I started modelling soil resistance (Yes exactly where Andrei told me not to start). Next progress meeting I met my second TU Delft supervisor Dr. Kevin Duffy, who recently promoted on axial pile capacity in sands. As the reader will discover in a bit, sand is not silt, but his knowledge on axial capacity was exactly the next puzzle piece that I needed for my research. I discovered that shaft friction is based on effective stress and this effective stress is reduced by increasing pore-water pressure. This could be the crux of my problem and it felt like my Eureka moment. One week later this theory was proven by a paper of my third TU Delft supervisor Dr. Miguel Cabrera. It felt for a moment as if my idea was stolen but from the moment I discussed the research with Miguel, I was happy to have him in the supervisory board as well.

With the board completed and this thesis to be defended, my part of the pile run research comes to an end. I want to thank Andrei for the way he approached the supervision. His open minded meeting to meeting approach gave the freedom to research what I found interesting. His knowledge and experience on the other hand gave enough pressure to not come up with a stupid story. Up to the reader if I succeeded. Miguel, I want to thank you for the flexibility to jump last minute on the project. You answered exactly the remaining fundamental soil mechanics questions I had which made the pieces fall together. Your input hammered the thesis to a more deepening level. Kevin, I want to thank you for all the knowledge on pile driving and the insights I gained during the extra discussions we had. You provided me new questions (as a Dr. should) that made me understand the topic better and better. You created the link between pile driving and soil fundamentals for me. Not only in discussion, but also in literature contributions, as your papers had the highest score in my plagiarism scan. I want to thank Thijs for the practical link he made between the research and the Heerema operations. I remember foremost the end of the 1st progress meeting where you were praising the discussion while I was still high in frustration. I learned a lot on how to approach such a thesis. Throw 90% away to obtain the knowledge for the final result. Last but for sure not least, Soheib. I enjoyed everyday working together with you and I hope to beat you again with ping pong while working on the same project offshore. Your direct and demanding attitude was exactly what I needed to deliver everyday. Sometimes your words do not tell the work or argumentation is bad, but your face explains enough. The way how you guided me through my thesis was a 5 star treatment which I had to earn myself. You prefer the numbers sometimes but I prefer working with engineers as pragmatic and honest as you are.

The last paragraph is for my family and friends, who supported my as well during this journey. I want to thank mum for the love and the fact that you are always present when I need help. I enjoyed especially my writers camp the last two months back home. Sometimes it feels like you are the only real engineer at home. Dad, I was so lucky to have you so investigated in the research. You asked me the right questions, improved my argumentation and pinpointed the aspects that where important. I feel proud that we can share the title Ir. in a couple of days. A title that raised in prestige with the experience of the last 6 months. I hope you will both keep the family together and continue to enrich my life with your knowledge, as you have done for the last 25 years. An, you where to make me smile after long days of study. You are the only one in the world that was willing to listen to long monologues of my daily discoveries which I really appreciate. After explaining pile driving for one hour you claimed that the topic is easy. Would say job well done. It turned out that you are better in almost all aspects of performing an academic research. Thanks to my brothers, room mates and the guys from Vic for forming my personal foundation throughout the years. Not to forget the DSDH, the band that made me swing through Civil Engineering. As last the Foundation team at Heerema, that made me feel welcome and you guys where always open to help and discuss. Loved being part of your team this months.

Otto Robert Schultze
Delft, November 2025

Abstract

The phenomenon of unexpected pile runs during pile driving, also known as 'dropfalls', in silty transitional soils remains a subject of limited understanding. These occurrences have the potential to result in damage to the pile, hammer, and the occurrence of costly installation delays. In response to the growing demand for renewable energy and the spatial constraints of nearshore sites, offshore wind farms have emerged as a promising solution. In the last fifteen years, there has been a marked increase in the dimensions of offshore wind turbines, with monopile foundations now reaching diameters of up to 10 m. However, the installation of these large foundation piles can be hindered by dropfalls, which occur when the bearing resistance of the soil is decreased.

This study investigates the theoretical mechanisms by which excess pore-water pressure is generated in contractive silts during impact hammering. This temporarily reduces shaft friction and induces dropfalls. The primary objective of this study is to improve pile-run predictions, thereby enable the implementation mitigation measures. Firstly, the interaction between soil and pile under impact loading is reviewed, with particular emphasis on the hydro-mechanical response of silty soils. It is demonstrated that silts may exhibit behaviour similar to undrained soil during driving. Such behaviour has been shown to result in the accumulation of pore pressure within transitional layers, leading to a reduction in effective stress along the pile shaft.

The application of insights to a case study at the Changhua offshore wind farm (Taiwan) is then undertaken, where drop-falls occurred at depths of 16–25 m. The conclusion drawn from this study is that soil permeability and contractivity have a significant influence on the bearing capacity of the soil. In light of the aforementioned conclusions, the thesis proposes the incorporation of these variables into Soil Resistance to Driving (SRD) methods for the purpose of forecasting dropfalls. The contractivity is in this thesis assessed with help of the state parameter, which describes the difference in void ratios. Lab tests on borehole samples and plotting of CPT data on an SBT_n chart were used to identify semi-permeable soil layers. The findings contribute to the advancement of mechanistic understanding of pile runs in silty soils, thereby providing a predictive framework for engineers to ensure safer, more efficient large-diameter foundation pile installations in transitional soil environments.

Contents

List of Figures

List of Tables

Nomenclature

Abbreviations

Abbreviation	Definition
AH	Almd & Hamre
CD	Contractive/Dilative
CPT	Cone Penetration Test
EPWP	Excess Pore Water Pressure
ESP	Effective Stress Path
GSD	Grain Size Distribution
IFR	Increment Filling Ratio
OCR	Over Consolidation Ratio
OD	Outer Diameter
PLR	Plug Length Ratio
PWP	Pore Water Pressure
SBT_n	normalised Soil Behaviour Type
SRD	Soil Resistance to Driving
SWP	Self Weight Penetration
SWPPH	Self Weight Penetration Pile plus Hammer
TSP	Total Stress Path
YSR	Yield Stress Ratio

Symbols

Symbol	Definition	Unit
c	Wave propagation speed in pile ($\sqrt{E/\rho}$)	[m/s]
D	Cone/pile diameter	[m]
e	Void ratio	[–]
E	Young's modulus	[Pa]
G	Elastic shear modulus	[Pa]
h	Pile embedment depth	[m]
I_c	Soil behaviour type index	[–]
I_r	Rigidity index (G/s_u)	[–]
J	Damping coefficient in wave equation	[s/m]
k	Permeability	[m/s]
L	Embedded pile length	[m]
m_h	Hammer mass	[kg]
m_p	Pile mass	[kg]
n	Stress exponent in Q_{tn}	[–]
p_a	Atmospheric (reference) pressure	[Pa]
P_a	Atmospheric pressure	[Pa]
Q_t	Normalised cone resistance	[–]
Q_{tn}	Normalised cone resistance with stress exponent	[–]
R_{static}	Static soil resistance	[N]
R_{total}	Total soil resistance during driving	[N]
R^*	Effective pile radius	[m]
R_f	Friction ratio	[%]
s_u	Undrained shear strength	[kPa]
t	Time	[s]
u	Axial displacement	[m]

Symbol	Definition	Unit
v	Penetration velocity	[m/s]
V'	Normalised velocity (vD/c)	[–]
W_h	Hammer weight	[N]
W_p	Pile weight	[N]
x	Position along pile axis	[m]
z	Depth below ground surface	[m]
Δz	Soil layer thickness	[m]
δ	Interface friction angle	[°]
ε_1	Axial strain	[–]
ε_v	Volumetric strain	[–]
γ	Estimated soil unit weight	[kN/m^3]
γ_w	Unit weight of water	[kN/m^3]
ν	Poisson's ratio	[–]
ϕ'	Effective internal friction angle	[°]
Ψ	State parameter ($e - e_{cs}$)	[–]
ρ	Density of pile material	[kg/m^3]
$\sigma'_r c$	Radial effective stress set up by pile installation	[kN/m^2]
σ'_{rf}	Shaft radial effective stress at failure in clays	[kN/m^2]
σ'_v	Total vertical stress	[kN/m^2]
$\sigma'_v 0$	Initial vertical effective stress	[kN/m^2]

1 Introduction

Most offshore structures are supported by large open-ended steel piles driven into the seabed. Examples include conventional oil and gas jacket platforms, wind turbines and AC/DC converter stations. These piles resist loads from the superstructure and from environmental wind and wave forces. Wind turbines in particular are founded on a single large pile called a monopile. This chapter describes problems associated with installing these foundation piles and outlines the research needed to improve understanding of their installation.

1.1. Research problem

In the ongoing energy transition, the quest for more marine renewable energy is leading to an increase in the number and size of offshore wind projects worldwide (EU 2025). Offshore wind power is currently the most developed renewable energy source available at sea (Negro et al. 2017). Over the last few years, the size of offshore wind turbines has increased, resulting in greater energy generation. These larger turbines require larger monopiles, with diameters of up to 11 metres, to support the structure (SIF 2025). Increasing the size of the pile also requires a heavier hammer. This increases weights to thousands of tonnes, thus increasing the risk of pile run. As energy projects expand into more challenging environments, pile running has become a growing concern within the offshore industry.

Firstly it is important to explain pile driving shortly. In general, a pile design is made that provides sufficient strength to support a super structure. The installation of this pile consists of multiple steps. The pile is stabbed and lowered to self weight penetration under its own weight. Then the hammer is placed on top. This additional mass could result in extra pile penetration. After the hammer is placed on top, the pile is driven to target penetration. This pile driving has two main failure mechanisms: Pile refusal and pile run. Refusal means that the hammer cannot provide enough energy to the system to penetrate through a soil layer. Pile run is an uncontrolled descent of the pile because the bearing capacity is less than the weight of the pile and hammer. It is up to the contractor to pick a hammer that is strong enough to reach target penetration while controlling the pile descent.

Pile run is not a new phenomenon in foundation pile installation. In fact, when controllable, it can help to achieve total penetration depth with less effort. This uncontrolled descent can potentially damage the hydraulic controls of the pile hammer, lead to sling failures or cause the hammer to fall into the water. It is also possible that the hammer will slam onto the pile again, which could damage the flanges. In all these cases, work is halted, resulting in high costs for the contractor and client. Static analyses are typically carried out to calculate the strength of the soil and predict the self-weight penetration (SWP), assuming that the pile's weight and static soil resistance are equal at the SWP level. At the SWP level, relatively little shaft resistance has developed, meaning the static equilibrium remains at a critical threshold. However, if the soil's bearing capacity diminishes for any reason, a pile run will follow.

The Soil Resistance to Driving (SRD) methods used to predict soil strength during pile driving, are based on empirical research attempting to establish a relationship between CPT data and bearing capacity. This means that each SRD method is applicable only to new projects in comparable environments, as it is based on specific boundary conditions. Secondly, most SRD methods only consider sandy and/or clay soils. However, transitional soils, such as silt, have their own characteristics that are not taken into account, resulting in inaccurate drivability calculations.

Inaccurate predictions of soil bearing capacity, coupled with an increasing risk of dropfalls due to larger pile dimensions and heavier hammer weights, can result in unexpected dropfalls causing substantial damage and downtime. This compels the industry to seek knowledge on how to identify dropfall risks in new areas.

1.2. Research objectives

This research aims to address the challenges of pile run prediction in transitional soils by:

- Investigating the hydro-mechanical interaction between impact-driven piles and transitional soils under axial loading.
- Developing a risk-based framework to predict dropfalls during installation, with the use of SRD-based methods.

To provide context on the objectives, the hydro-mechanical interaction relates to changes in pore water pressure (PWP) in transitional soils due to the impact of pile driving, and how this affects the soil's bearing capacity. This objective focuses on transitional soils because the relationship between pile driving and the soil skeleton for this soil type is not clearly defined.

The second objective is the primary goal of the thesis and requires the theoretical knowledge obtained in the first objective. The idea is to create a step-by-step plan that assesses dropfall risks based on CPT data, since CPT is the most commonly used test for easily obtaining continuous soil profiles. Using the basic soil fundamentals and test it on a field case helps to create a generally applicable framework for the industry. In addition, it is necessary to identify the soil parameters that facilitate more precise prediction of the SRD in transitional soils.

This is beneficial for the analysis of driveability and the subsequent risk assessment of the contractor. Two failure mechanisms for pile driving have been identified: Pile run and pile refusal. Pile refusal is defined as the state in which a foundation pile is unable to be driven deeper into the ground due to the presence of an impenetrable obstacle, such as rock or boulders. This phenomenon is often observed when the effective energy of the hammer is inadequate for additional penetration. The contractor's objective is to predict the occurrence of one of the two failure mechanisms.

1.3. Scope and limitations

This research focuses on the impact hammering of pin piles in transitional soils, with a particular focus on pile-soil interaction under axial loading. The designed criteria from subsection 2.5.4 are tested using a case study near Changhua in Taiwan. All boundary conditions beyond the scope of this research are taken from that project. This means that the pile dimensions and hammer type are predefined and do not change between cases. Consequently, only the soil properties change. It also means that human interaction, such as the movement of the crane operator, is not being researched.

The main soil types of interest for this study are transitional soils, such as silts and clayey sands. Transitional soils demonstrate mechanical properties that are neither wholly consistent with that of sands nor that of clays, exhibiting characteristics that are intermediate between these two categories. The main characteristics of interest are the permeability and particle sizes. As addressed in the research problem lies the research gap in the soil behaviour region between clays and sands. The focus will not be on stratified soil layers and their behaviour, except when they show partially drained behaviour as mechanical property. The project details are explained in section 3.1. The main limitation is that the presented theory is only tested on dropfalls at six locations. This helps to test the theory, but does not prove the provided underlaying mechanism. Other key limitations include:

- The distance from CPT to the pile is approximately 10 meters, which introduces an element of uncertainty with respect to the soil stratigraphy.
- If present, direct hammer output data is used. Otherwise hammer info data is reconstructed as precise as possible. The hammer data is not 100% accurate, so it is compared with the blowcount sheets of the responsible engineer offshore.
- The validation of frameworks is confined to pin piles. The scalability of the system to other pile sizes, such as monopiles, remains to be empirically validated. Changes to other pile dimensions alter the contribution of shaft friction versus tip resistance.
- The decision has been made to utilise a select group of three SRD methods for the calculation of soil resistance. Motivation is given in section 3.3. Assumptions are also made when correcting the raw CPT data, but these are kept to a minimum.
- The CPT correlations that are used for soil classification and strength parameter calculations are very uncertain.
- Viscous effects and drag forces are neglected in the analytical model. The reason for it is further explained in section 2.7.

1.4. Research questions

The primary research question explores the potential for soil failure mechanisms resulting in a dropfall in transitional soils during impact driving. This involves pile-soil interface behaviour, fundamental soil mechanics and soil resistance to driving predictions for quantification. The main research question is as follows:

What is the primary mechanism that initiates a dropfall of an offshore monopile during impact pile driving in transitional soils?

The following sub-questions provide further insights into the governing mechanisms and the ability to predict a pile run:

- How does impact pile driving cause soil resistance reduction in transitional soils?
- How can the dropfalls observed in the Changhua case study be evaluated against the theoretical criteria for the proposed framework?
- To what extent can static SRD-based predictions of shaft and tip resistance anticipate the depth and occurrence of a dropfall?

1.5. Research method

The research is structured in three phases: theoretical framework development based on soil fundamentals, case-study validation and a predictive assessment with SRD methods. These phases are described below in more detail.

Theoretical framework development. To answer the question of how does impact pile driving cause soil resistance reduction in transitional soils, a comprehensive literature review is first conducted to characterise soil–pile interaction under impact loading at both particle scale and system scale (shaft and tip resistance zones). Existing models, including the Mohr-Coulomb criterium, Bolton's stress-dilatancy relations and the fluidisation concept, are integrated into a conceptual framework. From this analysis, explicit failure criteria (contractivity and partial permeability) are derived in order to define the conditions under which successive hammer blows will trigger a loss of bearing capacity and thus a dropfall.

Case-Study Validation. In order to address the question of how the dropfalls observed in the Changhua case study can be evaluated against the theoretical criteria for the proposed mechanism, borehole logs and CPT profiles from the six sites with dropfalls are assembled. For each site, the state parameter is computed and soil layers classified on Robertson's SBT_n chart to identify contractive, semi-permeable soil layers. Subsequent to this, the observed dropfall depths will be overlaid on these classifications in order to verify whether they coincide with layers that meet the two aforementioned theoretical criteria.

Predictive Assessment with SRD Methods. The objective of this study is to evaluate the extent to which static SRD-based predictions of shaft and tip resistance can predict the depth and occurrence of a dropfall. To this end, three state-of-the-art SRD models (Alm & Hamre, Maynard, Unified Method) are applied to the Changhua CPT data. Predicted static shaft and tip resistances are compared to the actual dropfall depths in order to evaluate the predictive performance. The results will demonstrate the capabilities and limitations of static SRD approaches for forecasting pile run risks in transitional soils.

1.6. Literature gap

A literature gap was identified in the pile-soil interaction in transitional soils for pile installation based on a literature study. The fundamental mechanisms describing this interaction during impact driving have yet to be defined. Although research on this mechanism exists, it is not linked to applications in industry. A more general gap exists between research and industry in terms of calculation methods used to quantify soil strengths. While many options exist for determining specific soil parameters using laboratory tests, the industry is limited to CPT tests. While laboratory tests provide variables that help create a pile design, a continuous soil profile is required for driveability to prevent installation failure due to local imperfections. Laboratory tests only provide precise parameter identification for certain depths, which creates a risk of not capturing complete soil behaviour. This is why CPT data is still widely used as the main input for driveability analysis.

Moving on to SRD methods, it is evident that there is a research gap as there is no method calibrated for large-diameter foundation piles in silty soils. Silt is often treated as sand, despite having different mechanical properties. Most methods are tested on piles with diameters under two metres. These two factors make SRD

predictions unreliable. The industry is calling for new methods to describe these soil layers. This thesis focuses on the transitional soil response during impact driving in order to gain an understanding of the governing mechanisms during pile driving. Calibrating the sensitivity of SRD method parameters is beyond the scope of this thesis as this would not contribute to our understanding of silt behaviour.

1.7. Thesis outline

The structure of this research is summarised below, providing an overview of the contents of each chapter:

- **Chapter 1: Introduction**
  - Problem definition and thesis motivation
  - Outline of research objectives and questions
- **Chapter 2: Literature Review**
  - Description of soil fundamentals and governing theoretical mechanisms
  - Summary of existing knowledge on soil mechanics and pile driving
- **Chapter 3: Methodology**
  - Explanation of the soil investigation
  - Project details and explanation of the SRD methods
- **Chapter 4: Results**
  - Plots of relevant soil parameters for the case study
  - SRD outcomes over depth compared with observed dropfalls
- **Chapter 5: Discussion**
  - Interpretation and evaluation of the performed research
  - Applicability of the theory and practical recommendations
- **Chapter 6: Conclusion**
  - Answers to the main research question and sub-questions

2
Literature review

This chapter reviews literature relevant to this research, providing insights needed to achieve the study's objectives. Firstly, the report zooms out to watch the trends in the offshore wind market and the accompanied so called 'pile run' problem in offshore foundations. Secondly, the drivability of foundation piles is explained and the relevant input factors are discussed. The soil fundamentals that influence the bearing capacity are elaborated on. Finally the CPT test is explained and the equations used to calculate CPT correlations are provided. This literature review a steady foundation for the research.

2.1. Offshore wind market

The offshore wind energy sector has experienced significant growth in recent years (Lee and F. Zhao 2021). This has been driven by technological advances and environmental requirements (Netherlands Enterprise Agency 2023)(Bilgili et al. 2023). Offshore wind has become a key component of global renewable energy strategies. Governments worldwide are setting ambitious renewable energy targets to combat climate change, bolstering investments in offshore wind projects (Osborne 2024). Most countries have their first targets placed in 2030, creating a high demand for wind turbine installation the upcoming years. Figure 2.1 below shows that offshore wind energy deployment could reach more than 193 GW by 2029, according to McCoy et al. (2024). Most of the wind turbines are nowadays build in the shallow sea areas with bottom fixed foundations. The turbines are connected to the seabed with jacket structures or monopiles.

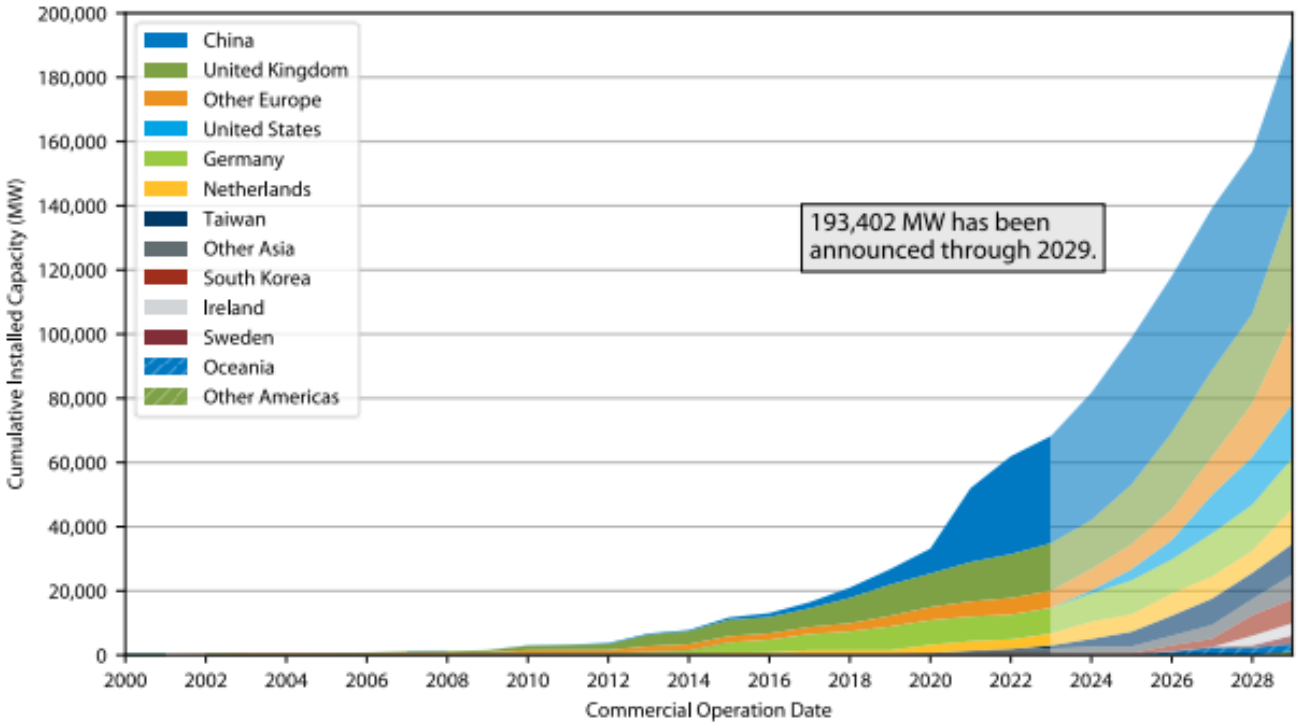

Figure 2.1: Estimated cumulative fixed-bottom and floating offshore wind capacity by country based on developer-announced CODs in 2023 (McCoy et al. 2024).

One of the primary trends in the technological growth of offshore wind turbines is the movement toward larger-rotor machines with higher hub height. This increase in size gives an increase in total weight of the wind turbine as well, requiring larger monopiles, which leads to even more weight of the total turbine (Bilgili et al. 2023). This increase of size and the accompanied grow of potential power generation is visible in Figure 2.2.

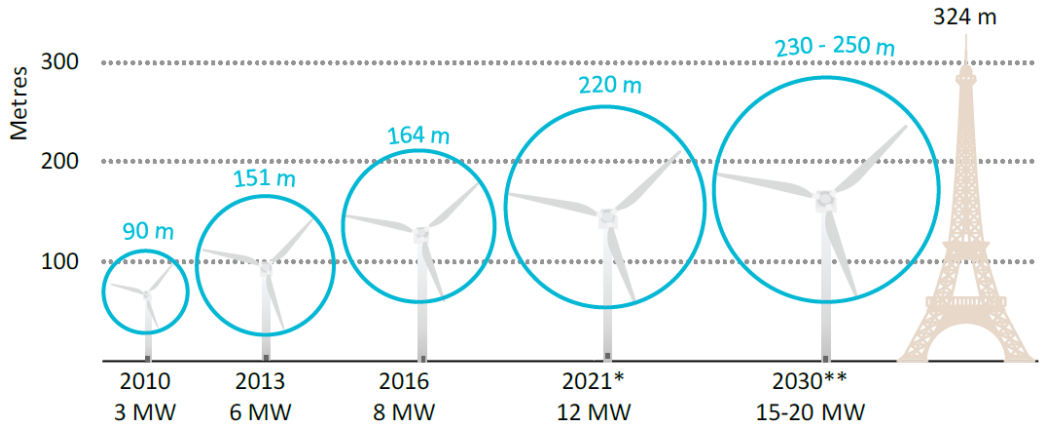

Figure 2.2: Global evolution of the largest commercially available wind turbines (International Energy Agency 2019).

2.2. Offshore foundations

Steel pipe pile is widely used to construct the foundations of offshore structures because it requires less installation effort than a closed-ended pile under the same soil conditions (Salgado et al. 2002)(M.F. Randolph 2003)(Paik and Salgado 2003). As described in section 2.1, the wind turbines are growing, requiring larger diameter monopiles to support the loads generated from the weight of the structure itself, wind and waves (Sun et al. 2016). These monopiles are currently dominating the offshore wind market, but as projects shift to deeper water other foundation types are chosen. Jacket and pin piles are used to support jacket and tripod superstructures. Jacket piles are also characterized by substantial diameters up to 4 meters. Three other foundations which are not further discussed in this thesis are mooring lines, anchor piles and suction caissons. Mooring lines anchor a floating structure to the seabed. Anchor piles hold offshore floaters in place and are able to transfer loads vertically compared to mooring lines. Suction caissons are fixed platform anchors with normally large diameters than piled foundations. They lower themself by creating a water pressure difference. In Table 3.1 the typical pile dimensions presented.

Table 2.1: Typical dimensions for Jacket Pile and Monopile (Maynard et al. 2019).

Typical Dimension	Jacket Pile	Monopile
Embedded length (m)	65	30
Diameter (m)	2.5	7.5
L/D (m)	26	4
Tip thickness (mm)	55	70
Side area (m^2)	325	450
End area (m^2)	0.1375	0.525

As pile dimensions increase, the complexity and technical demands of the installation process also grow. The installation process typically consists of four main stages, as illustrated in Figure 2.3:

1. **Placement of pile guide frame:** A steel template is lowered to support pile positioning during stabbing and driving of the pile.
2. **Stabbing of monopile:** The monopile is lifted into the guide frame and allowed to penetrate under its own weight until initial embedment (SWP) is achieved. Hitting a soft soil layer can already cause a punch through.
3. **Placement of follower and hammering:** A follower is seated on the pile head, and an impact hammer drives the pile to target depth through controlled blows. Placing of the follower and hammer can initiate a punch through. This thesis researches dropfalls during the impact driving phase.
4. **Template removal and superstructure installation:** The guide frame is retrieved. A transition piece for the turbine or a different super structure is installed atop the driven foundation pile.

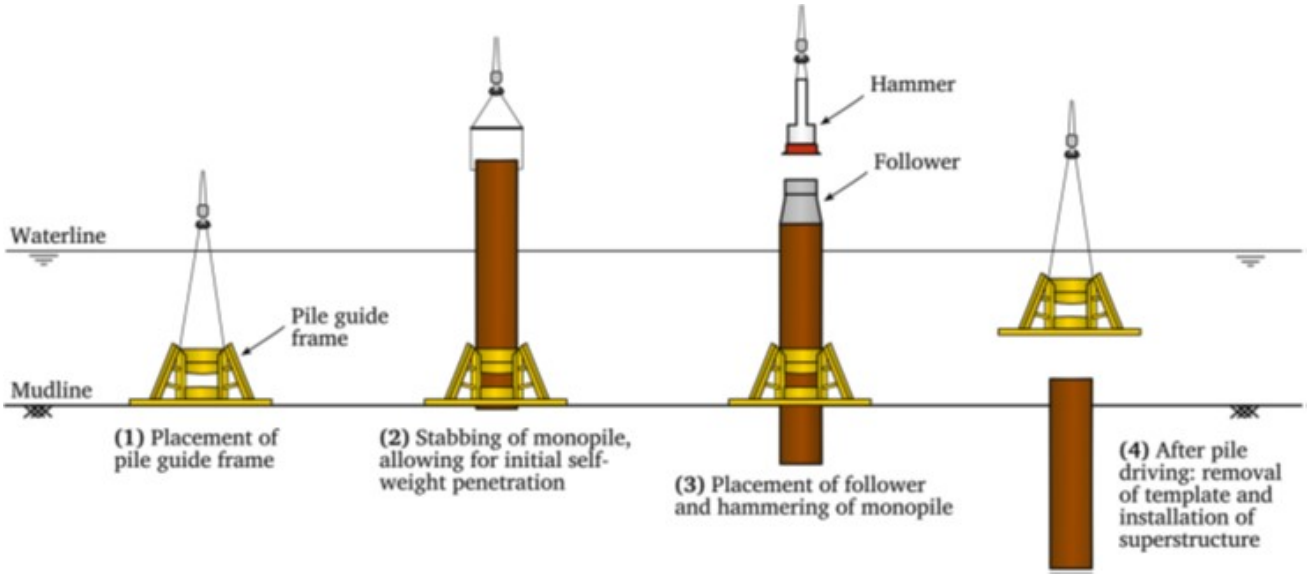

Figure 2.3: Example of a monopile installation process (Duffy et al. 2025).

2.3. Soil fundamentals

This section describes fundamental behaviour of soil that help understanding the governing mechanisms in the pile-soil interaction.

2.3.1. Soil stresses

The basic principles that determine stress in soils are primarily based on the concept of effective stress, which is critical in soil mechanics. Effective stress is the stress that contributes to soil deformation and strength, excluding pore water pressure. This principle is essential for understanding both saturated and unsaturated soil behaviour. The fundamental relationship of stresses in soil is described as follows by Terzaghi's stress principle and written by Verruijt (2001):

$$\sigma = \sigma' + u \tag{2.1}$$

where:

- σ is the total stress (N/m^3);
- σ' is the effective stress (N/m^3);
- u is the pore water pressure (N/m^3).

The principle of effective stress is foundational in soil mechanics, serving as the basis for understanding soil behaviour under various conditions (Zhao et al. 2016). It influences the stress-strain rate over time (Alpan 1970), further explained in subsection 2.3.8 and provides insights into the mechanical behaviour of soils under different stress conditions, emphasizing the critical state line where soil transitions from elastic to plastic behaviour (Atkinson and Bransby 1987). In stress and strain relationships, it is important to distinguish between compression and distortion. The behaviour in these two types of deformation is completely different. Deformations in shear are usually much greater than those in compression. Moreover, in compression the material becomes progressively stiffer, whereas in shear it becomes progressively softer (Verruijt 2001). This is not the case when compact soil is exerted under shear. For compact soils, shear results in dilation and thus increasing effective stress.

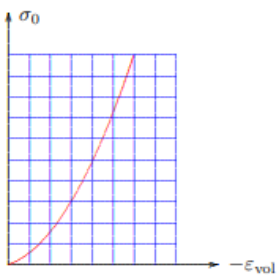

Figure 2.4: Stiffness in compression (Verruijt 2001).

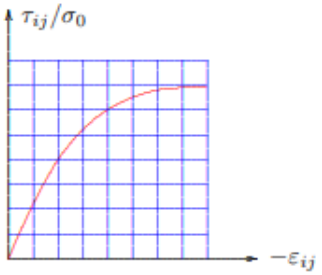

Figure 2.5: Stiffness in shear (Verruijt 2001).

The principle of effective stress is essential to understanding soil mechanics and influences how soils respond to external forces. It determines soil properties under drained and undrained conditions, which are explained in Subsections 2.3.5 and 2.3.6. Understanding these principles is essential for predicting soil behaviour.

2.3.2. Grain size distribution

Grain size distribution (GSD) is a fundamental characteristic that determines the physical and hydraulic properties of soils. It influences soil classification, behaviour and various soil properties. The three main soil types for offshore foundations are sand, silt and clay. The distribution of gravel, sand, silt and clay particles affects soil texture, which in turn affects soil properties such as porosity, permeability and water holding capacity. For example, soils with higher silt and clay content tend to have higher water retention and different mechanical properties compared to sandy soils (Ural and Görgün 2019).

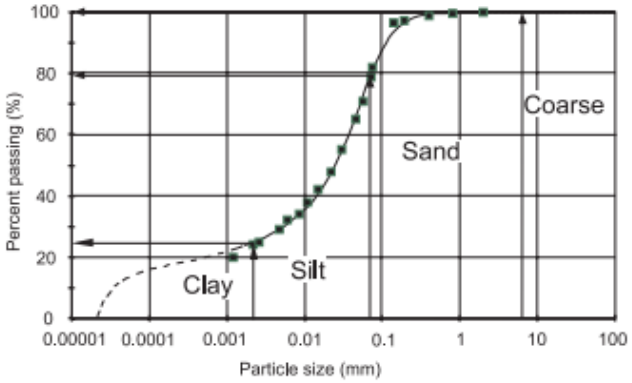

Figure 2.6: Determination of the soil fractions according to the USDA classification, when using the unimodal equation (Fredlund et al. 2000).

Soil type	min. (mm)	max. (mm)
clay	-	0.002
silt	0.002	0.063
sand	0.063	2
gravel	2	63

Figure 2.7: Soil type classification based on particle size (Verruijt 2001)

Traditional methods like sieve analysis and hydrometer analysis are commonly used to determine GSD, especially for coarse and fine particles, respectively. These methods involve physical separation and measurement of soil particles. Also several mathematical models are used to represent GSD curves (Fredlund et al. 2000). The results of two different models are presented in Figure 2.6 and Figure 2.7 above, which shows that there are no clear boundaries between the different soil types. The distribution of grain sizes, including parameters like average size and dispersion, plays a crucial role in predicting permeability (Masch and Denny 1966), which is further elaborated on in subsection 2.3.4.

2.3.3. Soil classification

Soil classification is based on index properties, which are determined by classification tests. These tests are described below:

- Particle-size (grain-size) analysis by sieving, which is used to determine gradation parameters.
- Plasticity characterisation by Atterberg limit tests, which are used to obtain the plasticity index and place fine-grained samples on the plasticity chart.

Combining particle-size and Atterberg-limit information ensures robust identification of sands, silts and clays. Soil samples are obtained by making boreholes from which soil layers are extracted (Das 2006). subsection 2.3.2

explains more on grain size distributions that follow from a sive analysis. An example of the Atterberg-limits is shown in Figure 2.13. The limits are typically determined using the Casagrande device.

For samples that contain significant fines, the liquid limit (LL) and plastic limit (PL) are determined following standard laboratory methods on the soil samples. The plasticity index (PI), which quantifies the plastic range of the soil, is defined as:

$$PI = LL - PL \tag{2.2}$$

The PI is a measure of the plasticity of a soil. As such, the PI indicates the amount and type of clay present in a soil (Kaliakin 2017). In general:

- Soils with a high PI tend to be clay.
- Soils with a lower PI tend to be silt.
- Soils with a PI near zero tend to have little or no fines (silt or clay) present.

The particle size and plasticity index classify the soil type. The problem is that these indicating parameters are only determined with lab tests on soil samples taken from a borehole. They cannot be directly derived for a continuous soil profile provided by a CPT. P. Robertson (2010) suggested a method to classify soil based on CPT correlations. A clear description of how this analyss is performed is given in section 2.4. This method is involved with more uncertainty than lab tests on the soil samples. The advice is to classify soil with particle size or plasticity index, as is done in the case study from this thesis with the information gathered from the borehole samples. The process of obtaining a borehole log is described in subsection 3.2.1.

2.3.4. Permeability

Grain size determine soil permeability, which is the measure of how easily water can move through soil. Larger grain sizes generally lead to higher permeability, while smaller grain sizes result in lower permeability (Shepherd 1989). Permeability *(k)* is basically the volume of water that can pass through one square meter per second and is represented in Equation 2.3 as:

$$q = -k\frac{dh}{ds} \tag{2.3}$$

Figure 2.8: Equation for soil permeability (Darcy 1856)(Whitaker 1986)

soil type	k **(m/s)**
gravel	$10^{-3} - 10^{-1}$
sand	$10^{-6} - 10^{-3}$
silt	$10^{-8} - 10^{-6}$
clay	$10^{-10} - 10^{-8}$

Figure 2.9: Permeability of different soil types (Verruijt 2001).

The sorting of grain sizes, which refers to the uniformity of particle sizes, also affects permeability. Well-sorted soils with uniform grain sizes tend to have higher permeability compared to poorly sorted soils (Huang et al. 2019). Soil can in practice be divided into two categories: coarse-grained and fine-grained soils, with as described their difference in permeability. The mechanical differences between these two categories are relevant for the calculations of the SRD, as it influences the drainage conditions, described in the next subsections. Figure 2.10 below provides pictures of the structure of different soil types, sorted on permeability and grain size.

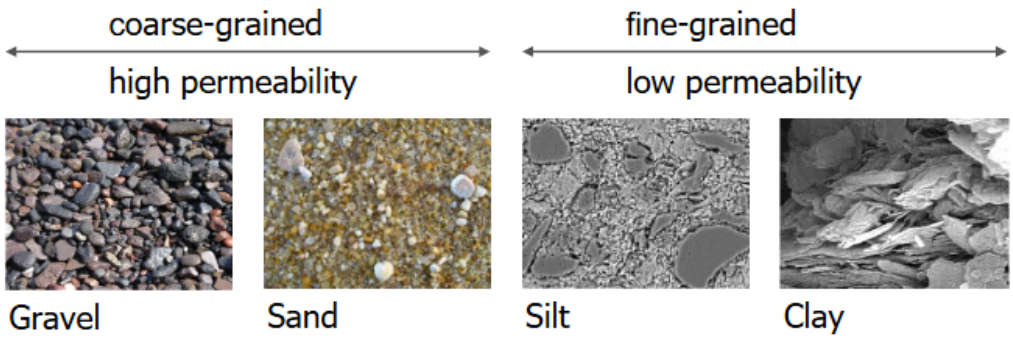

Figure 2.10: Pictures of different soil types, ordered on grain size and permeability (Kementzetzidis 2024).

2.3.5. Drained conditions

Coarse-grained soils have been shown to exhibit distinct mechanical properties in comparison to fine-grained soils. The high permeability of the medium leads to conditions of drainage. In conditions of drained loading, the application of load is gradual, or alternatively, the soil permeability is high, resulting in the unobstructed flow of water out of the soil skeleton, without the development of excess pore pressures (Δu). In other words, all load changes are taken by the soil skeleton (Lambe and Whitman 1969). The soil is described by the following key mechanical properties:

- **Shear Strength:** The shear strength of coarse-grained soils increases with the proportion of gravel, particularly when the gravel is uniform in size. The internal friction angle also increases with coarse grain content (Ardouz et al. 2022), plotted in Figure 2.11. This means that in drained conditions the soil has higher shear strength and is thus able to build up more shaft friction than undrained soils.
- **Dilatancy:** Coarse-grained soils exhibit significant dilatancy, which is the volume change tendency during shear (Du et al. 2023). This positive dilatancy is plotted in Figure 2.12, as the volumetric strain increases under loading. Well-graded soils show greater dilatancy compared to poorly-graded soils, leading to higher peak friction angles in drained conditions (Ahmed et al. 2024).
- **Particle Breakage:** Under stress, coarse-grained soils undergo particle breakage through fracture. The rate of particle breakage increases with larger differences in particle size distribution before and after testing (Du et al. 2023). Particle breakage forms a risk in carbonated soils (CAPE Holland 2024).
- **Influence of Gradation:** Soils with a wider gradation exhibit greater dilatancy and shear strength. The critical state lines in void ratio-mean effective stress space move downward as gradation widens, indicating higher mechanical strength (Ahmed et al. 2024).

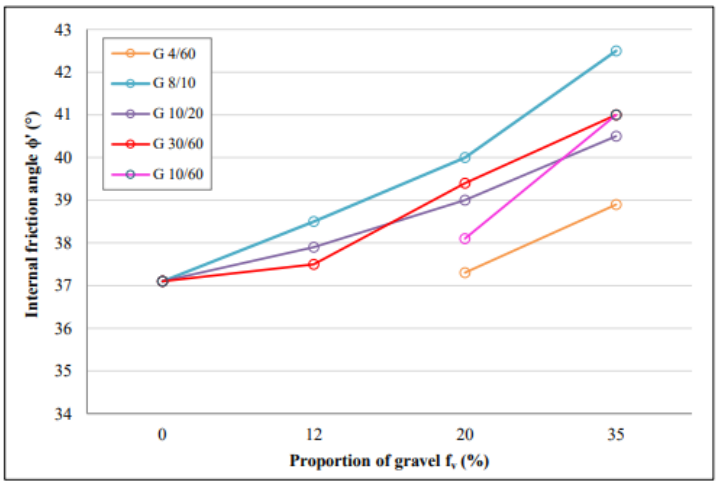

Figure 2.11: Evolution of the internal friction angle ϕ' as a function of the volume proportion of gravel (Ardouz et al. 2022).

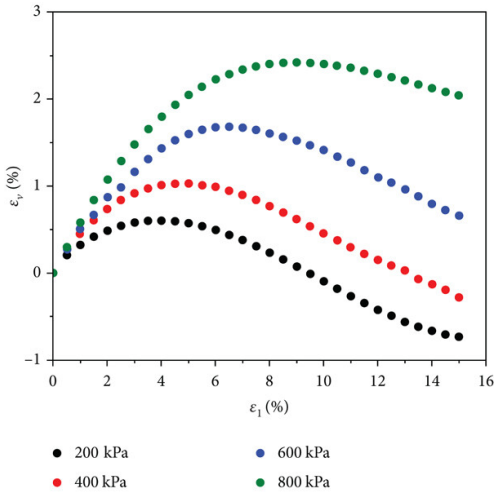

Figure 2.12: The volumetric strain ϵ_v versus axial strain ϵ_1 curves under different effective stresses (Du et al. 2023).

2.3.6. Undrained conditions

In water-saturated soils, the pore water pressure (u) relieves the contact forces between the grains. The same way that solids submerged in fluids weigh less. When loading is applied so rapidly, or the soil permeability is so low, there is no movement of water and excess pore pressures (positive or negative) are able to develop (Wu et al. 2019). Undrained conditions are most common in fine-grained soils as they have low permeability. In unsaturated soils, volume change in undrained conditions is related to over consolidation ratios (OCRs) and pore air volume (D. Sun et al. 2008). Atterberg limits, which include the liquid limit, plastic limit, and plasticity index, are determining the undrained conditions of fine-grained soils. These limits, shown in Figure 2.13 are used to estimate the undrained shear strength of soils. More importantly, they classify the soil type based on the plasticity limit. This is described in section 4.1. The undrained shear strength at the plastic limit is significantly higher than at the liquid limit, often 30-35 times greater (Karakan 2022). The undrained shear strength of clay (s_u) is not increasing, with increasing axial shear, as this is taken by the pore water pressure. This is visualised in Figure 2.14.

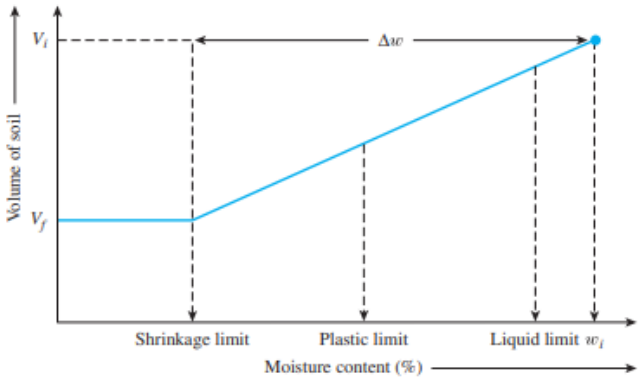

Figure 2.13: Definition of the Atterberg limits (Das 2006).

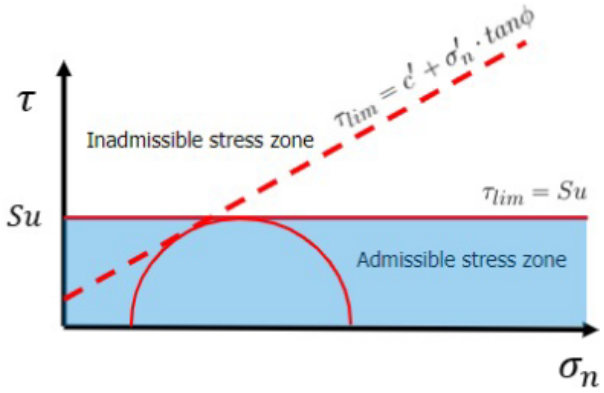

Figure 2.14: Undrained shear strength s_u (Kementzetzidis 2024).

Than silty soils are left, which form the partially drained soil category. Silty soils often experience partial drainage during testing and loading, which affects the interpretation of soil properties. This is particularly evident in Cone Penetration Tests (CPT), where partial drainage can lead to inaccurate estimates of soil properties if not properly accounted for. In undrained conditions the tip resistance, the pore pressure distribution and its dissipation depend on the rigidity index $I_r = G/s_u$, where G is the elastic shear modulus and s_u is the undrained shear strength. The first may be expressed as:

$$G = \frac{3(1-2\nu)}{2(1+\nu)} \cdot \frac{(1+e)\sigma'}{\kappa} \tag{2.4}$$

where ν is the Poisson's ratio, e is the void ratio, κ is the permeability and σ' is the mean effective stress (Ceccato and Simonini 2017). The consolidation behaviour of silty soils under partially drained conditions is influenced by the soil's permeability and the rate of loading. The coefficient of consolidation can be estimated through dissipation tests, which are affected by the degree of drainage during penetration. The partially drained behaviour of silty soils necessitates careful consideration in geotechnical design and analysis. Existing soil behaviour charts and correlations may not accurately capture the behaviour of silty soils, requiring tailored approaches for site characterization and engineering applications (Liu et al. 2022).

2.3.7. Normalised velocity

The normalized velocity is a dimensionless parameter that accounts for the effects of penetration rate on soil response during testing. It is particularly significant in fine-grained soils, where penetration rate can influence pore pressure generation and, consequently, the measured cone resistance (García Martínez et al. 2016). The effect of the above discussed soil drainage can be taken into account using as normalising parameter, the normalised penetration velocity (Finnie and M. F. Randolph 1994):

$$V' = \frac{vD}{c} \tag{2.5}$$

where v is the penetration velocity, D the cone diameter, and c the consolidation coefficient. For open-ended steel piles, take wall thickness t instead of the diameter. Indeed, the consolidation process close to the advancing cone is not only affected by the permeability, but a significant role is also played by the compressibility of the soil, the probe diameter, and penetration velocity. Accordingly, Equation 2.5 describes the relation between penetration rate, pile size and consolidation coefficient, which is related to soil drainage state. These parameters are plotted against each other in Figure 2.15, indicating that one soil type can have different drainage behaviour, based on penetration speed (Finnie and M. F. Randolph 1994). Note that this thesis invests the initiation of a pile run, not the behaviour during a pile run. This means that the velocity is (almost) zero, giving small relative velocity values.

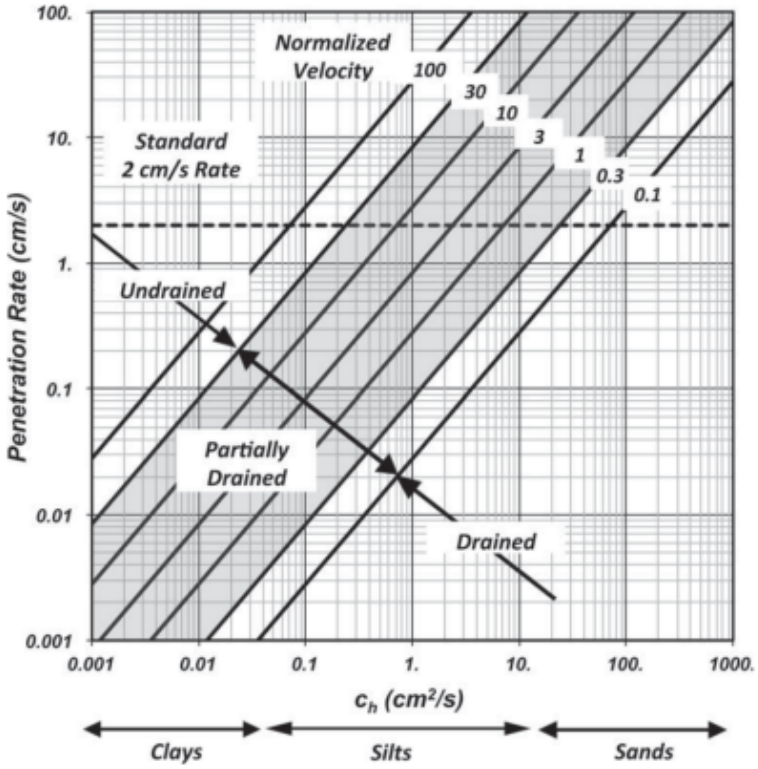

Figure 2.15: Field decision chart for 10 cm^2 cone presenting relation between consolidation, penetration rate and normalised velocity (J.T. DeJong et al. 2013).

As by higher penetration rate (pile run) the soil behaviour turns more undrained, the total resistance drops (Finnie and M. F. Randolph 1994). This drop is 55% for shaft friction (Carneiro et al. 2016) and 90% for tip resistance (Finnie and M. F. Randolph 1994). Further research has been conducted on this topic, from which the results are visible in Figure 2.16. For transitional soils are the changes in penetration resistance difficult to define, as the drainage conditions are often unknown around the CPT and pile. Intermediate soils should therefore be examined on a case-by-case basis, with particular attention to the soil's coefficient of consolidation and the probe diameter (Duffy et al. 2025).

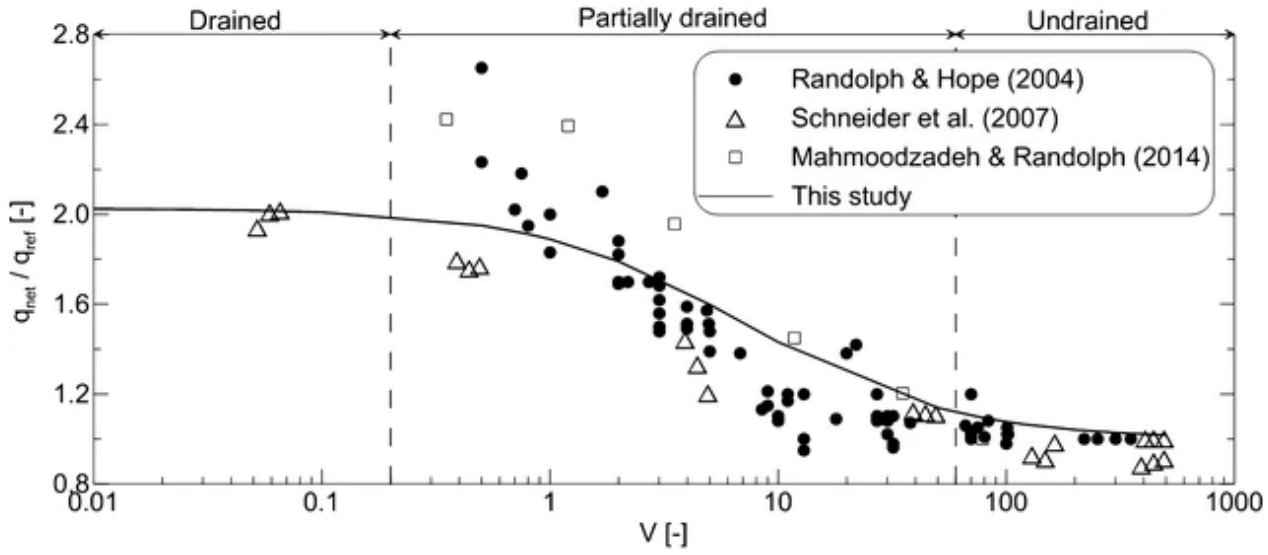

Figure 2.16: Resistance ratio over normalized velocity, comparison with experimental data on kaolin (Ceccato and Simonini 2017).

2.3.8. Consolidation

Consolidation occurs as water is squeezed out of the soil's pore spaces, leading to a reduction in volume and an increase in soil density over time. This process continues until the excess pore water pressure, generated by an increase in total stress, is fully dissipated. The consolidation coefficient is relevant for drainage behaviour, as it describes the relation between the permeability and the compressibility (Verruijt 2001):

$$c = \frac{k}{m_v \gamma_w} \tag{2.6}$$

- c = Coefficient of consolidation
- k = Coefficient of permeability
- m_v = Coefficient of volume compressibility
- γ_w = Water density, 10.25 [kN/m^3] for salt water

2.4. Cone Penetration Test

This section provides an explanation of the Cone Penetration Test (CPT) test and the correlations that can be calculated with the CPT results. The CPT, a Dutch invention from the 1950s that was called the Dutch Cone Test, is a widely used method for soil investigation, providing rapid, continuous, and reliable measurements of soil properties. The CPT is based on pushing a penetration cone of approximately 35 mm with constant velocity (20 - 25 mm/s) into the soil. During the penetration test the values of the cone resistance q_c and the local skin friction f_s, respectively are recorded. Sometimes pore pressure is also recorded (P. Robertson 2016). The friction ratio is defined as the percentage of sleeve friction, f_s, to cone resistance, q_c at the same depth (Rocscience Inc. 2021). The raw q_c value is corrected for the pore pressure influence on the measurement to obtain the corrected cone resistance q_t. The used correction described in Equation 2.7 is suggested by P. Robertson (2010).

$$q_t = q_c + u_2(1 - a) \tag{2.7}$$

Where:

- q_t: corrected cone tip resistance
- q_c: measured cone resistance
- u_2: measured PWP at CPT shoulder
- a: cone area ratio. $a = 0.75$ commonly used for CPT tests offshore by Fugro

CPT is effective in determining the number and thickness of soil layers, providing a detailed profile of subsurface conditions. The test data can be used to classify soils based on behaviour characteristics, which are more indicative of in-situ conditions than traditional textural classifications. For soil identification, the CPT results may be normalised to yield the normalised cone resistance, Q_{tn}, and the normalised shaft resistance, F_r. When these values are plotted on the SBT_n chart (see Figure 2.17), the soil behaviour type becomes apparent. The contours of the state parameter, I_c, can be used to approximate the SBT_n boundaries. The generally circular shape of the I_c contours provides a reasonable fit to the SBT_n boundaries in the central region of the chart (P. Robertson 2016). This SBT_n chart is presented below in Figure 2.17, with the classification table next to it to categorise the soil type.

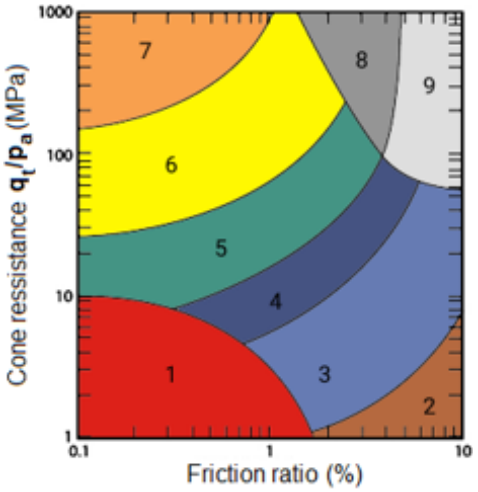

Figure 2.17: CPT Soil Behavior Type (SBT) chart (P. Robertson 2010).

Zone	Soil Behavior Type (SBT)
1	Sensitive, fine-grained
2	Organic soils - clay
3	Clay - silty clay to clay
4	Silt mixtures - clayey silt to silty clay
5	Sand mixtures - silty sand to sandy silt
6	Sands - clean sand to silty sand
7	Gravelly sand to dense sand
8	Very stiff sand to clayey sand *
9	Very stiff fine-grained *

Figure 2.18: Soil Behavior Type (SBT) Classification by Zone (P. Robertson 2010).

2.4.1. CPT correlations

A summary is presented of the interpretation methods for the CPT results. Identification of soil stratigraphy in terms of general soil behaviour (and to a lesser degree soil type) is a more important feature of CPT than other investigation techniques (Fugro 2021). Empirical research has correlated these measurements to other soil parameters (P. Robertson 1990)(P. Robertson 2010)(P. Robertson 2016). This subsection offers a comprehensive overview of the employed correlations and their respective references, in addition to a detailed list of the variables utilised.

The soil properties saturated unit weight γ, effective stress σ'_v and total stress σ_v, calculated according to P. Robertson (2010):

$$R_f = \left(\frac{f_s}{q_t}\right) \cdot 100\% \tag{2.8}$$

$$\gamma = \left(0.27 \log(R_f) + 0.36 \log\left(\frac{q_t}{p_a}\right) + 1.236\right) \gamma_w \tag{2.9}$$

$$\sigma'_v = \sum \Delta z \left(\gamma - \gamma_w\right) \tag{2.10}$$

$$\sigma_v = \sigma'_v + z\,\gamma_w + \sigma_{v0} \tag{2.11}$$

- R_f: friction ratio
- fs: local skin friction $[Pa]$
- γ: estimated soil unit weight $[kN/m^3]$
- p_a: atmospheric (reference) pressure, 101 [kPa]
- σ'_v: total vertical effective stress at depth z, obtained by summation of layer contributions [kN/m^2]
- Δz: thickness of the soil layer [m]
- σ_v: total vertical stress at depth z [kN/m^2]
- z: depth below the ground surface [m]
- σ_{v0}: initial vertical stress at the seabed surface (initial surcharge) [kN/m^2]

The normalised cone resistance and friction ratio parameters for soil classification are also calculated as following by P. Robertson (2010):

$$Q_t = \frac{q_t - \sigma_v}{\sigma'_v} \tag{2.12}$$

$$Q_{tn} = \frac{q_t - \sigma_v}{p_a}\left(\frac{p_a}{\sigma'_v}\right)^n \tag{2.13}$$

$$F_r = \frac{f_s}{q_t - \sigma_v} \times 100 \tag{2.14}$$

$$I_c = \sqrt{\left(3.47 - \log Q_{tn}\right)^2 + \left(\log F_r + 1.22\right)^2} \tag{2.15}$$

- Q_t: normalised cone resistance
- Q_{tn}: normalised cone resistance with variable stress exponent
- n: stress exponent
- F_r: normalised friction ratio (%)
- f_s: sleeve (shaft) friction [MPa]

The stress exponent n is according to Zhang et al. (2002) calculated with Equation 2.16. Use a root cause finder function to solve I_c, Q_{tn} and n.

$$n = 0.381\, I_c + 0.05\, \frac{\sigma'_v}{p_a} - 0.15 \tag{2.16}$$

P. Robertson (2016) suggested to update the SBT_n chart with new soil behaviour types and the incorporation of a contractive–dilative (CD) boundary. This updated chart is shown in Figure 2.19. A CPT-based boundary between contractive and dilative soils depends on many variables (e.g., in situ stress state, soil plastic hardening), and there is a transition between ideal soils that are predominately contractive to soils that are predominately dilative at large shear strains. The CD boundary may be represented by Equation 2.17 and the modified soil behaviour type index I_b with Equation 2.18.

$$\text{CD} = 70 = (Q_{tn} - 11)(1 + 0.06F_r)^{17} \tag{2.17}$$

$$I_b = 100(Q_{tn} + 10)/(Q_{tn}F_r + 70) \tag{2.18}$$

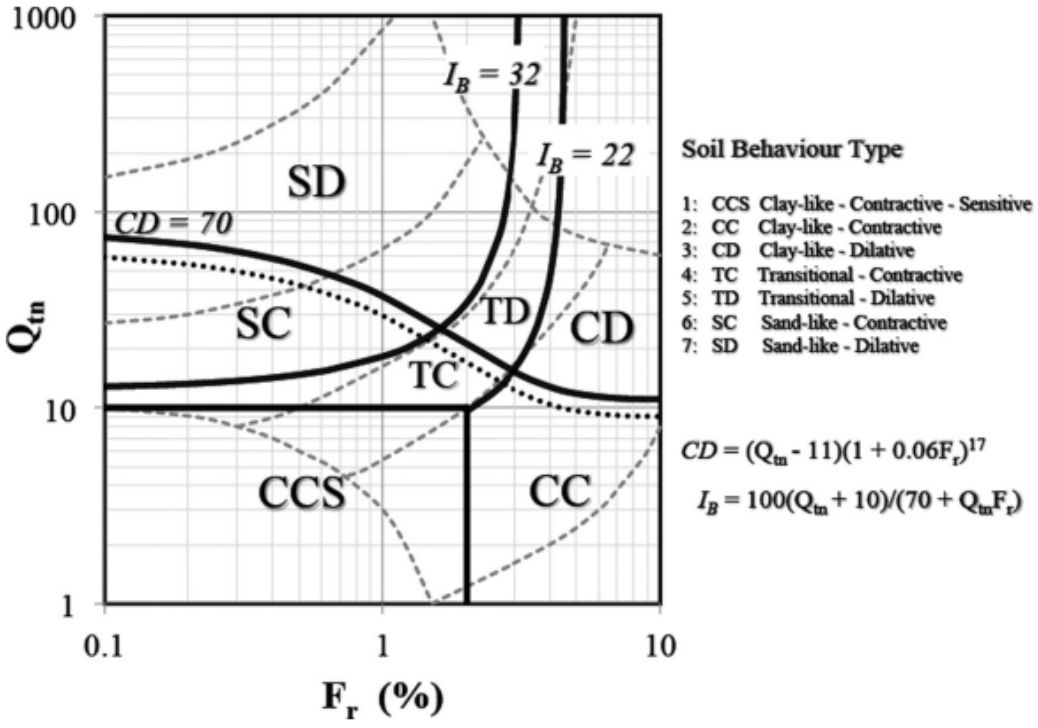

Figure 2.19: Proposed updated SBT_n chart based on Q_{tn}–F_r (solid lines show soil behaviour type boundaries, and dashed lines show boundaries), suggested by P. Robertson (2016)).

2.4.2. State parameter

The state parameter Ψ quantifies a soil's relative density and its tendency to contract or dilate under undrained shear. It is defined as:

$$\Psi = e - e_{cs}(\sigma') \tag{2.19}$$

where

- e: the current void ratio,
- e_{cs}: the void ratio at the critical state. This parameter is effective stress dependent.

There is spoken of the initial state parameter Ψ_0 when the soil is undisturbed. Jefferis and Been (2016) state that an initial state of around $\Psi_0 = -0.06$ is necessary on average to ensure that net dilation occurs at peak ϕ. According to Ayala et al. (2023) occurs the shift in dilative–contractive behaviour at $\Psi_0 = -0.064$. This boundary is highly case dependent and thus not directly applicable on different soils. The void ratios are measured with lab tests to obtain the state parameter. These lab tests are not performed for this case study, so the CPT correlations from Robertson (2022) are used to quantify the degree of contractive/dilative behaviour. The calculations performed for this thesis are described in Equations 2.20 to 2.22. For CPT-based interpretation, a clean-sand equivalent normalized cone resistance $Q_{tn,cs}$ is first defined by:

$$Q_{tn,cs} = Q_{tn}\, K_c \tag{2.20}$$

$$K_c \approx 15 \; - \; \frac{14}{\left(1 + \frac{I_c}{2.95}\right)^{11}} \quad \text{for } I_c \leq 3.0 \tag{2.21}$$

where

- $Q_{tn,cs}$: the clean-sand equivalent normalized cone resistance, valid for ($I_c < 3.0$)
- K_c: correction factor for fines content

The term K_c is introduced by K. Been et al. (2012) to account for partially drainage of the CPT measurements. P. Robertson (2010) then correlated the state parameter to $Q_{tn,cs}$ for sand-like soils ($I_c < 3.0$). This means that no state parameter is calculated for the clay layers in this thesis. Equation 2.22 provides the CPT correlation with the state parameter, suggested by Robertson (2022).

$$\Psi = 0.56 \; - \; 0.33 \log\left(Q_{tn,cs}\right) \tag{2.22}$$

The magnitude of Ψ represents a potential shear strength loss: higher positive values signal greater potential strength loss, while more negative values signal greater potential strength gain. Robertson (2022) suggests for soils with a contractive state parameter ($\Psi > -0.05$) to use the liquefied undrained shear strength for stability calculations. This liquefied undrained shear strength ratio $s_{u(liq)}/\sigma'_{vo}$ is given in Equation 2.23 for sand-like and transitional soils ($I_c < 3.0$). This ratio is not directly returning in the used SRD methods from section 3.3, but it does provide a way of quantifying strength loss.

$$\frac{s_{u(\text{liq})}}{\sigma'_{v0}} = 0.0007 \exp\left(0.084\, Q_{tn,cs}\right) + \frac{0.3}{Q_{tn,cs}} \tag{2.23}$$

Robertson his normalised Soil Behaviour Type (SBT_n) chart can be used to plot the undrained liquefied shear strength and visualise vulnerable soil types for this strength loss, displayed in Figure 2.20. If this quantification is applicable to soil resistance to the driving of monopiles, this should be investigated. However, it states that the fluidisation mechanism in contractive soils could lead to significant strength loss. In the Changhua case study analysis, the state parameter is used to quantify the level of contractivity of the pile runs that occurred.

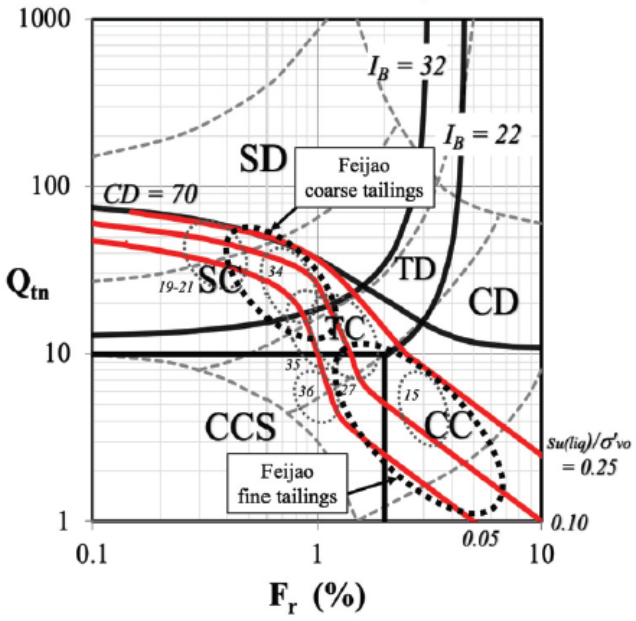

Figure 2.20: CPT-based SBT chart showing contours of large strain $s_{u(liq)}/\sigma'_{vo}$ and case history data of flow liquefaction failures (numbers represent cases presented by P. Robertson (2010)). CC, clay-like – contractive; CCS, clay-like – contractive – sensitive; CD, clay-like – dilative; SC, sand-like – contractive; SD, sand-like – dilative; TC, transitional – contractive; TD, transitional – dilative (Robertson 2022).

2.5. Pile-soil interaction transitional soils

In this section, two mechanisms are addressed. The first concerns the interaction between the soil skeleton and the pile, which is split into two zones: the pile tip, which governs end-bearing capacity, and the pile shaft governing the shaft friction. Soil–shaft interaction is analysed at the micro scale in the latter to explain the overall soil response.

Once the influence on the soil skeleton has been defined, the second mechanism analyses how transitional soils respond to pile driving in terms of changing bearing capacity. Changes in shaft friction or end-bearing resistance can trigger a dropfall. This analysis focuses particularly on how soil permeability and compaction control the response of silty layers to impact loading, which are the primary variables investigated in this section. Based on these two mechanisms, a theoretical framework is developed to characterise the fundamental behaviour of transitional soils under impact loading. chapter 4 applies this framework to the Changhua case study to test its capacity to explain unexpected dropfalls during pile installation.

2.5.1. Influence impact hammering on soil skeleton

Firstly, it is important to establish how the hammer blow is absorbed by the soil in both the axial and lateral directions. Initially, the impact of the hammer causes the pile toe to displace. As illustrated in Figure 2.21, this induces compression in the soil layer beneath the pile tip. Even the slightest displacement causes the soil skeleton to undergo plastic deformation: the soil particles are forced together, resulting in an increase in effective stress. Consequently, a compression zone, a shearing zone and a crushing zone develop beneath the pile tip (NGI 2024). Under undrained conditions, pore water is not able to escape. This leads to a rise in pore-water pressure (PWP) such that $u + \Delta u > \sigma'$. According to cavity-expansion theory, the maximum bearing capacity may then be determined (Randolph et al. 1994). The shear angle, ϕ, and the dilation angle, ψ, are directly related to the relative density, D_r, and to the effective stress, σ', at failure via Bolton (1986) stress–dilatancy theory . The spherical cavity-expansion approach has given rise to several models linking pile-tip displacement to end-bearing capacity (Thooft et al. 1997). When applied to transitional soils, this mechanism demonstrates that, if the soil is less permeable than anticipated, pore-water pressures will increase in relation to the effective stress. As water is essentially incompressible, this does not necessarily result in a reduction in end bearing forces. This behaviour can be observed in a consolidated undrained triaxial test. This test simulates axial compression under undrained conditions: total stress capacity increases while shear strength decreases.

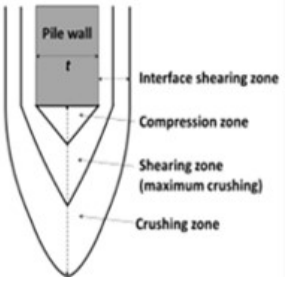

Figure 2.21: Pile toe loading zones as described by NGI (NGI 2024).

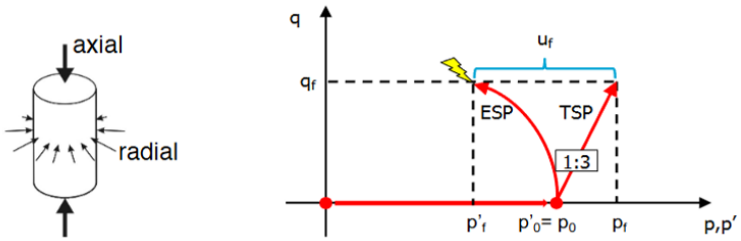

Figure 2.22: Triaxial Consolidated Undrained test highlighting fictive Total Stress Path (TSP) and Effective Stress Path (ESP) under axial loading conditions (Kementzetzidis 2024).

2.5.2. Pile shaft-soil interaction

Shear resistance along the pile shaft is mobilised from the moment even a minute displacement occurs. In terms of the soil–pile interaction, two zones must be distinguished: the interface layer and the far field. These correspond to Zones B and A in Figure 2.23. These two zones exhibit different relevant mechanical properties. The interface layer, approximately $10d$ of the particle diameter, is the stratum that experiences shear stress directly from the foundation pile. The behaviour of this layer can be explained via a direct shear test. When shear stress is applied by the pile, the particles slide over one another, resulting in the interface layer dilating. The relationship between shear stress and effective stress is described by the Mohr–Coulomb criterion in Equation 2.24. Here, c is a parameter that denotes the cohesion of the soil and takes a value of zero for sandy and silty strata.

$$\tau = c + \sigma' \tan(\phi) \tag{2.24}$$

The Mohr–Coulomb criterion operates in both directions. It ensures that the pile transmits shear forces to the adjacent particles in the interface layer. Conversely, it also demonstrates how the soil skeleton exerts bearing on the monopile. Having established that dilation occurs in the interface layer, consideration can be given to how the far-field layer responds. Zone A can be modelled mechanically as a spring that reacts to the expansion of the interface layer. At the microscale, Zone A undergoes continuous contraction and expansion, resulting in fluctuating effective stresses and variations in pore-water pressure as the inter-particle spacing is constantly changing. This leads to large strains in the soil formation.

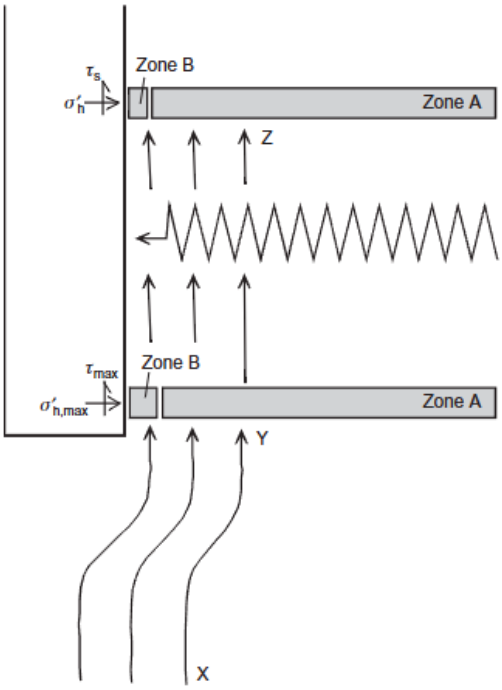

Figure 2.23: Kinematics of pile shaft-soil interaction close to the pile tip (White and Bolton 2004).

On a larger scale, the influence of dilation becomes more pronounced. The behaviour of soils in shear prior to failure can be classified into two main groups: soils that dilate at large strains and soils that contract at large strains. Saturated soils that contract at large strains have a lower shear strength in undrained conditions than in drained loading due to the consequent increase in PWP and reduction in effective stress (Robertson 2022). This mechanism essentially arises from the dilation of the interface layer in relation to the far-field zone. As a layer dilates, the pressure on the soil skeleton increases. This results in higher effective stress. In the case of a contractive layer, the far-field zone contracts. This causes the soil particles in the interface layer to lose contact. It thereby eliminates effective stress and the shear resistance mobilised on the pile. The pores in the interface layer then fill with water, forming a fluid film layer that moves along the pile surface. This phenomenon is known as fluidisation. Equation 2.1 demonstrates that the Excess Pore Water Pressure (EPWP) thus generated results in a reduction of effective stress and, applying the Mohr–Coulomb criterion, a corresponding decrease in the shear resistance on the pile.

2.5.3. Response transitional soils

In order to determine why inexplicable pile runs occur in transitional soil layers, a deeper investigation on mechanical properties of transitional soil is required. Transitional soils are typically characterised by silty textures and exhibit mechanical properties that are intermediate between those of sands and clays. Their behaviour during loading depends strongly on drainage conditions, relative density and the plasticity limit explained in subsection 2.3.3. Sands generally exhibit drained behaviour due to their high permeability. In contrast, clays predominantly exhibit undrained behaviour under short-term loading due to their low permeability. Their strength is mainly influenced by cohesive forces and the generation of EPWP. Transitional soils, such as silts, have intermediate permeability and can behave in either a drained or undrained manner depending on the loading rate. In the industry, an assumption often made for soil resistance calculations is that silty soils behave in the same way as sands under loading. However, Figure 2.9 indicates that clay has a permeability between that of clay and sand, which is why it is called a transitional soil. While it is not as bound to water as clay, the fine-grained structure of the soil makes it low permeable, as explained in subsection 2.3.4.

The combination of semi-permeable soil and EPWP because of impact loading can result in a decrease of effective pressure providing shaft friction. As mentioned above, the soil must be both contractive and permeable so that the pores in the contractive far-field layer are expelled and the interface layer fluidises. This phenomenon can be observed on a beach: when standing on saturated sand, one can see the water drain away and the sand dry. The same process occurs in the interaction zone between soil and pile. The issue with silt compared to sand is that, when pore-water pressures increase due to impact hammering, water in the silt layers cannot escape. This results in excess pore-water pressure (EPWP). Rosati et al. (2025) has demonstrated this theory through centrifuge tests.

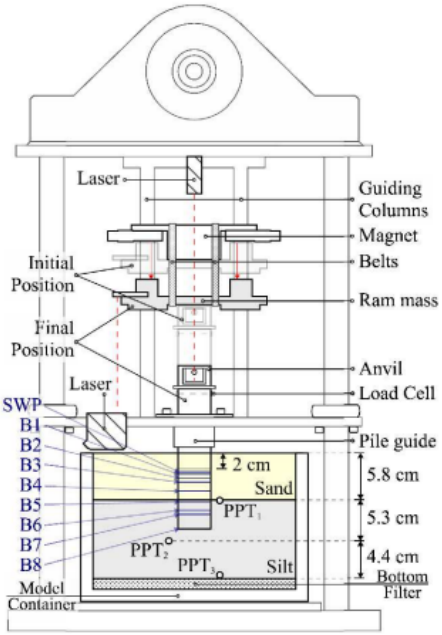

Figure 2.24: Experimental setup in centrifuge basket with pile depths resulting from blow 1 till blow 8 (Rosati et al. 2025).

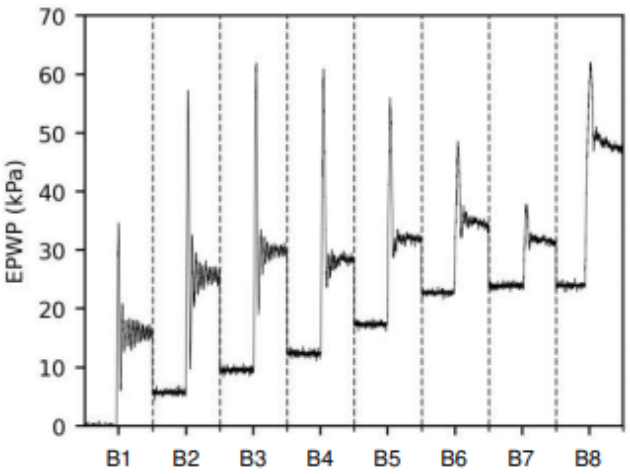

Figure 2.25: EPWP measured by PPT2 over the blow sequence (Rosati et al. 2025).

The authors hypothesized that pile runs result primarily from the accumulation of EPWP due to inadequate dissipation during repeated impact blows. Centrifuge tests simulated the installation of a monopile in stratified soil consisting of normally consolidated Viterbo silt overlain by dense Geba sand. Experimental results demonstrated a clear build-up of EPWP during consecutive blows, as measured by transducers embedded in the silt layer. This positive EPWP build-up was directly caused by the silt's low permeability and contractive behaviour, which induced a partially drained response between consecutive blows. The decrease in driving force observed in two consecutive blows performed in the silt suggests a reduction in unit shaft friction according to Rosati et al. (2025). This raises an important question: How do hammer energy (amplitude) and blow rate (frequency) influence the build-up of EPWP, and how can this influence be quantified?

2.5.4. Conclusions on pile-soil interaction transitional soils

During impact driving, the pile exerts a shear force on the soil, causing its particles to slide past one another. This results in fluctuations in inter-particle stress and pore-water pressure. If the surrounding far-field layer contracts, the particles in the interface layer lose contact and the effective stress decreases. In permeable soils, this process forces water from the far-field layer into the interface layer, creating a thin film along the pile shaft. This phenomenon is known as fluidisation. In partially drained conditions, pore-water pressure in the interface layer does not dissipate between blows. This leads to EPWP and a consequent reduction in shear resistance according to the Mohr-Coulomb criterium Equation 2.24.

This mechanism is triggered under two conditions:

1. The soil layers providing shaft friction are contractive.
2. The soil layers are partially permeable. It is essential that the EPWP is able to build up, but not quickly dissipate again.

Silt satisfies these conditions as a transitional soil type. Clay is not considered because the water within it is essentially bound and cannot therefore inhabit the far-field layer. The pertinent follow-on question is to what extent increasing frequency and amplitude affect the susceptibility of additional fine graded sand types to fluidisation. If pore-water pressure accumulates more rapidly than it dissipates, the soil will remain vulnerable to the phenomenon. If required to precisely check the drainage response, dissipation tests and variable rate CPT's can be useful (J.T. DeJong et al. 2013);(Duffy et al. 2025).

2.6. Drivability

Drivability analysis calculates whether the selected hammer and pile can achieve the targeted penetration depth without overstressing or causing structural damage to the pile, thus avoiding significant operational delays and additional financial costs. This section introduces the Smith pile-hammer-soil model, which uses a spring-based representation to simulate the dynamic interaction between the pile, hammer and soil. It also presents the mechanical way of modelling the soil and finally a schematisation of the drivability analysis.

The Smith model conceptualises the pile-hammer-soil system through discrete springs and dashpots representing pile segments, soil resistance and energy transfer from the hammer impact. The open-ended pile is modelled as a linear homogeneous elastic rod (Tsetas et al. 2021). The fundamental equation of motion (EOM) for one-dimensional wave propagation along the pile axis considering an elastic pile (Deeks and M. Randolph 1993), is given by :

$$\frac{\partial^2 u}{\partial t^2} - c^2 \frac{\partial^2 u}{\partial x^2} = 0 \tag{2.25}$$

where:

- u is the axial displacement of pile particles;
- t is the time;
- x is the position along the pile axis;
- c is the wave propagation speed within the pile, expressed as $c = \sqrt{\frac{E}{\rho}}$, with E as Young's modulus and ρ as the density of the pile material.

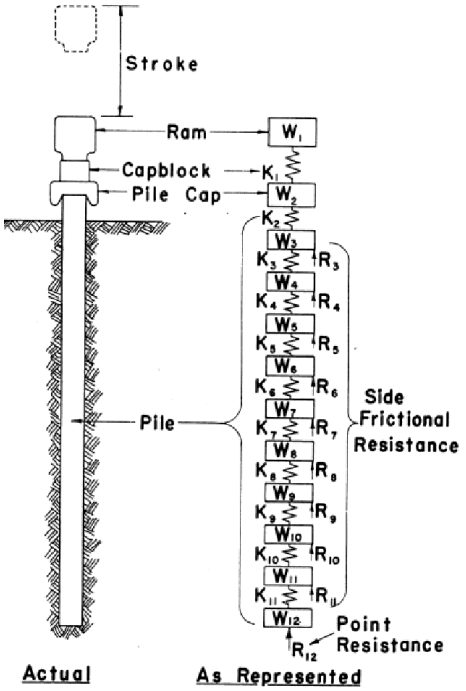

Figure 2.26: Pile-Hammer-Soil system as described by Smith (1960).

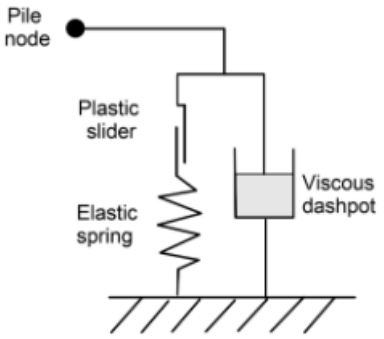

Figure 2.27: Traditional soil resistance (R) models described by Smith (1960) and Buckley et al. (2023).

The numerical solution of this partial differential equation (PDE) in Smith's approach uses the finite difference method, where the pile is discretised into segments and each segment interacts with the soil via elasto-plastic springs representing soil resistance to driving (SRD) and dashpots simulating dynamic resistance. The mechanical scheme is visualised in Figure 2.27. The Smith model solves this PDE by discretising both space and time. At each time step, the transmitted and reflected stress waves at the nodes are calculated based on local equilibrium and compatibility conditions (Patnaik et al. 1999). The soil resistance at each node is modelled as proposed by Smith (1960) Zandwijk et al. (1983):

$$R_{\text{total}} = R_{\text{static}} + J \cdot v \cdot R_{\text{static}} \tag{2.26}$$

where:

- R_{static} is the static resistance (SRD);
- J is a damping coefficient (sec/m);
- v is the pile velocity at the node (m/sec).

According to Byrne et al. (2018), pile drivability studies use wave equation analysis, typically implemented by software such as GRLWEAP or AllWave, to evaluate hammer-pile-soil interactions and solve it numerically.

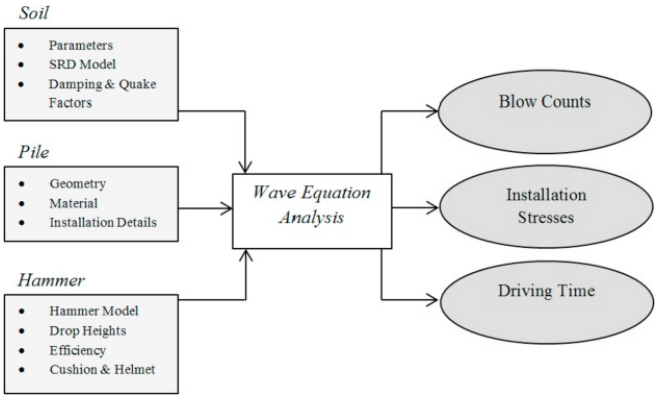

Figure 2.28: Schematisation of the input and output of a drivability analysis presented by Byrne et al. (2018).

Figure 2.28 the input and output parameters of the wave equation. These inputs are further analysed in this chapter to gain a broader understanding of the underlying principles of a drivability analysis. Wave equation analyses explicitly link input parameters (hammer, pile, soil conditions) to outputs (drivability predictions) by iteratively solving the wave propagation PDE. The adjustment of the soil resistance parameters has a direct effect on the impact predictions, allowing the hammer selection and driving strategy to be optimised. The relevant soil parameters are further elaborated on in section 2.3 and subsection 2.3.3 explains how these parameters are used for soil classification. Accurate drivability predictions are therefore dependent on static soil models, hammer efficiency and pile dimensions. Prendergast (2018) provided a more in-depth flow-chart of the drivability analysis shown in Figure 2.29.

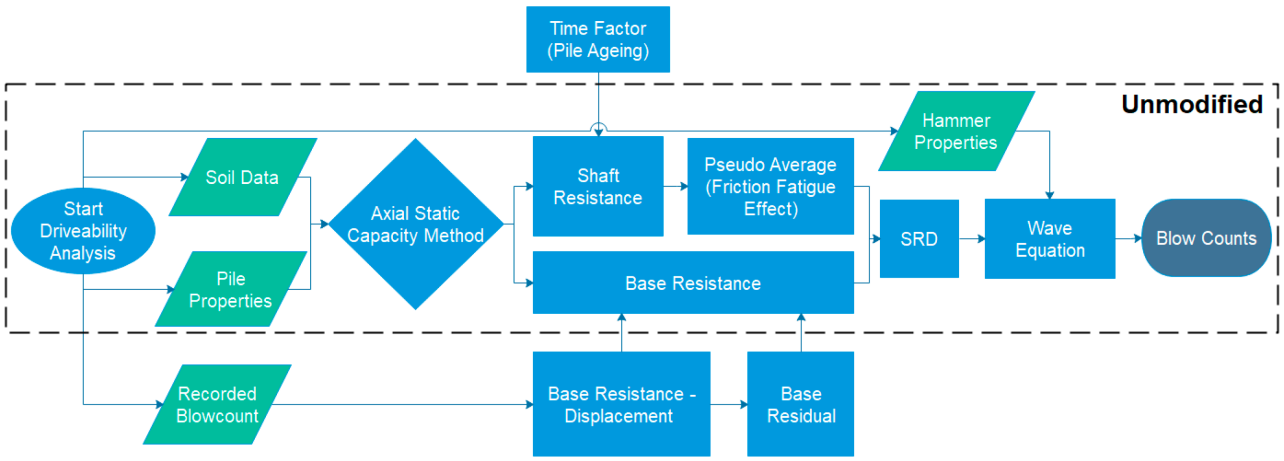

Figure 2.29: Flow-chart of driveability analysis procedure presented by Prendergast et al. (2020).

2.6.1. Impact hammers

In offshore foundation engineering, different types of hammers are used to install foundation piles. The two main types of hammer used are impact hammers and vibratory hammers. In thesis only impact hammering is considered. Traditionally, offshore foundations have been installed using impact hammers. These hammers deliver a series of blows to drive piles into the seabed. They are known for their reliability and have been widely used in the installation of monopiles, which are a common foundation type for offshore wind turbines(Meijers et al. 2017). The impact hammer system displayed in Figure 2.30 are described in the equations below:

$$F_h = \frac{v}{Z} \tag{2.27}$$

$$Z = E_p A_p C_p \tag{2.28}$$

- Fh: Impact force (N)
- v: Pile head velocity (m/s)
- Z: Impedance of the pile (Ns/m)
- E_p: Young's modulus of the pile material (Pa or N/m²)
- A_p: Cross-sectional area of the pile (m²)
- C_p: Axial wave speed of the pile (m/s)

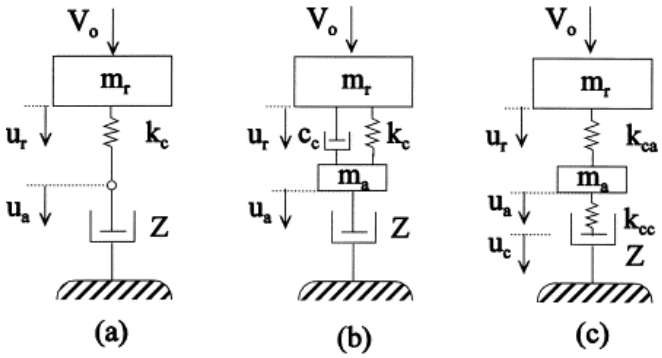

Figure 2.30: Three methods to model an impact hammer (Take et al. 1999).

2.6.2. Driveability framework

This thesis examines a static pile–hammer–soil system in which various parameters interact. In this study, the focus is exclusively on the variables that influence static equilibrium, while dynamic parameters are excluded from consideration. Although, they are provided in this theoretical framework to sketch the complete picture. The following four distinct categories of variables are defined:

- **Independent variables:** Parameters that are prescribed or controlled externally (e.g. CPT data and hammer efficiency).
- **Dependent variables:** Responses of the system that result from changes in the independent variables (e.g. shaft resistance, tip resistance).
- **Moderating variables:** Hammer and geometric factors that influence the relationship between independent and dependent variables (e.g. pile dimensions, hammer type).
- **Variables to investigate:** Specific parameters under study to validate the theoretical framework (e.g. state parameter, SRD).

The interrelations among these categories are summarised in Figure 2.31. This thesis investigates soil parameters that determine the soil behaviour. Note that the soil model is in this context a certain chosen SRD calculation method to link soil data in the form of a CPT to bearing capacities, usable for the wave equation analysis.

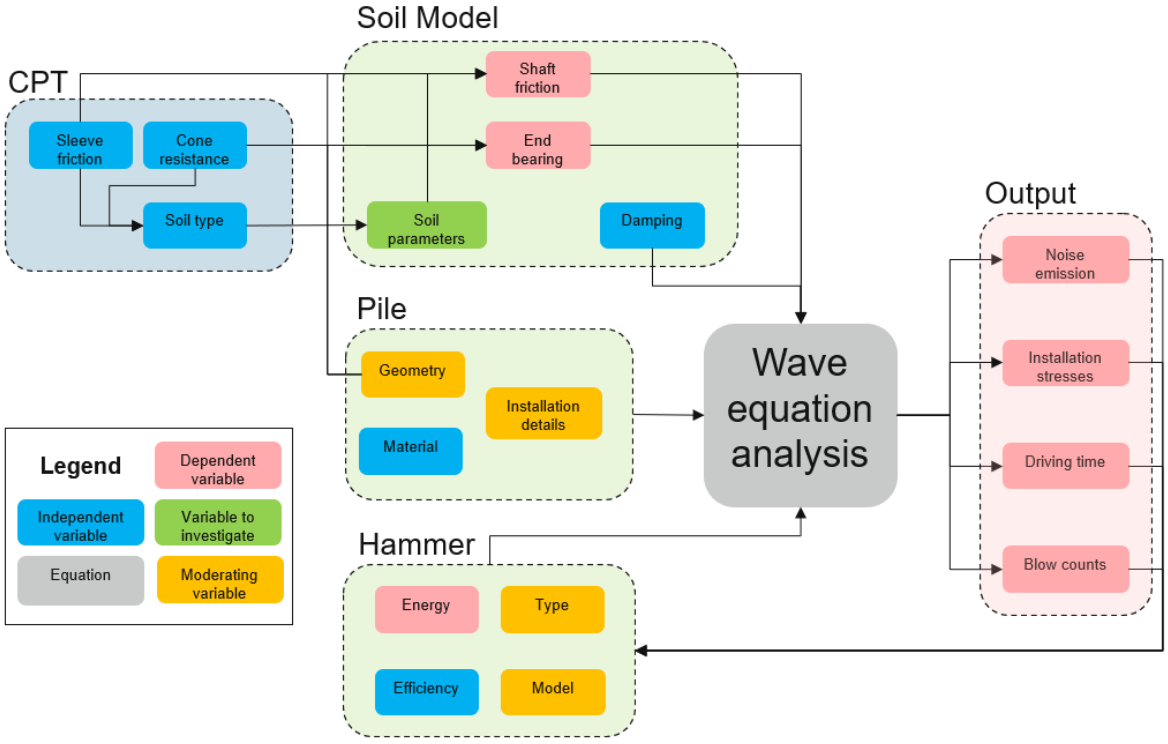

Figure 2.31: Schematisation of the relationship between the pile-hammer-soil system variables.

2.7. Pile run

A "pile run" (also termed pile free-fall (Erbrich and M. F. Randolph 2025)) refers to the sudden and uncontrolled descent of a offshore foundation pile during installation (CAPE Holland 2024). In case the total weight of the "pile driving system" (i.e. the combination of pile, upending tool and hammer) exceeds the Soil Resistance to Driving (SRD), pile run might occur. Usually, at this point in wave equation analysis software, no hammer blow count is predicted until a depth is found where the SRD increases sufficiently to support the weight of the pile driving system again (Thijssen and Roelen 2024). All the forces acting on a foundation pile during installation are displayed in Figure 2.32.

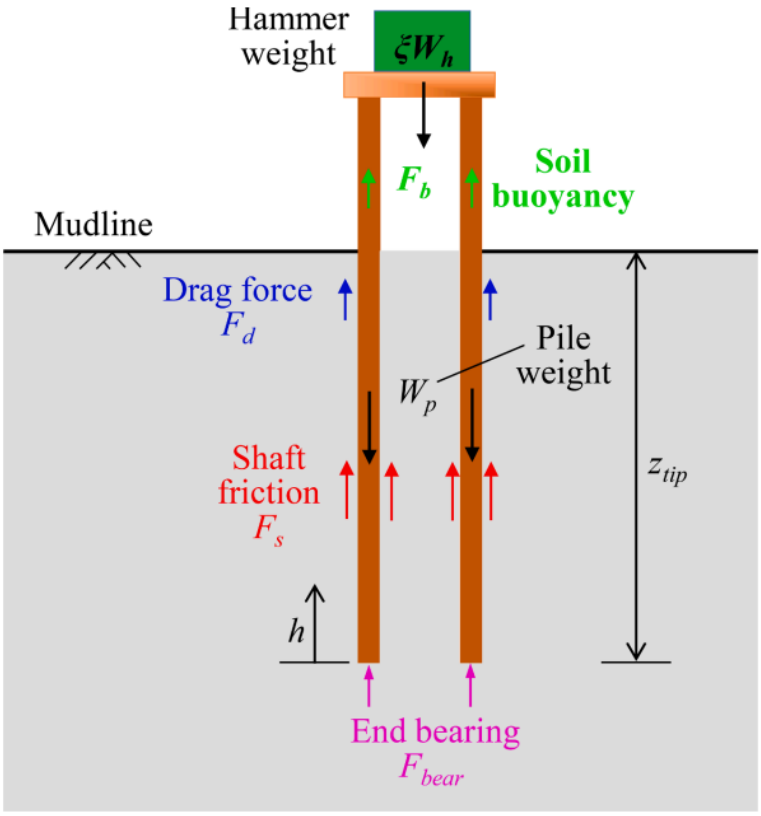

Figure 2.32: Forces acting on a pile during driving (L. Sun et al. 2022).

For the rest of the research, the pile run is divided into two types, known as 'dropfall' and 'punch through'. These definitions and the differences in their systems are explained below. Note that these definitions are used by Heerema and therefore in this thesis, but these terms are not used throughout the industry.

Punch Through refers to a scenario during monopile installation where the monopile suddenly penetrates a strong soil layer or scour protection while being partially suspended by the lifting equipment or monopile lifting tool. The main characteristic of pile run is that it occurs during the initial stabbing or placement phase of monopile installation, before active pile driving begins. Thus, pile run involves primarily a static or semi-static system, with the monopile partly hanging in the lifting gear.

Conversely, **Dropfall** occurs during active pile driving, where the monopile unexpectedly breaks through a strong layer or scour protection. This event happens during pile driving. Due to its dynamic nature, dropfall includes interactions related to the hammer-pile-soil system, as represented in Figure 2.32. Analytical static predictions for drop fall utilise methods based on Newton's second law (L. Sun et al. 2022). The problem is dynamically solved by a drivability model based on the wave equation (Meijers et al. 2017).

2.7.1. Analytical model

The most used analytical approach by researchers for assessing pile run is based on energy conservation equating the kinetic energy of the moving pile to the potential energy across a depth increment i, considering the different forces acting on the pile during penetration, presented in Figure 2.32 (Sun et al. 2016);(L. Sun et al. 2022);(Thijssen and Roelen 2024);(Duffy et al. 2025);(Kashichenula et al. 2025).

$$\frac{1}{2}(m_p + m_h)(v_{i+1}^2 - v_i^2) = (W_p + W_h - F_s - F_b - F_{drag} - F_{buoy})(z_{b,i+1} - z_{b,i}) \tag{2.29}$$

where

- m_p is the mass of the pile,
- m_h is the mass of the hammer,
- v is the velocity of the pile,
- W_p is the weight of the pile,
- W_h is the weight of the hammer,
- F_s is the shaft resistance,
- F_b is the base resistance,
- F_{drag} is the inertial drag force,
- F_{buoy} is the buoyant weight of displaced soil (and that acting on the pile and hammer if submerged),
- z_b is the elevation of the pile base.

Buoyant effects are particularly relevant for integrated structures where the foundations are integrated directly into the superstructure, like in skirted jackets or monopile towers (Duffy et al. 2025). Inertial drag force is generally considered negligible in sand (Dayal and Allen 1975) and is out of scope for this research. Viscous forces describe the frictional forces between pile and water. Chow et al. (2018) suggests to consider viscous forces when the pile penetrates through clay with a high normalised velocity. Duffy et al. (2025) suggests to neglect viscous forces for the analytical forcing model. This thesis investigates dropfall initiation in transitional soils, so vicous effects are neglected. The shaft friction F_s is the integral of the distributed load provided by the soil over the pile shaft, described by Equation 2.30. In the case of unplugged piles, also inner shaft friction is considered by adding the inner diameter to the outer diameter. The base resistance is the integral over the tip surface at pile tip depth, described by Equation 2.31 for unplugged piles.

$$F_\mathrm{s} = \pi D \int_0^L f_\mathrm{s}\, dz \tag{2.30}$$

$$F_\mathrm{b} = \frac{\pi(D_{out}^2 - D_{in}^2)}{4} q_b \tag{2.31}$$

Figure 2.33 gives an example of total resistance, pile velocity and blow counts based on a certain soil profile. The first observation is that according to API calculation method the total resistance drops in clay or silty clay layers. This soil resistance becomes even lower than the pile weight, which means that the soil fails and is not able to burry the pile any more, resulting in uncontrolled velocity increase and thus a pile run. The pile velocity and blow count graph demonstrates that every blow gives a certain velocity to the pile, lowering it into the ground. When velocity is observed without any hammer blows, there can be spoken of a dropfall.

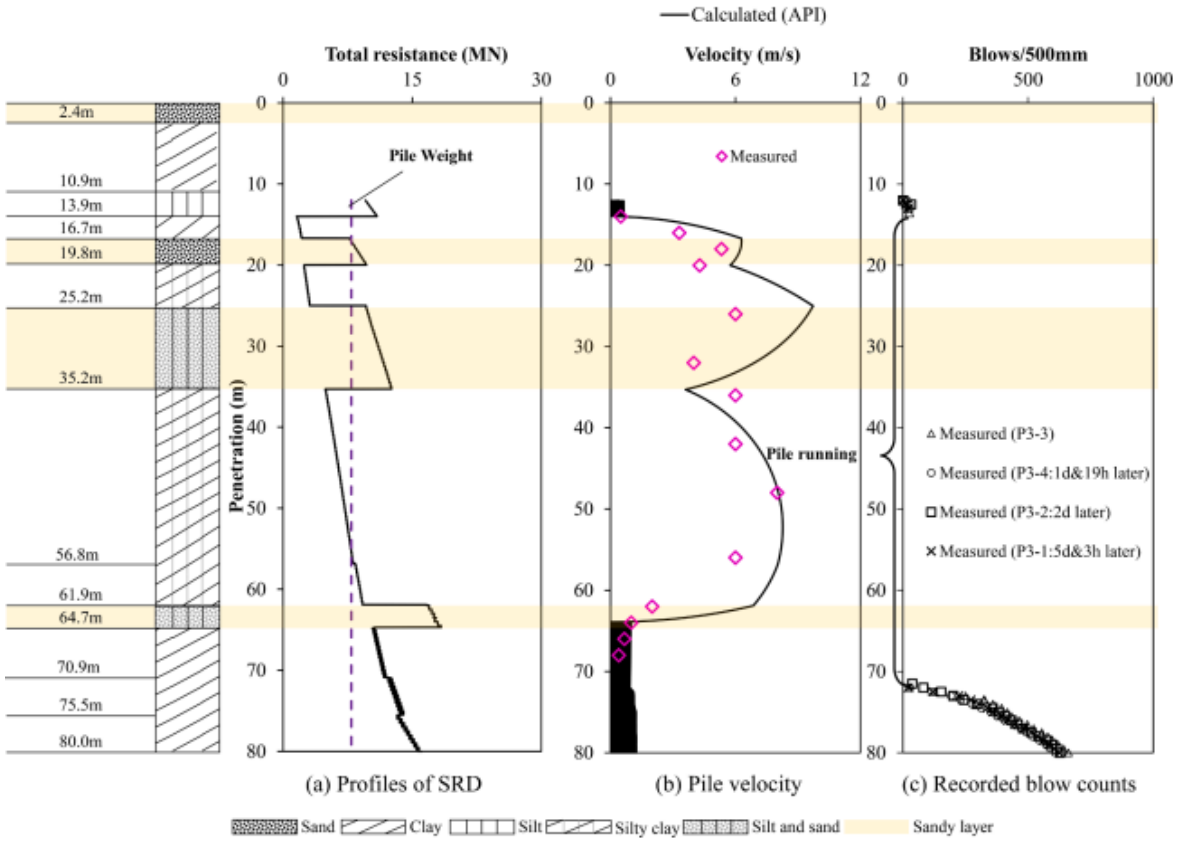

Figure 2.33: Example case pile run with profiles of total resistance, pile velocity and recorded blow counts (L. Sun et al. 2022).

2.7.2. Risks

Pile run itself is not a new phenomenon in pile driving. In fact, a controlled drop fall or punch through helps to reach the target depth, saving energy and time. The problem is that the larger foundation piles require heavier hammer, meaning that if the monopile drops and the hammer falls on the monopile, a huge impact force hits the monopile flanges and the hammer itself. Unexpected pile run during monopile driving can break the steel wires connected to the heavy hammer or cause the hammer to fall into the sea (Sun et al. 2016). Due to a sudden monopile through a strong layer or scour protection during pile driving of the monopile, there is a risk that the hammer, the hammer lift rigging and/or installation vessel crane is damaged as a result of shock loads. It can also damage the monopile (flange) or the monopile cannot be installed within the required tolerances (Tomic 2020).

Additionally, when a pile run occurs and the rigging sling is short, the pile hangs on the crane again, creating a huge momentum for the ship, destabilising it. This results in problems for the project execution as not to much pitch and roll are excepted during installation. The inherent risks associated with pile run lead to down time and thus high costs, as the ship and equipment are very expensive. Another problem is that these larger and heavier piles carry more inertia when set in motion, making it more challenging to halt their self-penetration process once initiated.

3
Methodology

This chapter outlines the two-stage methodological approaches adopted to investigate pilerun initiation in transitional soils. The theoretical framework from subsection 2.5.4 is tested on a case study to investigate whether the observed dropfalls can be explained by the proposed mechanism based on the literature review. This chapter describes the approach of this thesis to proof the two conditions that can trigger a dropfall:

1. The soil layers providing shaft friction are contractive.
2. The soil layers are partially permeable. It is essential that the EPWP is able to build up, but not quickly dissipate again.

The aim is to improve our understanding of the boundary conditions of this theoretical framework so that risks can be assessed more accurately in future projects. To this end, it is necessary to verify that both theoretical criteria are met at the point of dropfall initiation. This is done with the help of a case study. An explanation of the Changhua offshore wind project in the Taiwan Strait is provided in section 3.1 to provide the boundary conditions of the case study. Six monopile locations that exhibited unexplained dropfalls were selected for investigation. The pile run investigation comprises soil investigations and strength calculations.

The explanation for the applied soil investigation methods is provided in section 3.2. The methods used to assess soil are explained, and the implementation process is given step-by-step. The soil investigation methods involve classifying the soil stratigraphy using Robertson's SBT_n chart and computing the state parameter from CPT data. The aim is to identify transitional, contractive and semi-permeable soil layers. Borehole descriptions are then used to validate the CPT interpretations, providing a more reliable method of soil identification.

The soil investigation is followed by explanation of the implemented SRD methods in section 3.3. These methods are used to quantify soil strength in Newton. Three complementary CPT-based models are presented: the Alm & Hamre method, the Maynard method, and the Unified Method. These methods have been selected for this thesis as the state-of-the-art for assessing soil resistance to driving in transitional soils. The motivation and explanation of these methods is provided in subsection 3.3.1 to subsection 3.3.3. Other SRD methods are provided in Appendix C to provide background. The implementation and validation of the methods in a Python model is described in subsection 3.3.4

3.1. Case study description

This section provides a brief overview of the project details from the chosen case study in Changhua, Taiwan. A part is removed because of confidential reasons from this upload.

All Pin Piles have an outer diameter of 3099 mm and a wall thickness of 50 mm. Each jacket requires four pin piles, with lengths and weights defined in Table 3.1. Within each set of 4 pin piles, piles are identical and therefore interchangeable. The pile driving operations utilised an impact hammer from the company Menck, specifically identified as MHU-2100. This hammer has a in air weight of 3326 kN and rated energy of 2100 kJ, with a blow rate at maximum energy of 32 blows/minute, which comes down to 0.53 Herz.

Table 3.1: Overview of lengths and weights from investigated piles at six locations.

Pile location / WTG No.	Length [m]	Target penetration [m]	Weight [kN]
A2	74.5	73.00	2770
A3	75.5	73.75	2808
A5	69.5	68.25	2586
A6	77.5	75.75	2881
C4	66.5	64.75	2475
C6	76.5	74.75	2844

For this case study, only locations where pile runs occurred are considered. These locations comprise six of the twenty-one sites. The most pronounced pile runs were predominantly observed at the initial installation locations. The reduced incidence at later sites is attributed to more cautious pile driving following revised soil strength analyses. Additionally, the soil profile varies between sites due to the minimum spacing of 500 metres between turbines. Table 3.2 provides an overview of the dropfall events per pile at each location. The number of blows delivered prior to each event are also presented. The spacing between piles is sufficient to prevent interference with driveability. The energy per blow at the dropfall is approximately 10% of the maximum energy, i.e. around 210 kJ.

Table 3.2: Dropfall events during pile driving

Location	Pile	Dropfall depth [m]	Blows before dropfall
A2	A1	10.5 - 48.3	0
	A2	16.9 - 26.0	0
	B1	21.5 - 23.4	77
	B2	16.4 - 55.1	25
A3	A1	7.0 - 59.0	0
	A2	22.6 - 24.1	N/A
	B1	21.8 - 62.0	39
A5	A1	18.7 - 36.5	48
	B1	25.0 - 41.6	234
	B2	26.4 - 41.6	236
A6	A1	19.6 - 20.8	82
C4	A1	19.9 - 23.9	48
C6	B1	24.5 - 26.8	128

3.1.1. Driveability data

The driving-monitor `.pen` file is the primary raw record of pile installation The hammer data exports contain a series of measured quantities such as absolute depth, hammer stroke count, blows per penetration, average energy per blow and total energy per penetration. The processing objective is to convert the blow events into engineering summaries over depth intervals (here 25 cm), plot the average energy per depth interval, and present both the discrete blow counts and a continuous energy curve aligned with depth for direct comparison with CPT and SRD data.

The plot explains the following topics:

- **Blows / 25 cm** is a direct empirical measure of short-term resistance: large values indicate high soil resistance (slow penetration) whereas small values indicate low resistance (fast penetration). Sudden decreases to zero blows/25 cm may indicate a pile run event. Sudden increases often mark transition into stiffer strata.

- **Energy (kJ) per interval** reveals how much energy on average was delivered to the pile at each depth. Comparing delivered energy to resulting penetration also indicates the stiffness of the soil layers.

A simple Python script is used to parse the `.pen` file. For a number of locations, this data processing has already been carried out, with the relevant data being stored in an Excel file. The driveability values should be lower in transitional contractive layers according to the presented theory of section 2.5. Time stamps are not available for this project making it impossible to analyse the penetration rate. The resulting plot of this data processing provides a central tool to link in-situ geotechnical predictions with the actual driving performance and to identify depth intervals where pile runs or unexpected reductions in resistance occurred.

3.2. Soil investigation

This section elucidates the methodologies employed to ascertain the pertinent soil parameters from the Changhua case study. The soil assessment is performed using data from CPT tests and borehole logs. It is evident that both methods are extensively utilised within the industrial sector for the purpose of conducting driveability analysis, a process which involves the collection of continuous data regarding soil profiles. The investigation methods employed are designed to ascertain whether the soil in question fulfils the two established criteria:

- The soil layers providing shaft friction are contractive.
- The soil layers are partially permeable. Water must be able to flow into the interface layer but not quickly dissipate again.

By plotting the state parameter with depth and representing the soil layers on Robertson's chart, the influence of the degree of contractivity is examined. The borehole log and the soil behaviour type index, I_c, should indicate the presence of semi-permeable soils. It is important to note that I_c does not denote permeability, but merely classifies soil types based on CPT data (P. Robertson 2016). In this context, the category of transitional soils is regarded as partially drained and therefore satisfies the second criterion.

3.2.1. Borehole log

A borehole is a narrow-diameter vertical or horizontal shaft constructed for various purposes, including the extraction of liquids and/or gases, groundwater, or for geotechnical investigations prior to construction. Boreholes are constructed using a drill rig capable of drilling through both unconsolidated sediment and consolidated rock (Singh 2021). The borehole test provides crucial information on the soil stratification over the complete depth profile. The extraction of soil samples facilitates the assessment of distinct layers in terms of their specific soil properties, thereby enabling the acquisition of more precise information than that afforded by calculated CPT correlations. Borehole data is available at each location where piles are installed. However, only one borehole and one CPT are conducted at the centre of the jacket structure housing four piles. These piles are placed 18 metres away of each other. It can be deduced from the limited spatial coverage and the pile distances that soil variability between the piles and the borehole location is plausible. The distance from an individual pile to the location of the borehole and CPT is around 13 meters.

The boreholes were undertaken by the MV Mariner. A four-point mooring system was utilised to maintain position throughout drilling operations at all locations. The drilling operations were conducted using a motion-compensated offshore drilling rig mounted on the vessel's derrick, which was equipped with a hydraulic top-drive system. The soil drilling method employed a straight flush rotary system with an 8.5-inch outer diameter (OD) drag bit, in accordance with the standards set forth by the American Petroleum Institute (API). The implementation of 5.0-inch OD drill pipes was also in alignment with API specifications. The sampling procedure was conducted through the open-centre bit. The borehole was cleaned and stabilised by means of seawater in cohesive layers, while a mixture of Xanthan gum and seawater was utilised to prevent collapse of the borehole in cohesionless layers (Fugro 2018).

The samples obtained from the borehole excavations are tested for multiple soil properties. The analysis of soil samples is conducted and interpreted by Fugro. A number of significant parameters were determined for specific depths at multiple locations, including the plasticity limits, plasticity index and percentage fines passing 75 μ m sieves. It is therefore concluded that the soil classification output derived from these soil samples is reliable. The classification outcome is utilised to differentiate the soil layers for the SRD input. The allocation of all CPT depths to soil types, namely sand, clay or silt, is conducted manually. The results of the soil classification with the by borehole obtained soil samples are presented in section 4.1. The decision to present this in the results chapter is to ensure that the classification plots are kept close to each other, thus facilitating easier comparison.

3.2.2. Implementation CPT correlations

This subsection describes how the CPT data (ASCII .asc files) are processed and which empirical correlations are applied to obtain the normalised CPT parameters, the state parameter Ψ over depth, and the interactive SBTn plots used in the results chapter. The resulting parameters are the input for the SRD methods described in section 3.3. The workflow follows the correlations and procedures presented in subsection 2.4.1 and subsection 2.4.2 of this thesis and is implemented in Python for reproducibility. Key references for the equations and charts used are Robertson (2010, 2016) for the CPT correlations and K. Been et al. (2012) and Robertson (2022) for plotting the state parameter. Their equations are used throughout the implementation.

The primary input is the CPT ASCII export (`.asc`). The provided parameters by this file are depth [m], time [s], q_c [MPa], f_s [MPa] and u_2 [MPa]. If a pore-pressure value is absent the correction of q_c for pore-pressure influence cannot be performed directly. In such cases use the uncorrected q_c and results are annotated as having larger uncertainty. In this thesis al PWP values are presented and plotted over depth in Appendix A. The CPT-based workflow and equations used are the same as those described in the thesis.

Step-by-step processing and correlations The following stepwise procedure was executed for each CPT profile (depth-by-depth) to obtain the plotted parameters and SBTn visualisations.

1. Data quality checks and smoothing. Remove obvious spikes and interpolate missing values. Checking the values is important because one CPT file consists of multiple measurements. In this case a new CPT test is performed for every three meters. It aslso reduces sensitivity of single-point CPT irregularities.
2. Correct cone resistance for pore-pressure influence with Equation 2.7.
3. Compute friction ratio R_f with Equation 2.8 and estimate unit weight γ with Equation 2.9. Although the test results of the borehole soil samples are also providing precise γ values, their is chosen to use the CPT correlation of P. Robertson (1990). This makes that a continuous profile over depth is obtained.
4. Compute vertical stresses for each depth with Equation 2.10 and Equation 2.11. The running sum uses the estimated γ per depth interval.
5. Calculate normalised cone resistance Q_t with Equation 2.12 and friction ratio F_r with Equation 2.14.
6. Solve for the normalised cone resistance with variable stress exponent Q_{tn}, the soil behaviour index I_c and stress exponent n. Equations (2.13) to (2.16) are solved with a small root-finder (iterate n until I_c and Q_{tn} converge). In this thesis the brentq function from the SciPy package is used, as recommended by the Python CPyT package from Duffy (2023).
7. Apply fines-correction to obtain a clean-sand equivalent $Q_{tn,cs}$ with Equation 2.20 and Equation 2.21 for all soil layers with ($I_c < 3.0$). This correction accounts for partial drainage effects and fines content following K. Been et al. (2012).
8. Compute the state parameter Ψ from the CPT correlation with Equation 2.22 This correlation (Robertson, 2022) provides an estimate of Ψ where laboratory void-ratio data are not available. Positive Ψ indicates contractive (looser than critical-state) soil; negative Ψ indicates denser/dilative soil. A conservative critical threshold used in the analysis is $\Psi \approx -0.05$ (Robertson 2022).
9. Determine contractive/dilative and transitional zones. Using (Q_{tn}, F_r) and the updated $\mathrm{SBT_n}$ boundaries from P. Robertson (2016), each depth point is assigned an SBTn zone (TC, TD, SC, SD, etc.). The CD boundary and the modified index I_b are also evaluated to flag transitional contractive layers.
10. Post-processing and plotting:
    - plot the soil layers on the $\mathrm{SBT_n}$ with use of the Bokeh package to create interactive plots.
    - produce Ψ versus depth plots (with the chosen critical line $\Psi \approx -0.05$ annotated).
    - export a table with depth, q_c,f_s, q_t, γ, σ_v, σ'_v, Q_{tn}, F_r, I_c and $Q_{tn,cs}$ for SRD calculations. Add soil type column based on lab test results of the soil samples.
11. Validation of the soil parameters. Upload the CPT file as a text file in the UWA calculation tool (Lehane 2025). Download the parameter export excel file after the analysis and compare the individual parameters.

In summary, the implementation reads CPT `.asc` files, applies the standard Robertson corrections and normalisations, computes the soil stresses and the state parameter Ψ per depth, and visualises the results Ψ over depth plots and $\mathrm{SBT_n}$ charts to enable direct inspection and comparison with borehole logs and driving records. The mathematical basis and the equations used are documented in Chapters 2 and 3 of the thesis.

3.3. SRD Methods

This section reviews state-of-the-art SRD methods, explaining the reasoning behind their selection. It also describes how these methods convert CPT data into soil strengths, specifying the data for which they are most appropriate. The objective of all SRD methods is to convert CPT measurements into equivalent forces. These calculation procedures are developed through parameter fitting to specific datasets. Consequently, while all methods are grounded in physical principles, they are also empirical in origin. The used methods are the Alm and Hamre method, Maynard method and Unified method. The first two are created by back-calculating a pile database with assumed dynamic parameters. The Unified method is based on a large dataset where forcing is determined by pile load tests.

3.3.1. Alm and Hamre method

The Alm and Hamre (2001) method is a CPT-based approach that incorporates a friction degradation mechanism for the first time. The friction values were based on observed friction values from cone penetration tests (CPT), together with basic soil properties such as undrained shear strength and friction angles. The model was established based on back- from a number of offshore pile installations in typical North Sea soils, and the model generally predicted well in most cases. In particular, driving records through deep deposits of normally consolidated soils showed that the previous method over predicted the resistance to some extent. The method is directly correlated to measured cone resistances, which reduces variability. However, the method has been primarily calibrated for offshore piles in the range of 0.762 to 2.74 meters in diameter, making it less suitable for smaller-diameter piles that may experience partial plugging effects (Alm and Hamre 2001). Unplugged open-ended steel piles are assumed for the A&H method calculations.

Table 3.3: Summary of Alm and Hamre CPTu-based Model(Alm and Hamre 2001), as presented by Maynard et al. (2019).

SRD Component	Formulation	Empirical Fitting Parameters
Tip resistance q_{TIP} Clay	$q_{TIP} = C1 \cdot q_t$	$C1 = 0.6$
Tip resistance q_{TIP} Sand	$q_{TIP} = S1 \cdot q_t \cdot \left(\frac{q_t}{p_o}\right)^{S2}$	$S1 = 0.15$, $S2 = 0.2$
Side friction f_s	$f_s = f_{res} + \left(f_{si} - f_{res}\right) \cdot e^{k \cdot (d-p)}$	-
Clay initial friction f_{si}	$f_{si} = C2 \cdot f_{CPT}$	$C2 = 1$
Clay residual friction f_{res}	$f_{res} = C3 \cdot q_t \cdot \left(1 - C4 \cdot \frac{q_t}{p_o}\right)$	$C3 = 0.004$, $C4 = 0.0025$
Sand initial friction	$f_{si} = K \cdot p'_o \cdot \tan\delta$	-
Side residual friction	$f_{res} = S3 \cdot f_{si}$	$S3 = 0.2$
K (applied on both sides)	$K = 0.0125 \left(\frac{q_t}{p_o}\right)^{0.5}$	-

A summary of the equation and their empirical fitting parameters is provided in Table 3.3. As these parameters are based on case studies that use smaller pile diameters, they are not directly applicable on larger diameter foundation piles. An adjustment for the parameters is made by Maynard et al. (2019). The model is run in Python, with the in-house code of Heerema MC.

3.3.2. Maynard method

The research was applied to a drivability assessment large amount of 202 monopiles for a wide variety of geologies and pile geometries. Industry typically use research based on jacket piles, smaller test piles or in-house methods derived from past project experience. This has led to inaccurate predictions thought to be associated with the difference in size between pin piles and monopiles. The Maynard method does make adjustments on the Alm and Hamre method, based on the back analysis of these 202 monopile installations. The research recommends the empirical fitting parameters in Table 3.4. As for the A&H method unplugged piles are assumed, meaning that the inner and outer shaft friction is taken.

The improved method contains two adjustments. An update is made for high- to extremely high-plasticity clays with OCR 5–13. For these soils, coefficient C2 = 0.75 instead of 1. The other adjustment is made to the tip resistance in sand. The term with exponent S2 is removed to make the equations more simple and lower valued. Coefficient S1 is lowered from 0.15 to 0.1. This leads to reduction of the tip resistance in sand compared with the Alm & Hamre method. For the sands and clays, they concluded that a factor of 1.25 should be applied to the upper bound if soil is from the same nature as the studied database. For dissimilar soils, an increased factor should be considered (Maynard et al. 2019). The model is programmed in python and validated against the Alm and Hamre model.

Table 3.4: Summary of Alm and Hamre Model(Alm and Hamre 2001), with the proposed parameter adjustments by Maynard et al. (2019). Use C2 = 0.75 for high- to extremely high-plasticity clays with OCR 5–13

SRD Component	Formulation	Empirical Fitting Parameters
Tip resistance q_{TIP} Clay	$q_{TIP} = C1 \cdot q_t$	$C1 = 0.6$
Tip resistance q_{TIP} Sand	$q_{TIP} = S1 \cdot q_t$	$S1 = 0.1$
Side friction f_s	$f_s = f_{res} + \left(f_{si} - f_{res}\right) \cdot e^{k \cdot (d-p)}$	-
Clay initial friction f_{si}	$f_{si} = C2 \cdot f_{CPT}$	$C2 = 1^*$
Clay residual friction f_{res}	$f_{res} = C3 \cdot q_t \cdot \left(1 - C4 \cdot \frac{q_t}{p_o}\right)$	$C3 = 0.004$, $C4 = 0.0025$
Sand initial friction	$f_{si} = K \cdot p'_o \cdot \tan\delta$	-
Side residual friction	$f_{res} = S3 \cdot f_{si}$	$S3 = 0.2$
K (applied on both sides)	$K = 0.0125 \left(\frac{q_t}{p_o}\right)^{0.5}$	-

3.3.3. Unified method

The Unified Method is a CPT-based static axial capacity design method for driven piles in silica sand. This design approach is included in the 2022 edition of ISO-19901-4 replacing the four CPT methods (ICP-05, Fugro-05, NGI-05 and UWA-05) (K. Argyroulis 2022). Since SRD differs from pile axial capacity in terms of consolidation, stress equalization, and time effects(Prendergast et al. 2020). This new method captures key characteristics of driven pile. The method is shown to have higher reliability than existing approaches. the 'Unified database' and comprises 71 test piles in silica sand and 49 pile tests in clay. Full details of the 'Unified database' and the steps followed in its compilation are provided in B.M. Lehane et al. (2017). Bittar et al. (2022) advices to make a I_c based correction to $q_{t,sand}$, described in Equation 3.1. This is not applied in the implemented UM for this thesis. The reason for it is that Equation 3.1 is made to assign higher strengths to q_t of silt, which is not inline with the results.

$$q_t = \left[3.93I_c^2 - 14.78I_c + 14.78\right] q_{t,sand} \tag{3.1}$$

An update is made by Argyroulis et al. (2024), to make an SRD model in Sand of the UM axial capacity model. The UM was tested on 5 locations in the Netherlands, on which the following remark is made: 'Although this study is limited to pile diameters of 1.4 m (APM, RWG, SIF, HHTT terminals) and 0.76 m (EURIPIDES) it can be seen that the Unified Method, when slightly modified is capable of reproducing the hammer blows during installation.'(Argyroulis et al. 2024) The conclusion is that 70% of the shaft capacity is utilised during driving. So, for this thesis, the equations of Bittar et al. (2022) are used, with a shaft capacity reduction of 30%. The base resistance $q_{b0.1}$ is valid for displacements larger than 10% of the diameter. In the case of a large diameter, unplugged open pile, this displacement is 10% of D_{eq} ($= D \cdot A_{re}^{0.5}$), which is the case with pile run initiation. The calculation method is described in Table 3.5 for sands and silts and in Table 3.6 for clays.

The Unified method has an allowance for partially plugging, instead of assuming a unplugged open-ended steel pile. This is done by providing a measure of the level of soil displacement in any given soil horizon in the form of a relative area A_{re}. The equation is presented in Table 3.5. A_{re} is normally based on the Increment Filling Ratio (IFR), but in this thesis replaced by the Plug length Ratio (PLR). PLR is the average IFR during pile driving (Bittar et al. 2022). A_{re} varies between 1 for close-end piles and $\frac{4t}{D}$ for open-ended piles. For this thesis, piles with a outer diameter $D = 3.099$ meter and wall thickness $t = 0.05$ meter are used. This comes down to an relative area of $A_{re} \approx 0.1$.

Argyroulis et al. (2024) writes that the main difference in results between the Unified method and the other two used SRD methods is the incorporation of the internal shaft resistance to the external shaft formulation of open-ended piles, while the toe resistance is acting on the pile tip annular area. Contrary to these models, the UM accounts for the internal shaft resistance to the toe resistance formulation. This comes down that can be expected that the UM predicts lower shaft resistance and higher tip resistance compared to the other methods for large diameter open-ended steel piles. This makes it interesting to compare the methods in terms of total SRD results.

For clays, q_p is the average $q_{c,filter}$ value in the zone between the pile tip and $1D$ below the pile tip for closed-ended/plugged pile; or average q_t to a $20t$ deep (where t is the pile wall thickness) below the pile tip for large diameter, unplugged pile, which is the case for this case study (Lehane et al. 2020). For this thesis, the filter method of Boulanger and J.T DeJong (2018) is utilised to convert q_c into $q_{c,\text{filter}}$. $q_{c,\text{filter}}$ is used to calculate q_b This method was developed to address scale effects, rather than specifically for piles, although its application to pile foundations has been further tested by Chai et al. (2025). Furthermore, Bittar et al. (2022) recommend

Table 3.5: Unified CPT method for determination of τ_f and q_{b01} in sands and silts according to Bittar et al. (2022).

SRD formulation	Remarks
$\tau_f = 0.7\left(\frac{f_t}{f_c}\right)\left(\sigma'_{rc} + \Delta\sigma'_{rd}\right)\tan 29°$	$f_t/f_c = 1.0$ in compression, 0.75 in tension
$\sigma'_{rc} = \frac{q_t}{44} A_{re}^{0.3} \left[\max(1,\ h/D)\right]^{-0.4}$	$A_{re} = 1$ for closed-ended piles
$\Delta\sigma'_{rd} = \frac{q_t}{10}\left(\frac{q_t}{\sigma'_v}\right)^{-0.33}\left(\frac{d_{\mathrm{CPT}}}{D}\right)$	$d_{\mathrm{CPT}} = 35.7$ mm
$q_{b0.1} = \left[0.12 + 0.38\, A_{re}\right] q_p$	$Q_{\mathrm{base}} = q_{b0.1}\,(\pi D^2/4)$
$A_{re} = 1 - \mathrm{PLR}\left(\frac{D_i}{D}\right)^2$	
$\mathrm{PLR} \approx \tanh\left[0.3\,(D_i/d_{\mathrm{CPT}})^{0.5}\right]$	

Table 3.6: Unified CPT method for determination of τ_f and $q_{b0,1}$ in clays (Bittar et al. 2022).

SRD formulation	Remarks
$\tau_f = 0.07\, F_{st}\, q_t\, (h/D^*)^{-0.25}$	$F_{st} = 1$ for clays in zones 2–4 ($I_{z1} > 0$)
$q_{b0.1} = [0.2 + 0.6\, A_{re}]\, q_p$	$F_{st} = 0.5 \pm 0.2$ for zone 1 clays ($I_{z1} < 0$)
	$I_{zl} = Q_{tn} - 12\exp\left[-1.4\, F_r\right]$
	$D^* = \left(D^2 - D_i^2\right)$

this method for use in conjunction with the Unified Method.In comparison to the A&H model and the Maynard model, the UM method provides more tip resistance than shaft friction to the total SRD, which becomes more clear when plotting them in section 4.2 next to each other over depth. The model is programmed in python and validated with the UWA pile capacity calculation tool from Lehane (2025). This calculation tool implemented the UM sligthly different. The referencing of the UWA tool was followed for validation, after which adjustments are made based on Bittar et al. (2022) and the UM SRD method of Argyroulis et al. (2024). Validation for these methods is not possible as they provide driveability results instead of SRD values.

3.3.4. Implementation SRD methods

This subsection documents the practical implementation used to convert CPT-derived input data into SRD profiles, self-weight penetration (SWP) estimates and the final output tables and figures. The implementation is based on three SRD methods selected for this study (Alm & Hamre, Maynard, Unified) and follows the processing implemented in the analysis Python script.

The processing pipeline is described in two parts: (A) required input and preprocessing, (B) step-by-step transformations from the input `DataFrame` to the output `DataFrame`, SWP estimates and plots. All column names and formulae below follow the variable names used in the python sheet.

A. Required input

- Required input columns: `{ 'qt', 'fs', 'Depth', '`γ`', '`ϕ`', `σ'_v`, 'Soil_Type' }`. Use the CPT correlations if one of the input parameters is missing
- `Soil_Type` values: `{ 'SAND', 'SILT', 'CLAY' }`. Silt is only for soil layer distinguishing, but in calculations the sand equations are used for all methods.
- Units assumed in the input: q_t in MPa, f_s in MPa, Depth in metres, γ in kN/m^3, ϕ in degrees and σ'_v in KPa.

B. From input `DataFrame` to results

1. Convert cone resistance and sleeve friction to kPa by multiplying them with a factor 1000.
2. Compute layer thickness / depth increment. Create a column `Difference` = Δz as the difference between adjacent depth rows. This Δz is used to integrate distributed shaft friction over depth.
3. Method-specific parameter calculations. For each SRD method (AH, Maynard, Unified) the implementation uses method-specific empirical coefficients:
    - Calculate the method specific tip (q_{tip} or $q_{b0.1}$) and shaft resistances (f_{si} or τ_f) for each depth interval in kN/m^3.

- the Unified method uses filtered q_t (Boulanger & DeJong filter method) before applying the UM correlations.

4. friction-fatigue / depth dependent reduction factor calculations. A depth-dependent fatigue (or friction degradation) multiplier is computed, for AH and Maynard:

$$\texttt{friction\_fatigue} = e^{k(d-p)}$$

and for UM:

$$\texttt{friction\_fatigue} = \left(\max\left(1,\ \frac{\texttt{depth\_layer}}{\texttt{OD}}\right)\right)^{-0.4}$$

5. Compute distributed shaft resistance (per depth increment):

$$\tau_f = \Delta z \cdot (OC + IC) \cdot \tau_f$$

where $(OC + IC)$ are pile circumferences (outer and inner) and k_f is a method-and-soil dependent coefficient. Note that for UM only the OD is used. The cumulative shaft resistance is obtained with:

$$Q_{sf} = \sum \tau_f$$

6. Compute tip resistance (per depth point). Tip resistance is evaluated per depth using the cone-based tip correlation:

$$Q_b = q_{tip} \cdot A_{tip}$$

Note that the UM method takes A_{tip} as if the pile is fully plugged.

7. Computer total resistance (per depth point). Tip and shaft are summed to produce total method-specific SRD:

$$Q_{total} = Q_b + Q_{sf}$$

8. Determine SWP and SWPPH (Self Weight Penetration Pile plus Hammer) depths from cumulative SRD. SWP is defined as the first depth where the computed total resistance exceeds the submerged weight of the pile system. In code:

$$\texttt{SWP} = \text{first depth where } \texttt{Q\_total} > \texttt{Pile\_weight}$$

SWPPH (self-weight penetration with hammer) uses the pile + hammer weight threshold. If no depth meets the criterion.

9. Velocity and kinematic estimate (energy balance). An initial velocity v_0 is estimated from hammer energy and system mass:

$$v_0 = \sqrt{\frac{2\eta f E_{\text{rated}}}{m_p + m_h}}$$

where η and f are efficiency/cushioning factors (both taken as 0.9) and m_p, m_h are pile and hammer masses. For subsequent depth steps the script integrates accelerations from the net driving force:

$$F_{\text{net}} = W_p + W_h - F_{buoy} - Q_{sf,i} - Q_{b,i}$$

$$a_i = \frac{F_{\text{net}}\,\Delta z_i}{m_p + m_h}$$

$$v_i = \sqrt{\max\{0,\ v_{i-1}^2 + 2a_i\}}$$

The net force F_{net} equals the available weight minus the resistance components (shaft and tip) and buoyant/base contributions; the routine computes velocities for different assumptions (with and without friction fatigue) and stores them in columns such as `velocity`, `velocity_SWP_nff` etc.

10. Post-processing of the data and creation of plots. The full annotated `DataFrame` is exported to an Excel file per-method. Plots are generated showing: soil classification, q_t, SRD profiles, shaft and tip components.
11. Validation of the three SRD methods:

- AH method: Compare resulting forces with the Heerema inhouse results.

- Maynard method: Compare results with the AH results. Only differences should be present in sand tip resistance and high plasticity clays.
- UM: Compare resulting forces with UWA calculation tool (Lehane 2025).

The description above should enable reproduction of the script's behaviour and help integrate alternative SRD methods. In the case of stratified soil layers are the calculations performed as if it is a sand layer. When the soil has a silt-clay or silt-sand stratigraphy, the soil type is displayed as silt in the SRD and driveability plots.

4
Results

In this chapter, the results of the Changhua case study are presented and analysed in the context of the theoretical framework that has been developed in section 2.5. Firstly, the subject of Section 4.1 is the analysis of the soil stratigraphy with this being based on borehole logs and CPT data. The classification of soil behaviour types is facilitated by Robertson's SBT_n chart and the state parameter Ψ, and are compared against the observed dropfall depths. Next, Section 4.2 examines the SRD profiles computed via the AH, Maynard and Unified CPT methods. These profiles, alongside the cone resistance q_t, shaft and tip resistance components, are plotted as functions of depth and overlaid with the pile SWP and actual dropfall levels. Finally, Section 4.3 provides the driveability results of the case study. This allows for a comparison between predicted soil resistance and observed resistance during impact driving in transitional soils. Collectively, these results provide both retrospective validation of the proposed failure mechanism and practical insights for future drivability assessments.

4.1. Soil classification

The borehole logs at dropfall depths for all six locations are displayed below. Figure 4.1 to Figure 4.6 are not results, but obtained from soil investigation by Fugro. The figures are presented in this chapter to make them easily comparable with the other soil classification figures.

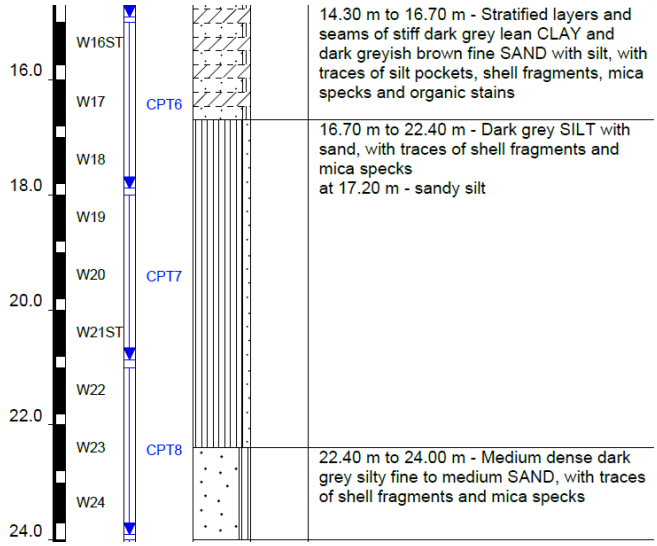

Figure 4.1: Borehole soil classification from 15 to 24 meters depth at location A2 (Fugro 2018).

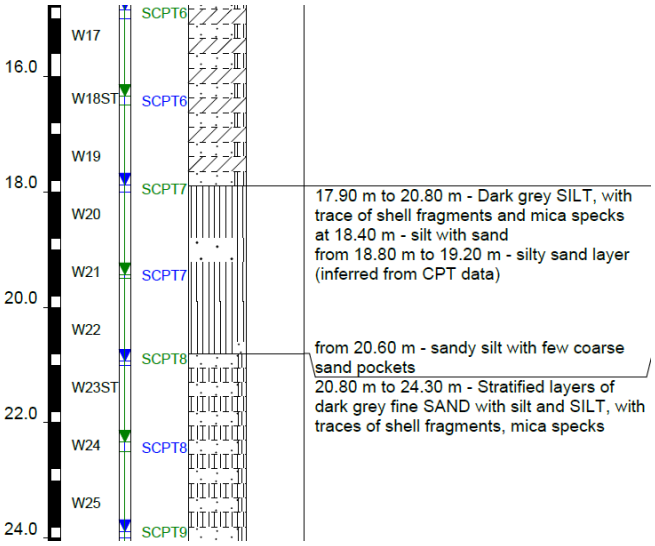

Figure 4.2: Borehole soil classification from 15 to 24 meters depth at location A3 (Fugro 2018).

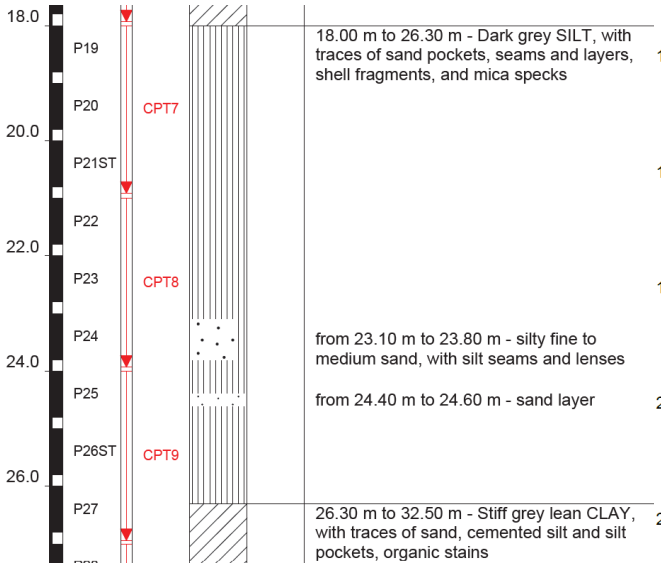

Figure 4.3: Borehole soil classification from 18 to 27 meters depth at location A5 (Fugro 2018).

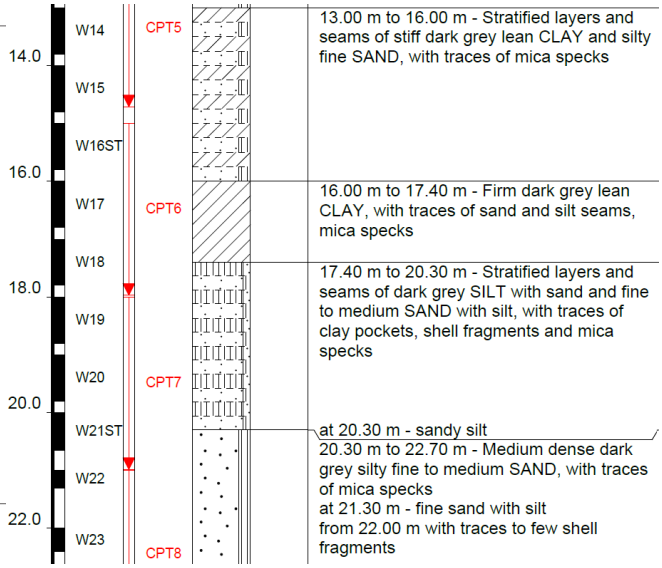

Figure 4.4: Borehole soil classification from 13 to 22 meters depth at location A6 (Fugro 2018).

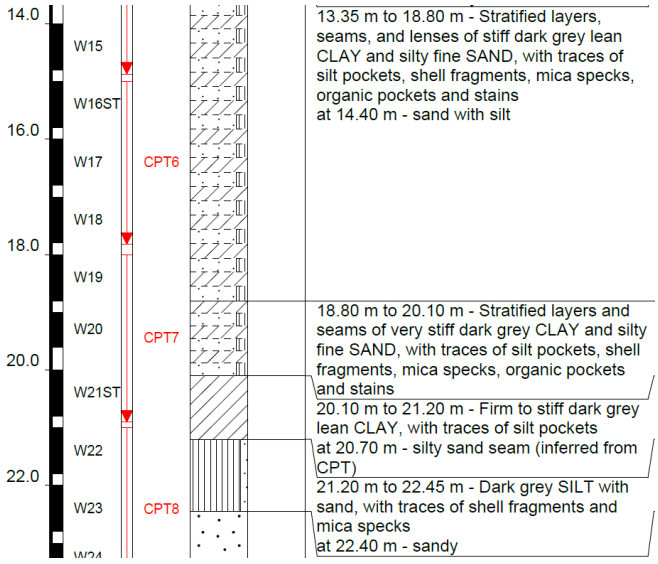

Figure 4.5: Borehole soil classification from 14 to 23 meters depth at location C4 (Fugro 2018).

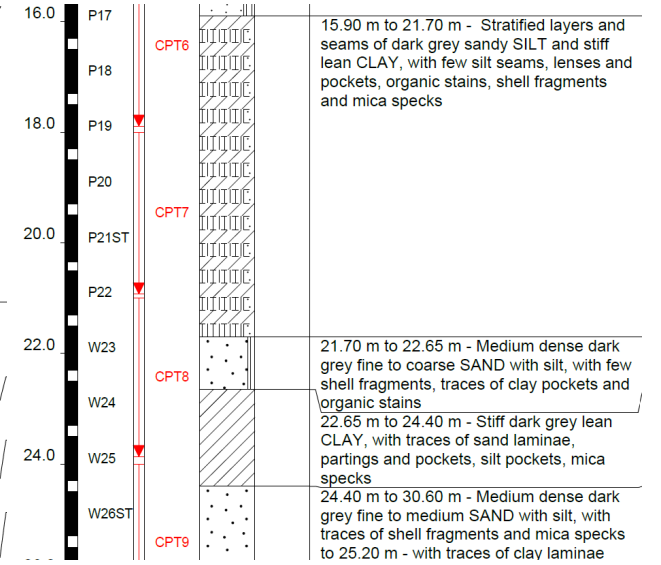

Figure 4.6: Borehole soil classification from 16 to 26 meters depth at location C6 (Fugro 2018).

Examining the borehole logs helps to determine whether transitional silt soils are present around the pile shaft at the dropfall depths. The presence of silty soils indicates partially drained behaviour. Observing the figures, silt layers are present at five of the six sites. Site C4 appears to be an exception, exhibiting stratified clay–sand layers and raising questions regarding their permeability. The fact that silt is present at almost all dropfall locations does indicate that silt is not providing enough bearing capacity, without even quantifying the resiting force. The soil classification results do also show many stratified sand-clay, sand-silt and clay-silt soil strata. It is more difficult to assign typical mechanical properties to these layers. It does indicate that mixed sand–clay strata may also be susceptible to strength loss during impact driving. The mix of sand, silt and clay does effect the permeability. This could make this layers susceptible to fluidisation of the interface layers as well. These soils are further analysed with the plotted CPT correlations on the SBT_n chart. It should be noted that the boreholes were logged at a distance of approximately 9.5 m from the individual piles, resulting in small deviations of the actual soil profile.

The soil layers from the borehole logs are plotted on the SBT_n chart from Figure 2.19 to determine whether the layers corresponding to the pile runs indeed comprise transitional contractive soils. Additionally, the state parameter is plotted against depth. The suggested critical state line at $\Psi = -0.05$ of Robertson (2022) is drawn with a red line. The results are based on empirical relationships with significant uncertainty.

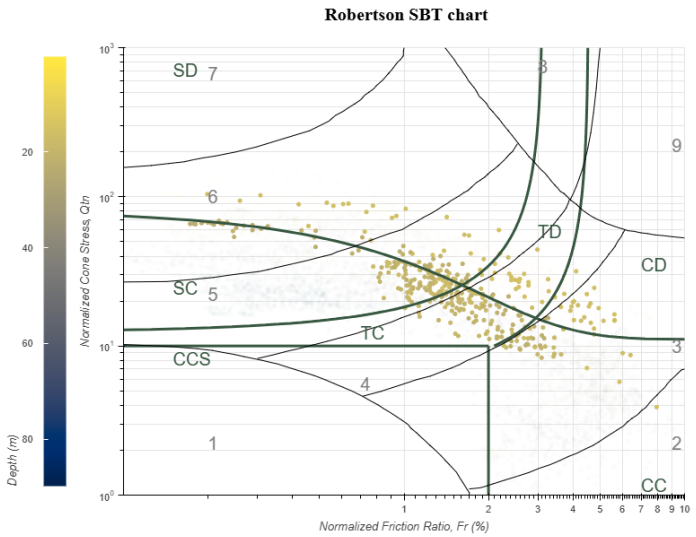

Figure 4.7: Soil layers plotted on SBT_n chart from 15 to 24 meters depth at location A2.

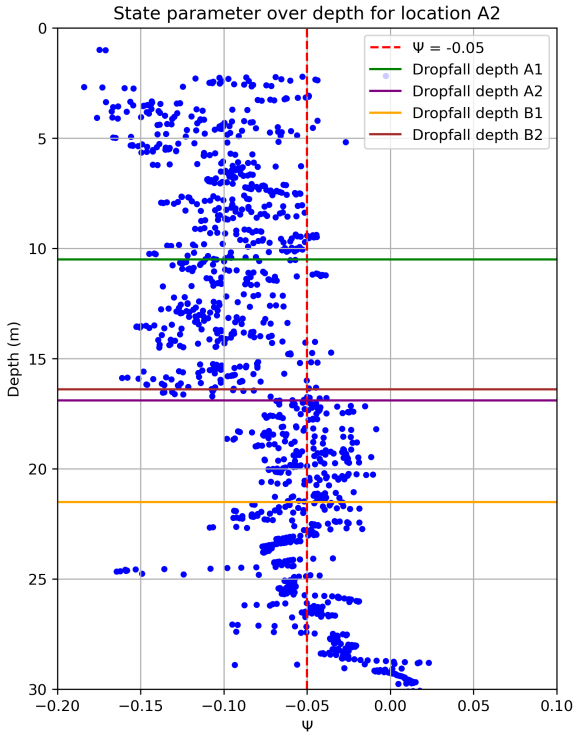

Figure 4.8: State parameter Ψ over depth for location A2.

The SBT_n chart for Location A2 shows that, based on the CPT correlations, the soils fall within the transitional/sandy contractive domain. This means that the strata fully satisfy the prerequisites for bearing-capacity loss. The state parameter shows that contractive soil conditions have not yet been attained at the dropfalls for A2 and B2, even though the pile runs occur immediately prior to a silt layer with higher state parameter values. The dropfall at a depth of 23 m accords entirely with the theoretical framework. The dropfall of A2 occurs at hammer stabbing and the dropfall of B2 after 25 blows. In contrast, the deeper dropfall of B1 required 77 blows.

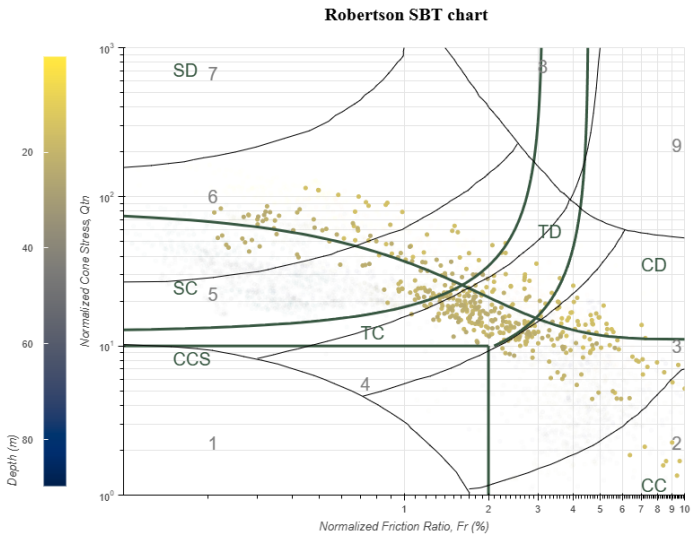

Figure 4.9: Soil layers plotted on SBT_n chart from 15 to 24 meters depth at location A3.

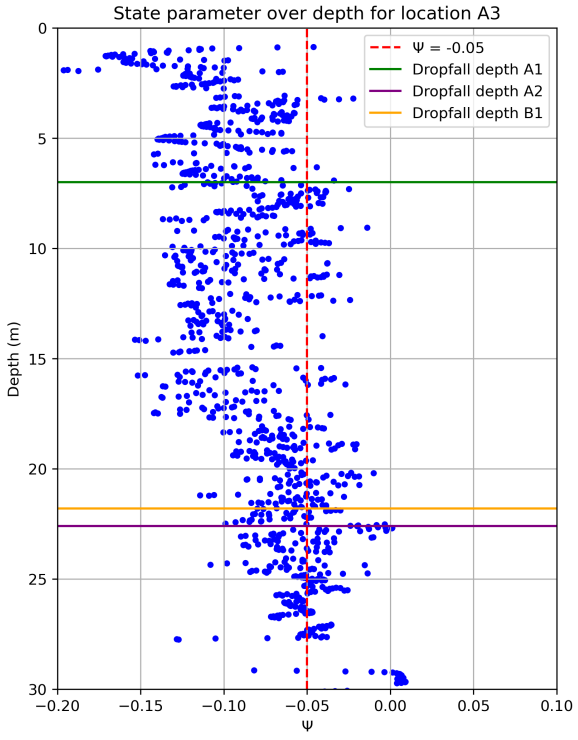

Figure 4.10: State parameter Ψ over depth for location A3.

At location A3, a clearly defined transitional contractive soil layer corresponding to the silt horizons of the borehole log is observed. When the dropfall depths and the state parameter are considered together, it is observed that the soils are around the proposed critical state line for dropfalls of A2 and B1. Only the blow count for B1 is known: 39 blows preceded the dropfall there.

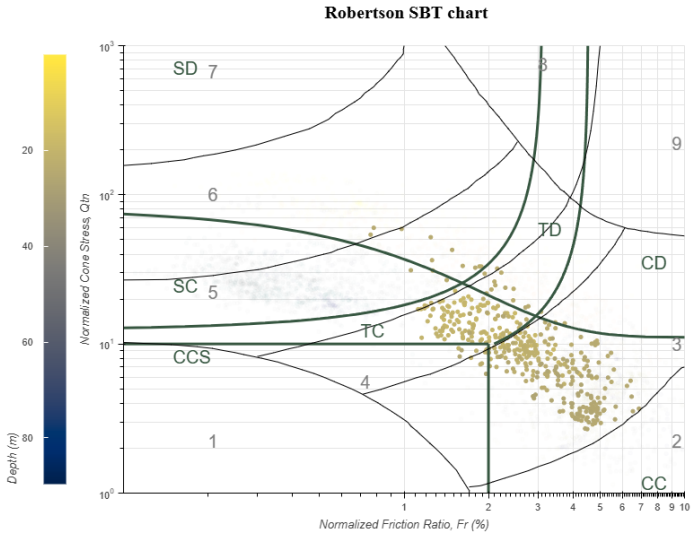

Figure 4.11: Soil layers plotted on SBT_n chart from 18 to 27 meters depth at location A5.

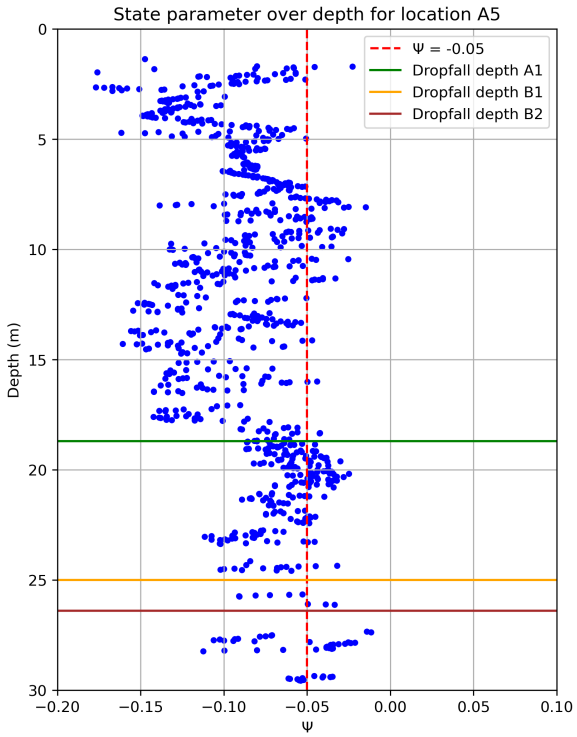

Figure 4.12: State parameter Ψ over depth for location A5.

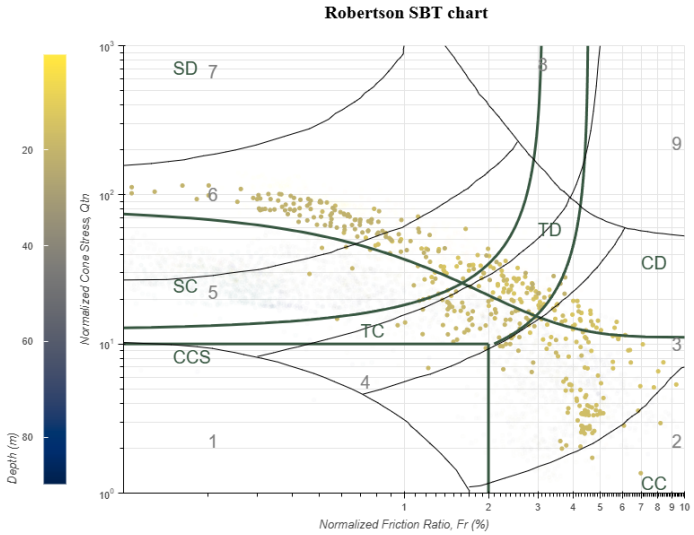

Figure 4.13: Soil layers plotted on SBT_n chart from 13 to 22 meters depth at location A6.

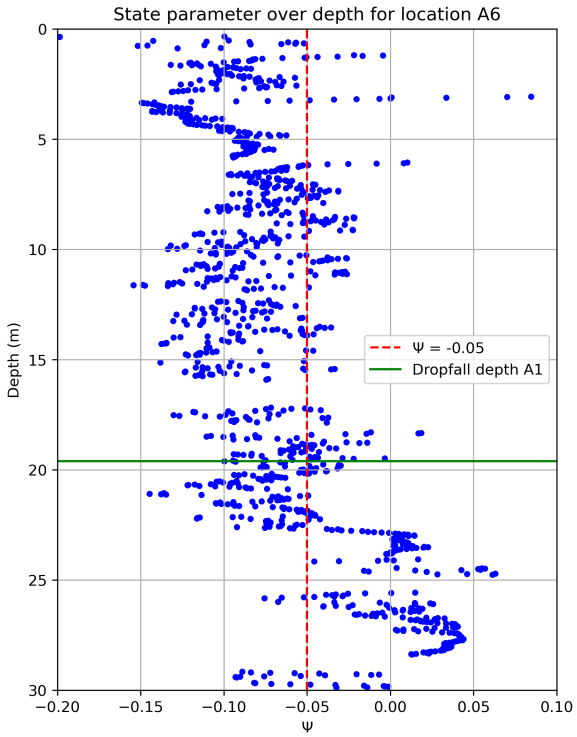

Figure 4.14: State parameter Ψ over depth for location A6.

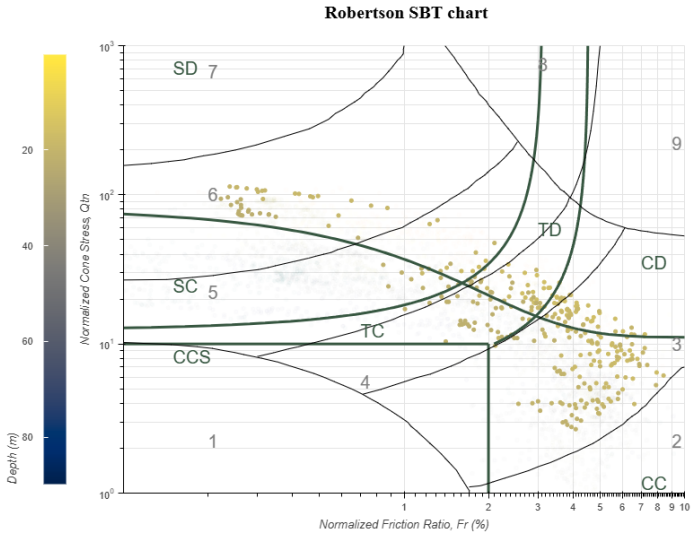

Figure 4.15: Soil layers plotted on SBT chart from 14 to 23 meters depth at location C4.

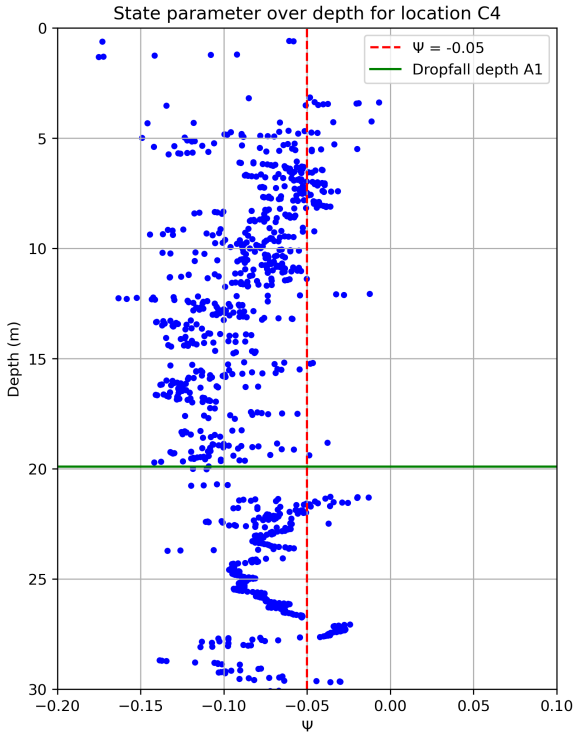

Figure 4.16: State parameter Ψ over depth for location C4.

At location A5, the SBT_n chart reveals a significant area of transitional soils, as well as weak clayey horizons. This corresponds with the borehole log, which shows a thick layer of silt surrounded by clay. At A5, it is noteworthy that the dropfalls occurred at the greatest depths and after the highest number of blows. As at location A3, the layer immediately above the pile tip exhibits a state parameter predominantly around the -0.05 threshold. In this instance, the larger amount of blows makes this location more vulnerable for EPWP because of dynamic driving effects.

Results from location A6 are less convincing. After 82 blows, a minor dropfall was observed. The soil appears predominantly dilative. Nevertheless, according to the plots, TC soil is still present around the pile tip. The question remains as to whether this is sufficient to trigger the dropfall. Likewise, Location C4 presents unconvincing results: here, the dropfall occurs within mixed sand–clay layers. This may be due to reduced tip resistance when the pile enters a clay layer at the start of the pile run. By contrast, location C6 is of particular interest, as contractive silt–clay layers are observed beyond the immediate pile tip. These layers continue to influence the overall bearing capacity and could account for the dropfall after 128 blows.

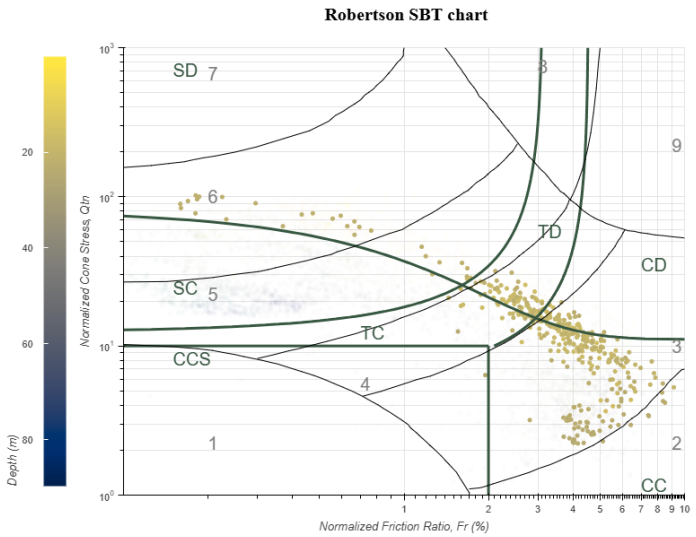

Figure 4.17: Soil layers plotted on SBT_n chart from 16 to 25 meters depth at location C6.

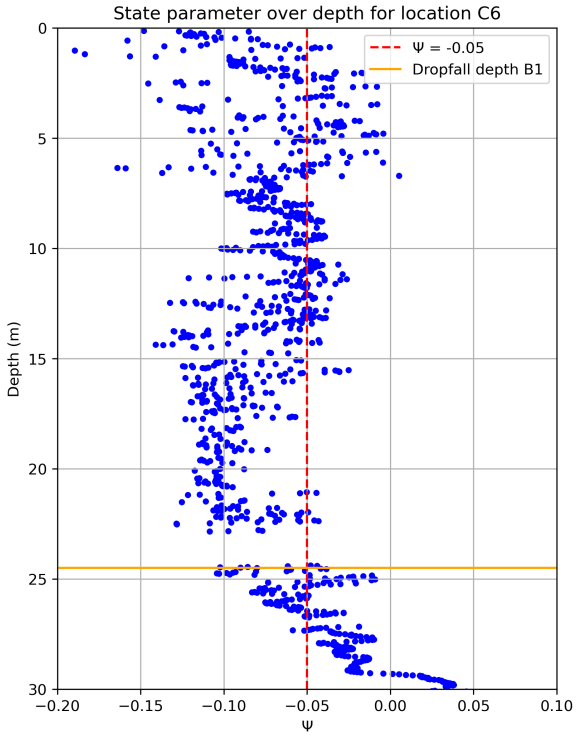

Figure 4.18: State parameter Ψ over depth for location C6.

4.1.1. Conclusions soil investigation

The theoretical criteria established in section 2.5 were evaluated in a case study near Changhua in Taiwan. This was achieved by classifying the soil layers at the depths of the dropfall to determine whether the proposed criteria were met. The first criterion is that the soil must be contractive, as assessed using Robertson's chart and the state parameter. The second criterion states that the soil must be semi-permeable so that, with each hammer blow, water is expelled from the far-field layer into the interface layer and cannot subsequently dissipate. This results in excess pore-water pressure and a reduction in shaft shear resistance. This requirement was also examined using Robertson's SBT_n chart and the borehole log resulting from lab tests. It is ultimately asserted that, in transitional (silty) soils, this mechanism can be the initiator of pile runs.

The primary observation is that the plots at five of the six sites indicate that both criteria are satisfied. Site C4 appears to be the sole exception, as the transitional strata were not present around the shaft at the time of dropfall initiation. However, the clay layer or the mixed clay–sand strata could explain the pile run in this case. Therefore, it can be concluded that the majority of dropfalls can be explained by analysing the contractive–dilative behaviour and permeability of the soils within the proposed framework. Examining the borehole logs and plotting the soil layers on the Robertson chart would provide further insight into their properties. It should be noted that CPT correlations inherently entail a degree of uncertainty. The plots of the state parameter, on the other hand, are less convincing. The majority of the points are located on the dilative side of the suggested -0.05 boundary, or around it. Interestingly, multiple locations have layers with a contractive tendency below the pile tip, which could be related to dropfall initiation. This is not in line with the proposed theoretical framework.

Although explaining dropfalls retrospectively is one thing, the true objective of this thesis is to predict future pile runs, or at least better assess the risks on pile runs. The theory articulates a novel failure mechanism and the case study provides a framework for testing the theoretical criteria in practice. This can be done by analysing borehole logs and by plotting CPT correlations on an SBT_n chart. The remaining question is how to determine the depth at which the static soil equilibrium fails. In order to answer this question, soil strengths must be assigned to layers. In the industry, this is achieved by converting the cone resistance q_c, and sleeve friction, f_s, derived from CPT tests into bearing capacity (in Newtons) using an SRD model. The next chapter will evaluate the extent to which these SRD methods can predict dropfall depths.

4.2. Changhua SRD results

This section plots the soil strengths over a depth of up to 30 metres for all six Changhua locations. Firstly, a plot of the soil stratigraphy is provided. Then the raw q_c data is displayed. Next, the SRD is plotted, followed by its components, F_{tip} and F_{shaft}. The vertical lines represent the pile weight (red) and the pile plus hammer weight (blue). The horizontal lines represent the dropfall depths, and the SWPs are shown in the same transparent colour.

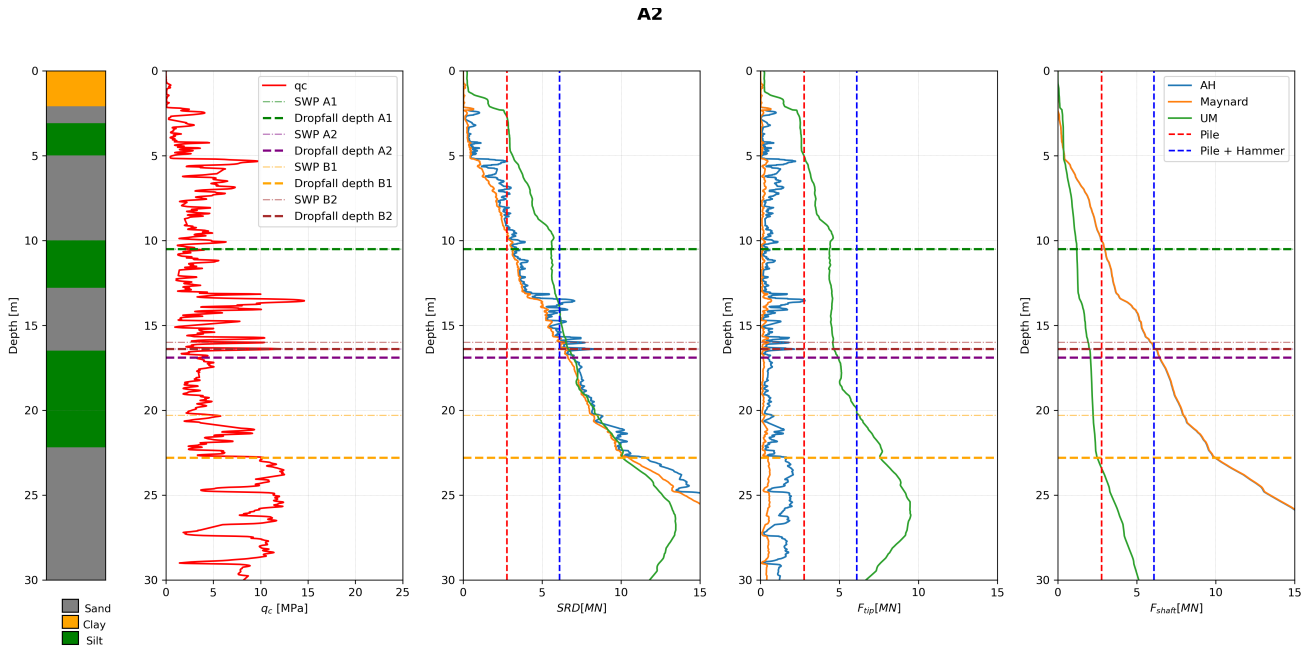

Figure 4.19: From left to right: soil classification, q_c, SRD, F_{tip} and F_{shaft} over depth for location A2, Changhua.

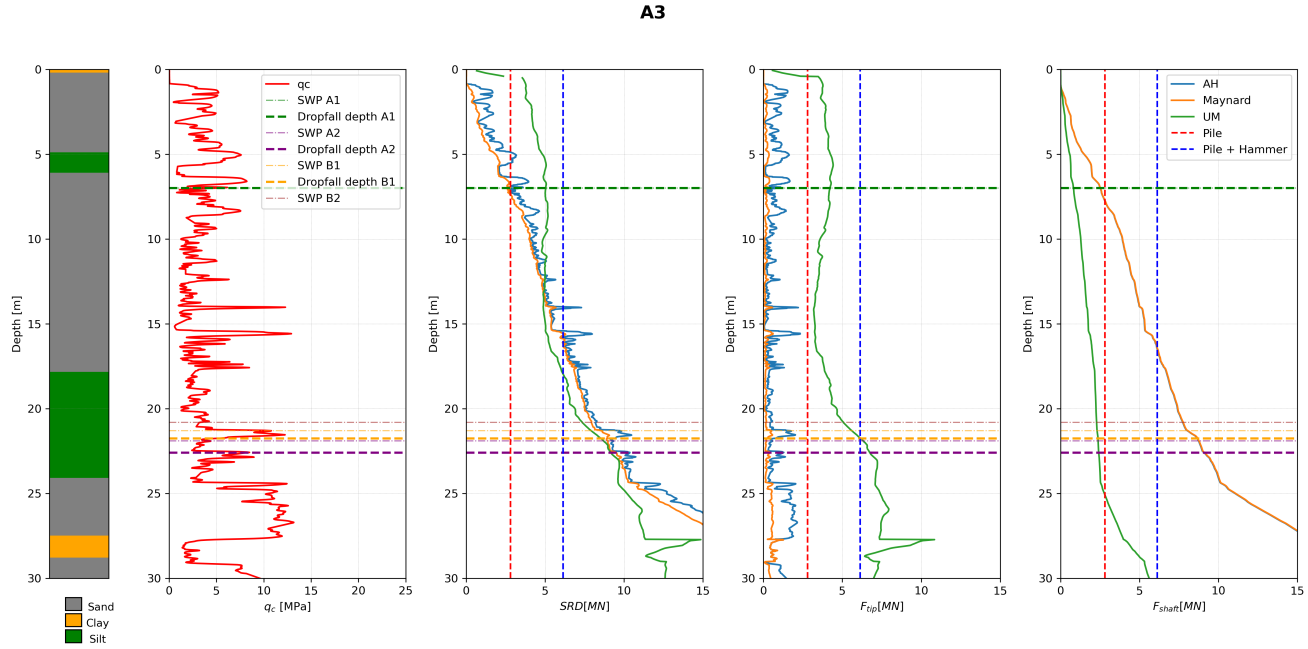

Figure 4.20: From left to right: soil classification, q_c, SRD, F_{tip} and F_{shaft} over depth for location A3, Changhua.

Considering the theory, the most interest is in dropfalls, not in punch throughs while stabbing the pile or hammer. At location A2, dropfalls of piles A2 and B2 are explainable by the drop in q_c just after the SWP is reached. That means that the piles are still in a critical zone in terms of the static equilibrium. Dropfall of pile B1 is mostly interesting, as a dropfall occurred at the moment the tip enters a strong sand layer, which should increase the tip bearing capacity. This means that a reduction of the shaft friction could explain the stability loss. The theory that

this silt layer from 16 to 22 meters loses its shaft resistance because of the impact hammering could be the answer on this loss of bearing capacity.

When observing the dropfalls from piles A2 and B1 of location A3, it is observed that both the pile runs occur in the silt layer. B1 happened just after a q_c reduction, but this is not the case for location A2. Again,this could indicate a loss of shaft friction, resulting in the dropfall. It is at least clear that all three SRD's are over predicting the soil strength around a depth of 22/23 metres.

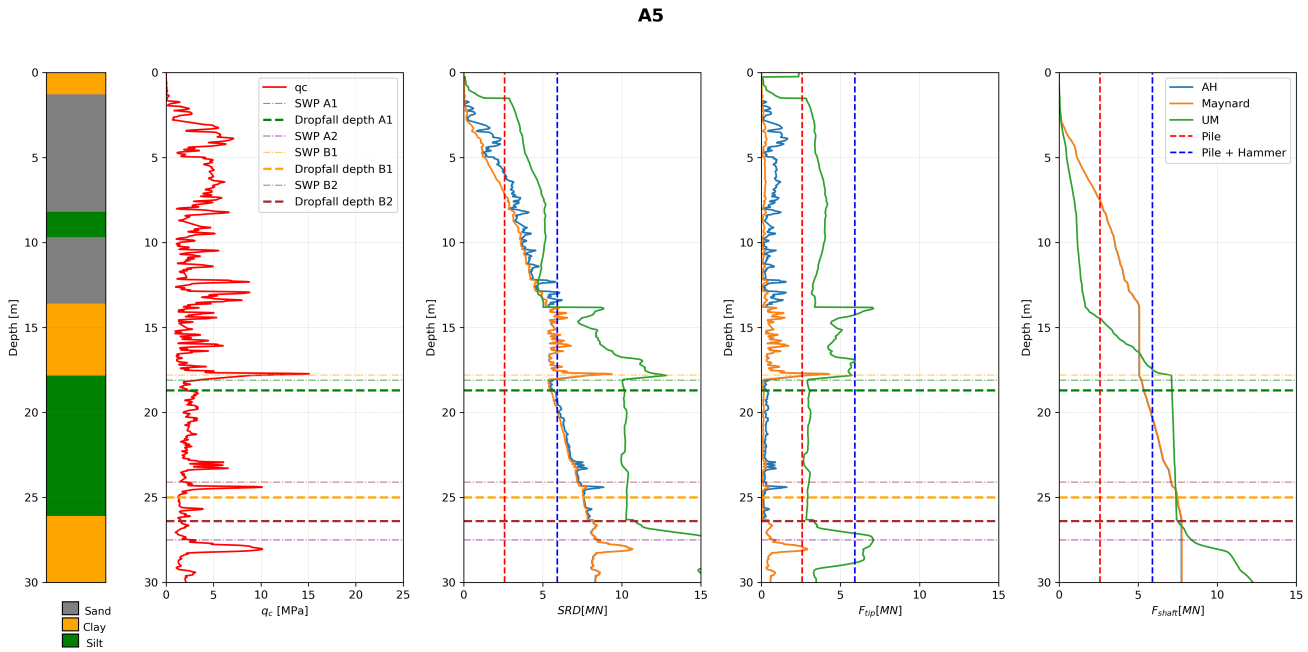

Figure 4.21: From left to right: soil classification, q_c, SRD, F_{tip} and F_{shaft} over depth for location A5, Changhua.

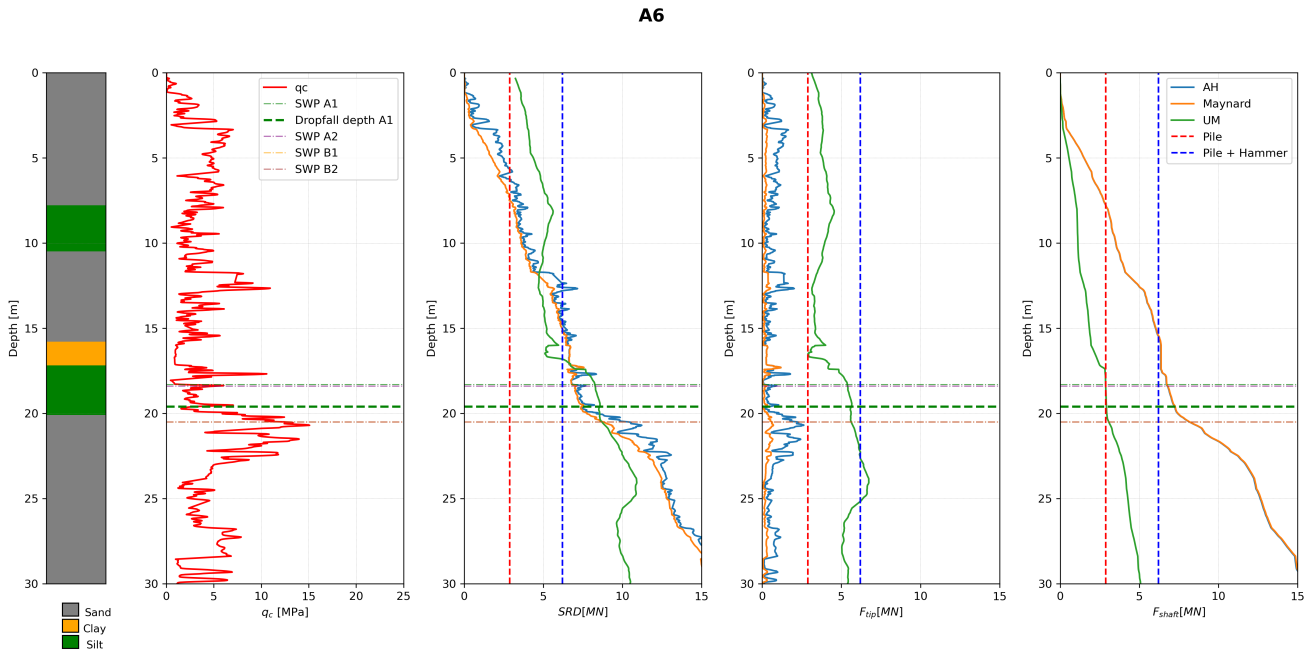

Figure 4.22: From left to right: soil classification, q_c, SRD, F_{tip} and F_{shaft} over depth for location A2, Changhua.

At location A5, three dropfalls are observed in and around the silt layer. The dropfall of pile A1 is correctly predicted by the A&H and Maynard methods. The other two dropfalls occurred at the end of the silt layer, without any indication of strength loss by the raw q_c profile or the SRD calculation methods. At location A6, a dropfall is observed at a unexpected depth. Again, the pile tip is almost in a stronger sand area resulting in

higher tip resistance. Still the pile drops which could be explained by the transitional contractive soil theory. As the SRD's are close to the pile plus hammer weight, a slight reduction of shaft friction in only the silt layer could already cause static instability.

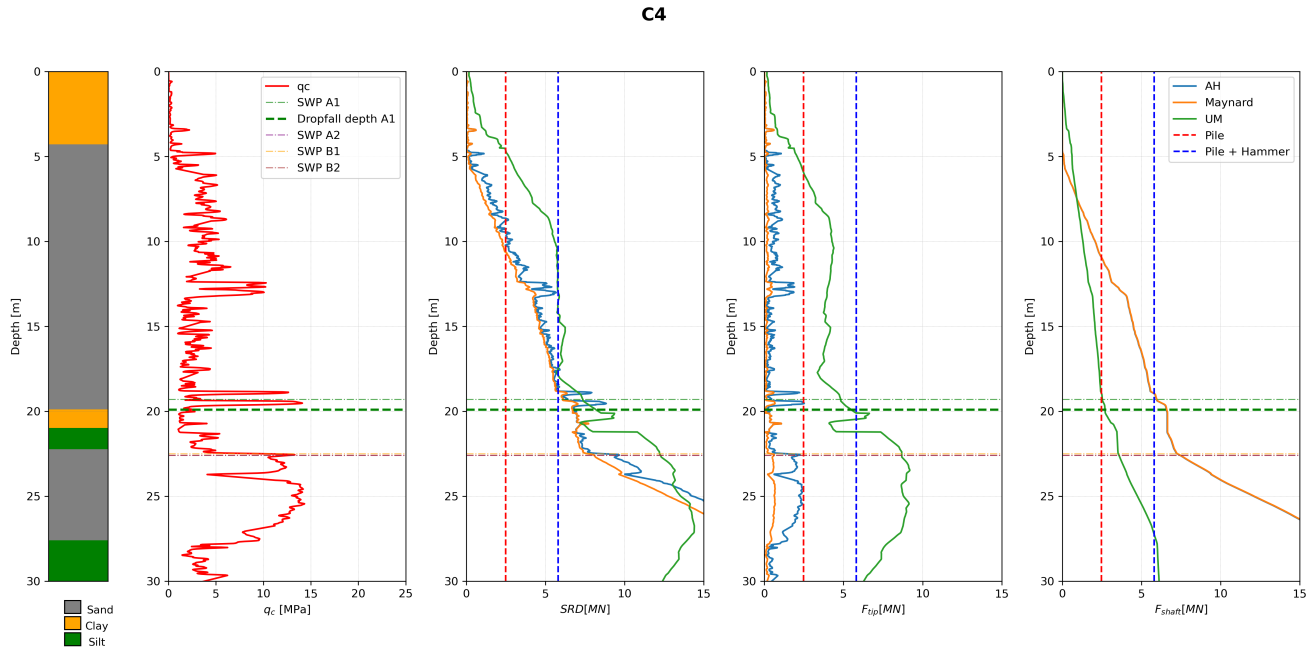

Figure 4.23: From left to right: soil classification, q_c, SRD, F_{tip} and F_{shaft} over depth for location C4, Changhua.

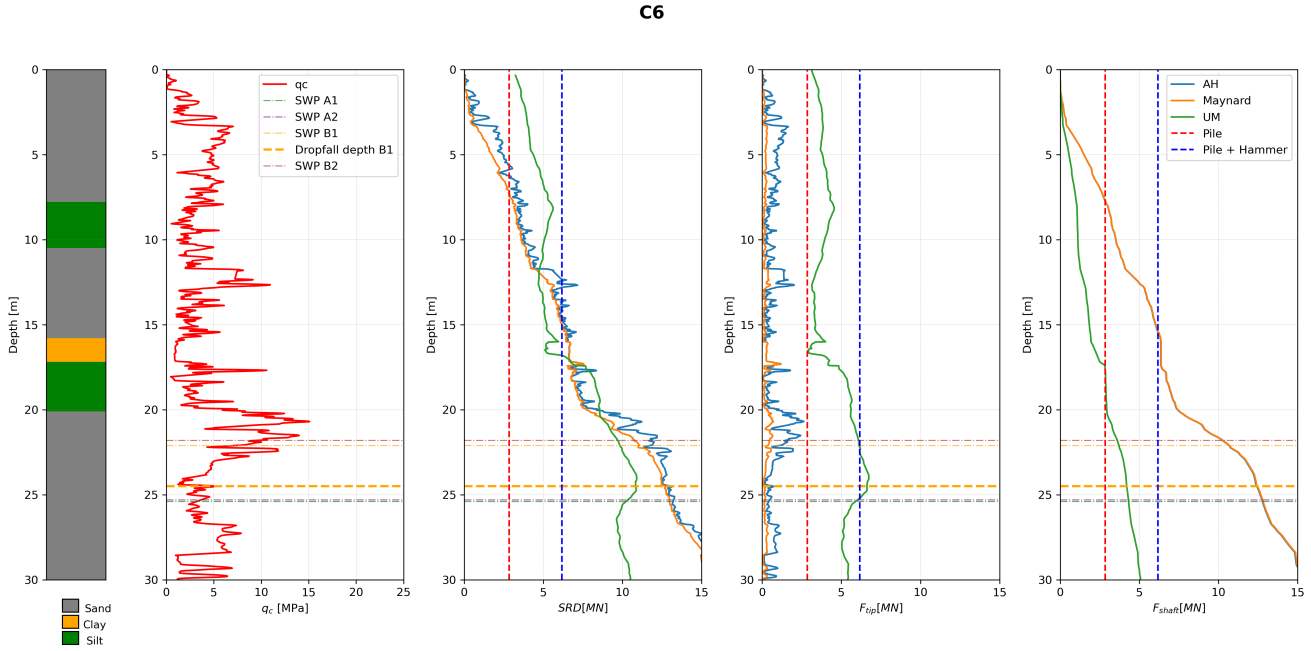

Figure 4.24: From left to right: soil classification, q_c, SRD, F_{tip} and F_{shaft} over depth for location C6, Changhua.

Location C4 does not show indications of a dropfall due to a silt layer. Here the dropfall can be easily explained by the entering of the weaker clay layer, resulting in a drop in tip resistance. This could somewhat be predicted by the SRD models as well. In the contrary, Location C6 does have a dropfall that is not predicted by the SRD models. Again tip resistance rises because of the strong sand layer. The silt layer from 14 to 22 meters could have a major influence on the shaft resistance predictions, especially for the A&H and Maynard methods.

4.3. Changhua driveability results

This section provides the driveability results and elaborates on the driving sequence to obtain insight on the dynamic resistance during driving in the silt layers. The silt layers at deeper levels should have less resistance to driving according to the proposed theory in this thesis. The blows per 25 cm and the average energy per 25 cm penetration are plotted next to the SRDs to compare expected resistance and real resistance. Note that the SRDs do not incorporated dynamic components. Blowrates for the Changhua case study are not available, so hammer frequency is not provided in the results of this thesis.

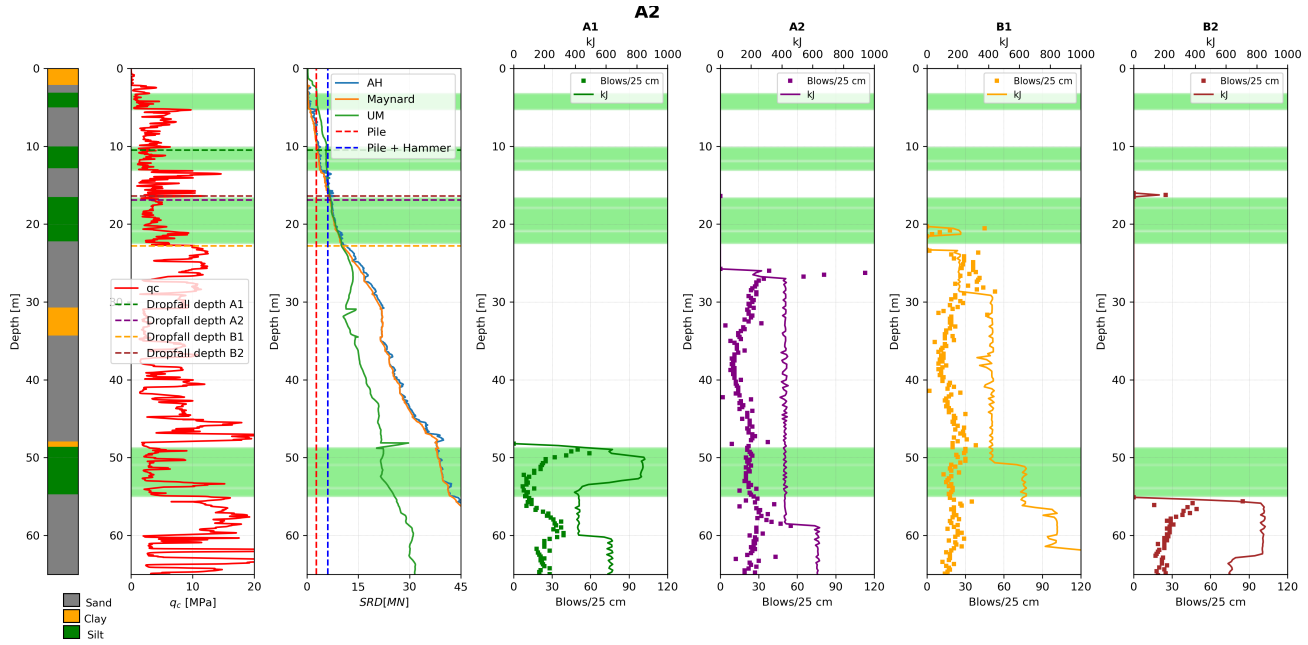

Figure 4.25: From left to right: soil classification, q_c, SRD and blow counts for all piles of location A2, Changhua. Driving order: B1, A1, B2, A2

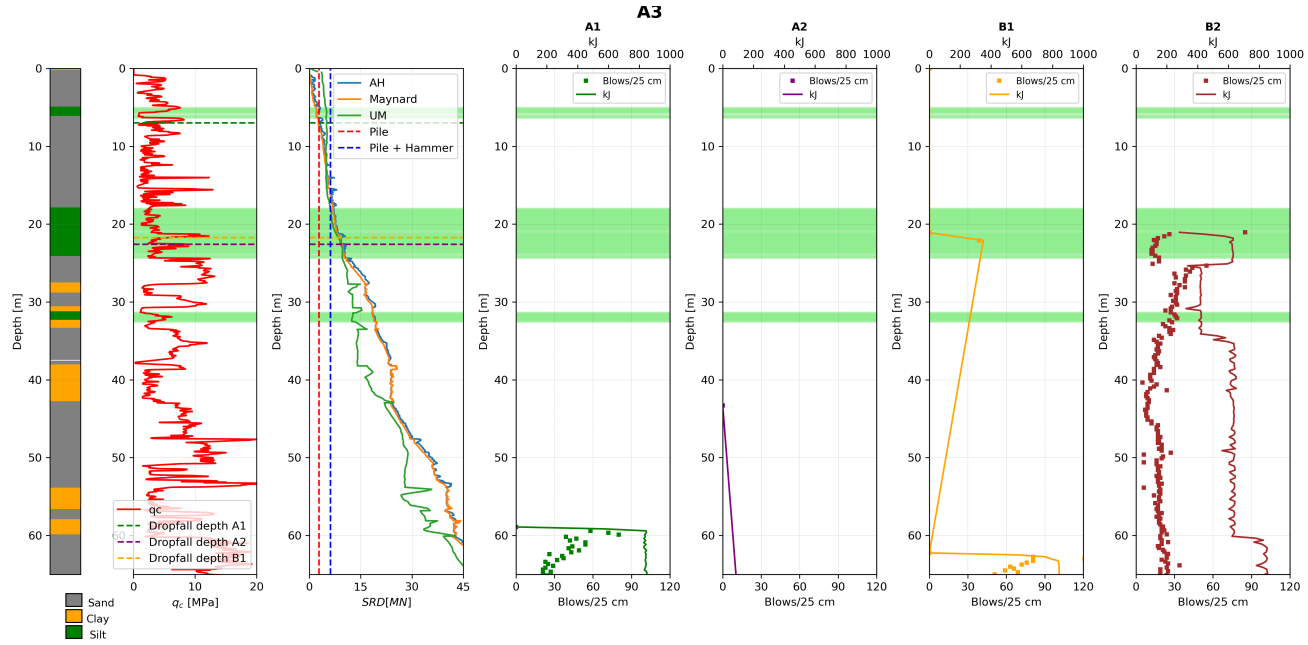

Figure 4.26: From left to right: soil classification, q_c, SRD and blow counts for all piles of location A3, Changhua. Driving order: B1, B2, A1, A2

The driveability results from 49 to 55 meters depth at location A2 are of interest as the piles encounter a major silt layer. This layer is weaker than the surrounding sand layers based on the q_c values, but still this layer should provide increasing strength because of more length over which shaft friction is mobilised. A1 shows a decreasing trend in energy and blows. Pile A2 has an increasing blows / 25 cm trend before hitting the silt layer, after which

the blow counts slightly decreases until the next strong sand layer. Increase in tip resistance because of the increase in q_c. Pile B1 on the other hand increases in energy, but decreases in the required amount of blows / 25 cm. The dropfall from pile B2 stopped arriving in the strong sand layer at 55 meters depth. Location A3 is not of added value as there is no silt layer present deeper in the soil. The hammer data of pile A2 is corrupted so ignore this results.

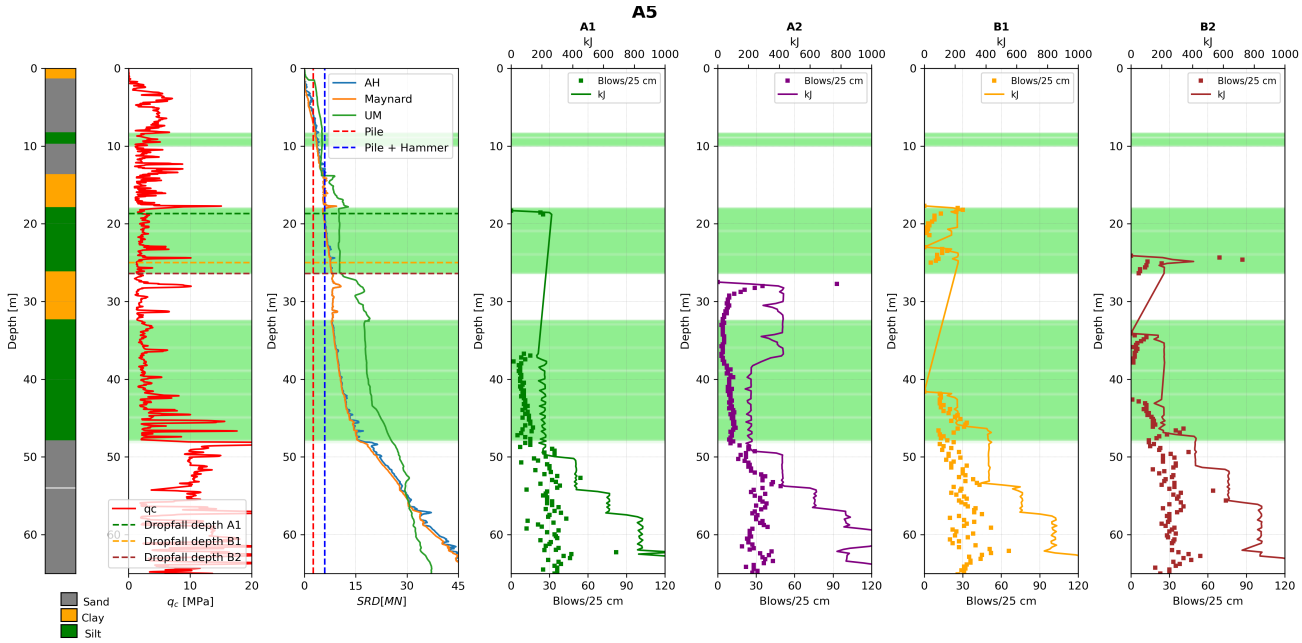

Figure 4.27: From left to right: soil classification, q_c, SRD and blow counts for all piles of location A5, Changhua. Driving order: B1, A1, B2, A2

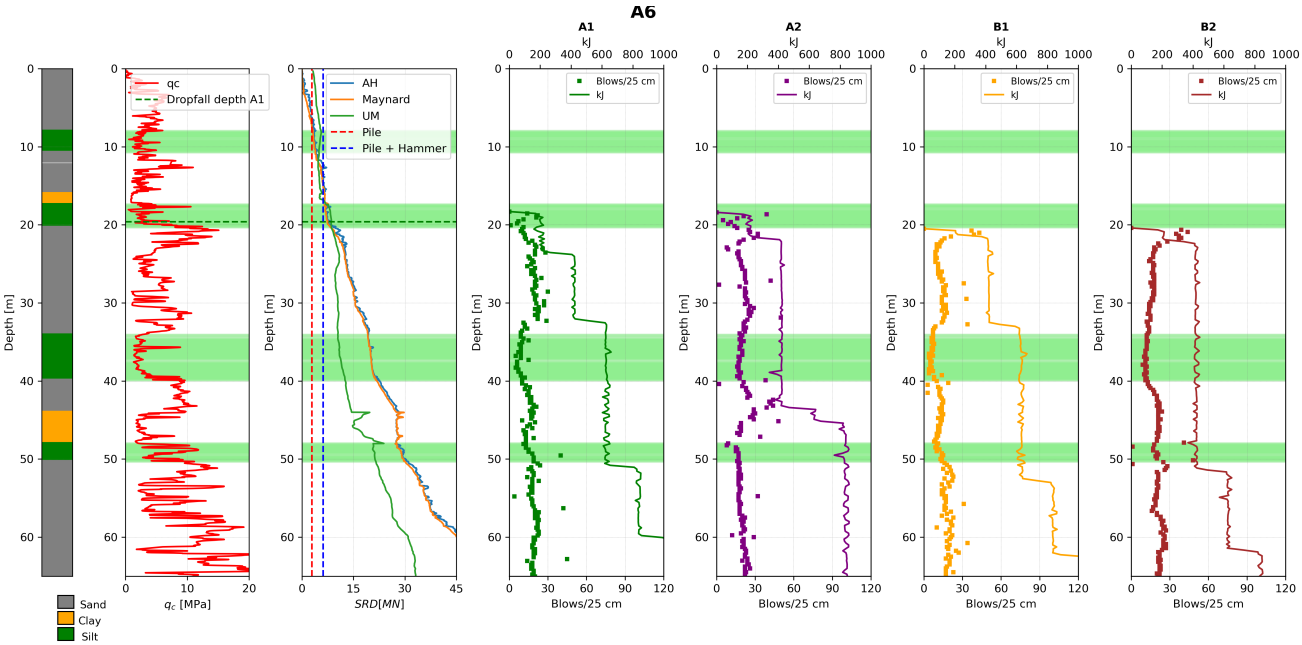

Figure 4.28: From left to right: soil classification, q_c, SRD and blow counts for all piles of location A6, Changhua. Driving order: B1, A1, B2, A2

Pile B2 from location A5 in Figure 4.27 shows a second dropfall from a depth of 38 meters to 43 meters based on the hammer data. This is presented as one dropfall in the blow count sheets made by Heerema. This indicates a strength loss in this layer. The silt layers have an overall tendency to have lo resistance to driving based on the other piles from location A5 and A6. It should be added that this low resistance is also visible in the raw CPT data. The SRD methods on the other hand predict an increase in static resistance, so an increase in driving resistance is than expected as well.

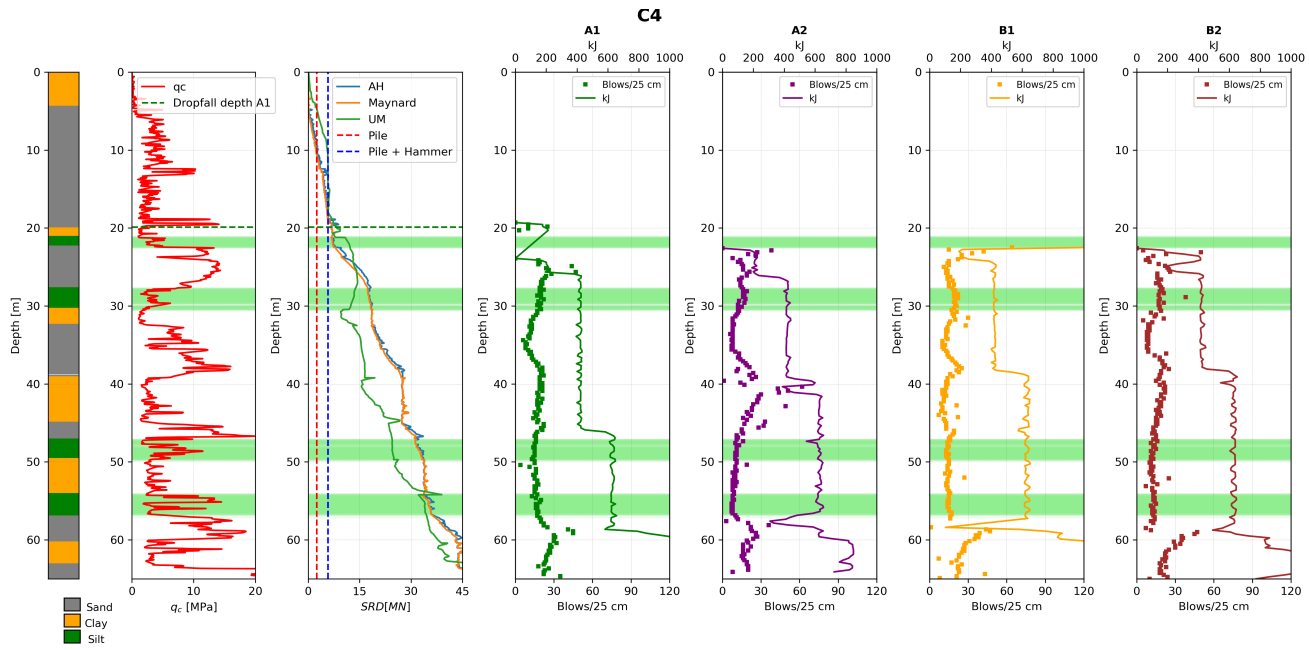

Figure 4.29: From left to right: soil classification, q_c, SRD and blow counts for all piles of location C4, Changhua. Driving order: B1, A1, B2, A2

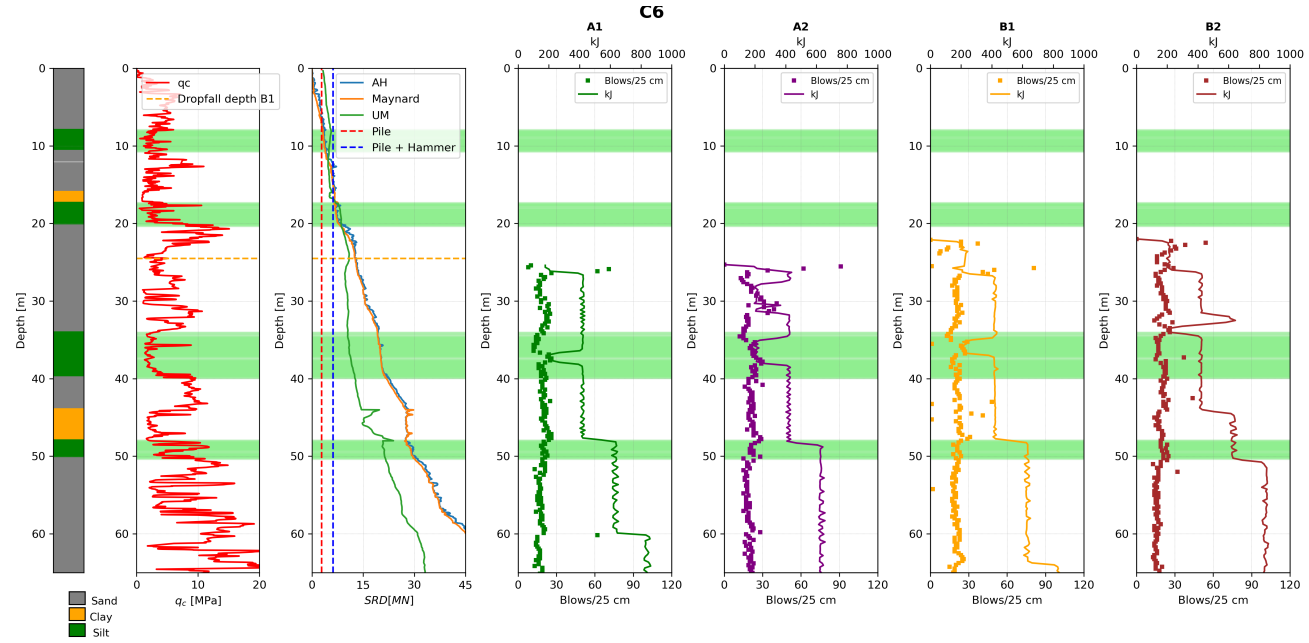

Figure 4.30: From left to right: soil classification, q_c, SRD and blow counts for all piles of location C6, Changhua. Driving order: B1, A1, B2, A2

Location C4 has a silt - clay - silt layer from 48 to 57 meters depth. The driveablitity is constant in this silt and clay layers indicating that the silt layers with higher q_c values contribute just as much to the resistance as the clay layer. The blows and energy increase significantly when the pile tip enters the sand layer. Location C6 shows that resistance is lower in the silt layers, which again can be explained following the CPT resistance. The CPT q_c values are mostly inline with the pile driving behaviour in the Changhua project. SRDs seem to overestimate the silt resistance to driving.

5 Discussion

5.1. Soil characterisation

The objective of the soil characterisation is to determine whether semi-permeable and contractive conditions are met at the dropfall levels in the case study. Locations A2, A3 and A5 have experienced the most dropfalls. Three pile runs occurred at A3 and A5, and four at A2. The other three locations had one dropfall each. Comparing these events with the SBT_n plots reveals that the majority of points at locations A2 and A3 are in the transitional contractive area. A5 also has a substantial point cloud in the TC area, but it extends further into the contractive clay area. These outcomes are supported by the results of lab tests on borehole samples. At locations A2, A3 and A5, the soil consists of a thick layer of silt. In contrast, A6, C4 and C6 contain more stratified soil layers consisting of mixtures of silt, sand and clay. This description of the boreholes at locations A6, C4 and C6 also explains why a large proportion of the points are not classified as transitional soil according to the CPT correlations. The results show that the greater the amount of transitional soil, the greater the probability of dropfall based on the case study. This is in line with the criterion that the soil must be semi-permeable.

The CD behaviour is plotted on the SBT_n chart and compared with the state parameter plots in order to investigate the contractive nature of the soil at dropfall depths. The first observation is that, for all locations, there are more points on the contractive side of the SBT_n chart than to the right of the -0.05 boundary. This is interesting, given that both methods are recommended by Robertson (2022). Again, the SBT_n charts for A2, A3 and A5 have most of their data points on the contractive side. The other three locations show a more dilative trend. This is different for the state parameter plots. In terms of fundamental terminology, the contractive behaviour of soil occurs when the current void ratio is greater than the critical state void ratio. The most accurate way to determine this state parameter is to measure the initial state parameter using laboratory tests. This was not performed for this case study. In this thesis, the normal state parameter is calculated from CPT data, which involves high uncertainty. This means that the boundary of the state parameter at $\Psi = -0.05$ is not thrust worthy, but still observations can be made in relative changes in the state parameter. It is still possible to make observations of relative changes in the state parameter. A total of 13 dropfalls were observed, of which six showed an increase in the state parameter around the pile shaft. These are location A2, pile B1; location A3, pile A2 and B1; location 5 pile B1 and B2 and less convincing location A6. The state parameter plots suggest that more contractive soil below the pile tip could initiate a dropfall. A significant shift in the point clouds to the right is observed underneath the pile tip for 10 out of 13 dropfalls. This indicates that, in this case study, contractive soils could cause a reduction in tip resistance, initiating a dropfall. This suggests that the bearing capacity is tip resistance dominated. This is also more in line with the theory of tip resistance reduction based on normalised velocity and drainage behaviour described by Finnie and M. F. Randolph (1994), J.T. DeJong et al. (2013), Carneiro et al. (2016) and Duffy et al. (2025). The concern with this theory is that a pile velocity must be present, while this is minimal at dropfall initiation. Further explanation on this theory is given in subsection 2.3.7. An attempt was made for this thesis to model this reduction, but the results where sensitive to assumptions in permeability and consolidation parameters. Duffy et al. (2025) also suggested that intermediate soils should be examined on a case-by-case basis. The relevant soil parameters where not available for this case study.

One of the difficulties encountered during the research was knowing how to describe the interbedded sand-clay soil strata. They cannot be classified as transitional soil layers per se. The mixture of the two soil types also influences the drainage properties of the soil layers. This has not been researched in depth in this thesis, but the dropfalls at locations A6, C4 and C6 do indicate that these layers also create a dropfall risk. Another interesting question is the extent to which contractive sands are susceptible to fluidisation through EPWP accumulation. Consequently, the applicability of the proposed theoretical framework to other soil types remains limited.

In conclusion, this case study demonstrates that dropfall risks can be identified based on the transitional nature of the soil layers. Based on the results, I would suggest a high dropfall risk if more than 50% of the data points are in the transitional contractive soil area of the SBT_n chart of Robertson (2022). For locations exhibiting a substantial quantity of transitional soil (i.e. > 20%), a reduced risk of dropfall persists. The assessment of this claim will be determined by the engineer's estimation in a future project. The recommendation in both cases is to support the classification with laboratory tests on the soil samples extracted from a borehole. The classification of soil type should be undertaken with greater precision, incorporating the plasticity limit and particle size as key factors in the analysis. The application of state parameter determination with CPT data offers no usable insights for this particular case study. The prevailing recommendation is to derive the state parameter from void ratios obtained through laboratory testing. This approach is more physics-based than CPT correlations. The utilisation of alternative parameters, such as relative density, should be explored in order to ascertain the CD nature of the soil. The findings of this research suggest that the state parameter is complex and necessitates further investigation into the soil samples. The main interesting observation from the state parameter is that more contractive layers seem to indicate a tip resistance loss. This provides a foundation for future research.

5.2. SRD

The results of section 4.2 are used to answer the question: To what extend can SRD models predict a dropfall. Except for the dropfall at location C4, the SRDs do overpredict the soil strength at dropfall depth, independent of the method used. The performance is measured by comparing the observed SWP of the pile and the pile plus hammer with the predicted SWP of the methods. Table 5.1 provides a brief overview of the mean errors and standard deviations for the AH, Maynard and Unified SRD method. The implementation of friction fatigue is distinguished in the results. Plots Figure B.1 to Figure B.12 visualise the error and deviation of the methods.

Table 5.1: Mean error and standard deviation of predicted SWP and SWPPH

Method	Maynard	Maynard FF	AH	AH FF	UM	UM FF
			Pile Pen			
Mean	12.0	5.1	14.1	6.5	18.2	15.5
Std.	4.73	4.56	4.21	3.43	4.50	7.02
			Pile + Hammer			
Mean	8.7	15.3	12.2	14.3	10.0	6.0
Std.	9.68	6.26	10.56	5.90	9.53	9.25

The trend indicates that models which do not incorporate friction fatigue underestimate the self-weight penetration depth. From a physical standpoint, incorporating friction fatigue in the calculation of self weight penetration is not a valid procedure. This is due to the fact that the soil is not exerted, and thus no reduction factor should be applied. The primary conclusion derived from the error calculations is that the SRD models employed are significantly deviating from the observed self weight penetrations. The discrepancy is so substantial that it calls into question the necessity of conducting a sensitivity analysis, or whether the models are simply not sufficiently accurate to justify their continued utilisation.

Moreover, a comparison of the methods can be made with regard to shaft friction and tip resistance. It is evident from the plots that the shaft friction of AH and Maynard is equivalent, given that the equations diverge exclusively in the context of high plasticity clays. When a comparison is made between the shaft frictions and the UM method, the former are shown to predict friction forces that are twice as large as those of the latter. This outcome is anticipated, given the shaft-focused nature of the AH and Maynard method. This is compensated in the tip resistance forces, resulting in almost equal (same order of magnitude) total resistance forces for all three methods. In more profound layers, the UM predicts reduced strengths due to diminished shaft friction. Incorporating friction fatigue into the analysis yields a different outcome. The AH en Maynard methods demonstrate a greater tendency for degradation due to friction fatigue.

This difference in tip or shaft resistance-based approach is of interest, as both resistances are the result of different mechanisms that create the force. Shaft friction is governed by the Mohr-Coulomb criterion and, consequently, the effective stress. The end bearing capacity of a pile is determined exclusively by the displacement of the soil beneath it. The governing mechanism is dependent on the soil type, a subject which is further elaborated upon in subsection 2.5.1. The increase in EPWP has been demonstrated to affect the effective stress and thus the shaft friction. This suggests that the AH and Maynard method are more susceptible to the previously described mechanism for shaft friction reduction. It is hypothesised that the tip resistance will increase in semi-permeable soils, since water is assumed to be incompressible in soil mechanics. Conversely, the presence of contractive soils within the pile can lead to a substantial reduction in bearing capacity.

It is recommended that further research be conducted on the failure mechanisms of silt at the pile tip during the impact pile driving process. This recommendation is based on the potential incorrectness of the assumption regarding the incompressibility water, as indicated by the results obtained. If the conclusion is to continue working with this SRD models, they should be updated for silty soil layers. Perform a sensitivity analysis on the shaft friction of the SRD methods to obtain a reduction factor for silty layers. This continues in the empirical nature of the SRD methods. Research the tip resistance in silt as the UM is tip resistance dominated and a physics based reduction of this end bearing capacity is preferable. The theoretical mechanism of this thesis suggests a reduction of the effective stress because of EPWP. This can be implemented in the AH and Maynard method by reducing σ'_v with 90% and in case of the UM reduce the radial effective stress σ'_{rc} with the same 90%. This calculation is performed for location A2 and A5 and the results are displayed in Figure 5.1 and Figure 5.2. The results of AH and Maynard are almost the same, so only Maynard is plotted.

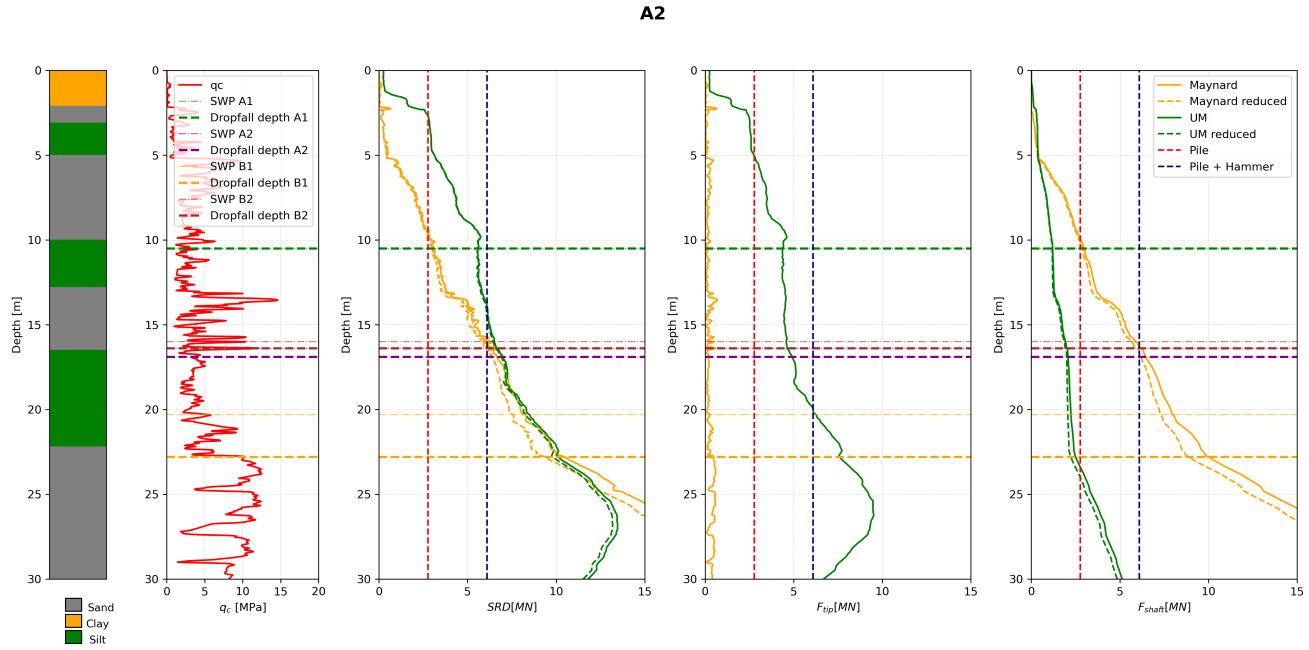

Figure 5.1: From left to right: soil classification, q_c, SRD, F_{tip} and F_{shaft} over depth for location A2 with 90% reduced effective stress.

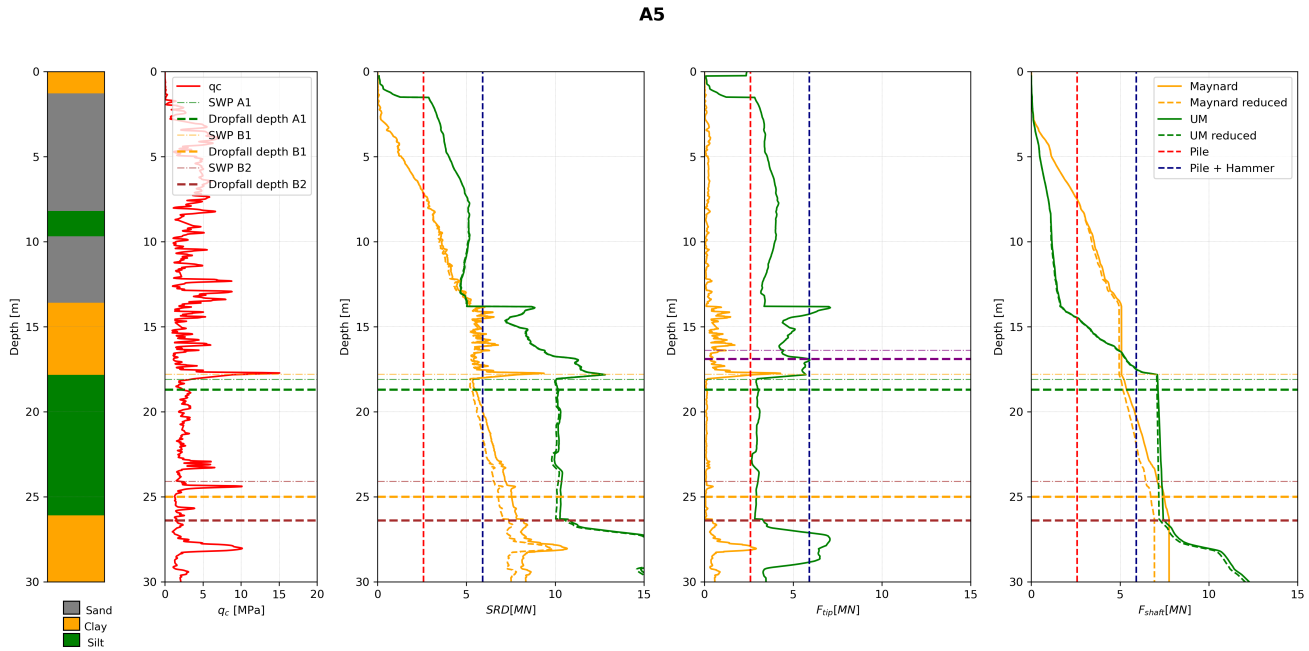

Figure 5.2: From left to right: soil classification, q_c, SRD, F_{tip} and F_{shaft} over depth for location A5 with 90% reduced effective stress.

The discrepancy between the original SRD values and the reduced effective stress values is marginal for both SRD methods. It is evident that implementing the proposed theory into existing calculation methods fails to provide a satisfactory explanation for the observed dropfalls, even when employing an extreme reduction factor of 90% for the effective stress in silt. This provides the insight that the SRD calculation methods do not support the proposed reduction of shaft friction because of EPWP. The state parameter plots exhibited a tendency of more contractive soil beneath the pile tip at dropfall depths. This finding may indicate that the SRD is predominantly governed by base resistance, as the effective stress reduction is inadequate to sufficiently mitigate shaft friction loss. It is evident that the UM is the most accurate method, as it employs base resistance as the governing mechanism. A reduction of this base reduction in contractive soils with the UM could lead to the desired results.

Consequently, SRDs are unable to accurately predict dropfalls in transitional soils based on the mean error and standard deviation of the outcomes of this case study. It is evident that the resistance predictions and the pile + hammer weight do indeed indicate a certain risk area. The findings of the study indicate that the identification of areas where the SRDs are proximate to the static equilibrium is advisable. This area is designated as a critical driving zone. In this case the UM seems to describe the governing mechanism the most accurate, so the advise is to reduce the base resistance of this SRD method for contractive soils. Subsequent to this, the soil properties should be thoroughly researched when there is a probability of transitional contractive soil being present in the critical driving zone. The utilisation of CPT correlations, in conjunction with borehole logs when available, is advised. In instances where this soil identification indicates contractive transitional soil, it is essential to implement mitigation measures.

5.3. Time-related effects

The primary observation is that resistance increases in accordance with the SRDs in the silt layers. However, the driving force does not appear to be increasing. The measurement of driving force is achieved through analysing the blows required to penetrate 25 cm and the average energy per blow for that depth increment. This finding suggests that the SRD methods may overestimate soil resistance in silt. The calculation methods may not accurately capture the true SRD, yet the CPT does evidently provide low q_t values in the silt layers. Despite the fact that the CPT is pressed into the soil rather than being hammered, the penetration mechanism is essentially analogous in both cases. The cone of a CPT is approximately 36 mm, and the wall thickness of the foundation piles is 50 mm. The driveability resistance appears to be in alignment with the q_t resistance, suggesting the potential for a CPT-based calculation method to be applicable. This low q_t in silt is again a hint towards tip resistance reduction because of undrained soil penetration. The CPT data also contains the measured PWP u_2 value of the test. Plotting this PWP can tell more about undrained penetration of the CPT, indicating that the soil is vulnerable to EPWP during impact pile driving. Locations A2, A3 and A5 are plotted in Figure 5.3 to Figure 5.5.

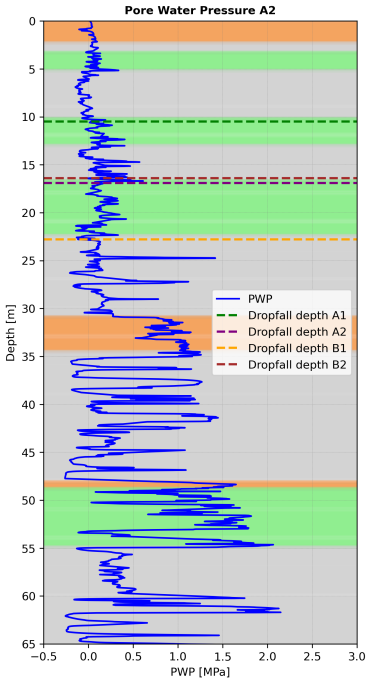

Figure 5.3: PWP over depth for location A2 before installation, measured with CPT

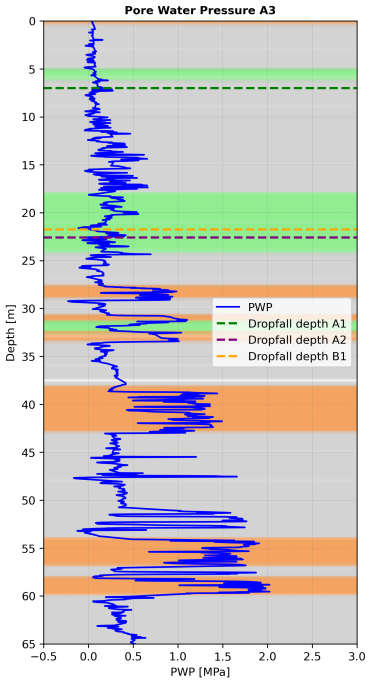

Figure 5.4: PWP over depth for location A3 before installation, measured with CPT

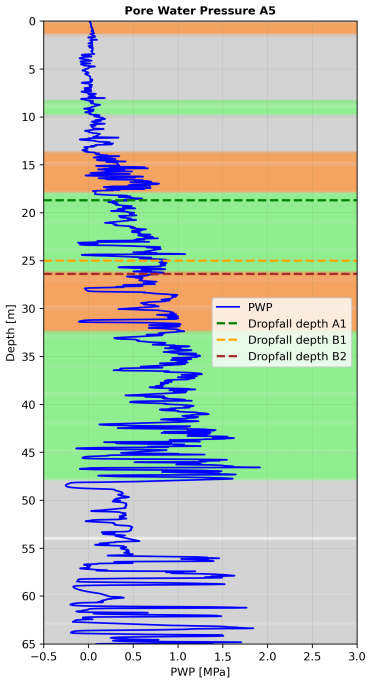

Figure 5.5: PWP over depth for location A5 before installation, measured with CPT

The observation in general is that the silt layers have higher PWP values than the sand layers. There is also a difference in PWP insight the silt layers, visible in Figure A.4. This phenomenon can be attributed to the distinct permeability characteristics of silt in comparison to sand and clay. As a transitional soil, this permeability is a challenging parameter to assess. While no direct correlation is observed between the PWP and the dropfalls, it is evident that silt is susceptible to undrained behaviour. This phenomenon exemplifies the capacity for the accumulation of EPWP. This satisfies the semi-permeable criterion. All the locations are plotted in Appendix A.

The order of driving is presented in the caption of the driveability plots. The order of pile driving is B1, A1, B2, A2 for all locations except A3. A3 was executed first and the piles where driven in the order B1, B2, A1, A2. After location A3, A2 was executed, then A5, A6, C4 and then C6. Interesting is that at the first locations more dropfalls where observed. The reason could be the soil type and the lack of experience with dropfall mitigation. These locations are at the west side of the field and the soil analysis shows more transitional contractive soils at these locations. The locations in question are situated on the western side of the field, and analysis of the soil reveals the presence of transitional contractive soils in these areas. Furthermore, the impact of pile driving on the soil surrounding the other piles at the same location could be a subject of investigation. An overview of the dropfalls and punch throughs in driving order is provided in Table 5.2. This highlights two aspects. The more locations installed, less dropfalls occurred. The installation of additional locations was found to be inversely proportional to the occurrence of dropfalls. It is also to be noted that the locations designated A2 to A6 are the initial sites to be equipped with the project's complete range of installations. In addition, the occurrence of dropfalls was most evident during the driving of the first pile at each location. The dropfall probability reduces per pile driven. This finding may be indicative of soil compaction resulting from impact hammering, leading to reduced contractility.

Pile	A3	A2	A5	A6	C4	C6
1	Dropfall	Dropfall	2x Dropfall	-	-	Dropfall
2	-	Punch through	Dropfall	Dropfall	Dropfall	-
3	Punch through	Dropfall	Dropfall	-	-	-
4	Dropfall	Punch through	-	-	-	-

Table 5.2: Overview of the dropfalls and punch troughs. Locations are in executive order.

5.4. Limitations

The principal limitation of this thesis is the absence of precise tests with which to quantify permeability and state parameter. The parameters under discussion were proposed as indicators for meeting the theoretical criteria for EPWP build-up. The precise permeability is a critical factor in determining the scale of undrained/drained behaviour, while the state parameter forms a scale in terms of CD behaviour. Whether this thesis constitutes the prevailing failure mechanism for bearing-capacity reduction is not a settled matter. An alternative theory concerning undrained penetration due to high relative velocity challenges the present thesis and is equally plausible, as demonstrated in subsection 2.3.7. This theory posits that increased penetration velocity induces undrained behaviour. The effects of this are evident in CPT tests conducted at varying rates. As shown in Equation 2.5, the soil property governing the quantification of normalised velocity is the consolidation coefficient. This parameter is of interest because it depends linearly on permeability and shear modulus, G. These variables are functions of the inter-particle pore structure, as is the degree of contractivity. Therefore, in terms of soil characteristics, this method of strength reduction also depends on the same intrinsic soil properties, although the precise micro-scale mechanism governing normalised-velocity-induced strength loss remains unclear. The establishment of precise parameters in future research is of critical importance for both theories.

The main limitation of SRD research is that the calculations are inherently empirical, meaning the analytical methods are always specific to the conditions and cannot be applied directly to new situations. In practice, this can result in assumptions being made about soil strengths that are not warranted, as they are based on correlations derived under different boundary conditions. This makes them theoretically inapplicable to new situations. However, it must be acknowledged that SRD methods are the only tool available to the industry for quantifying soil strength based on CPT profiles, making in situ measurements possible. Choosing an SRD model, averaging technique, and filter method makes a lot of assumptions that have a big effect on the result of the static analysis. But these assumptions have not been checked carefully. Although state-of-the-art methodologies were chosen that employed the most applicable variants, this does not necessarily imply that they represent the optimal qualitative approaches for this investigation.

The still unanswered question from regarding the time-related effects is: How do hammer energy (amplitude) and blow rate (frequency) influence the build-up of EPWP, and how can this influence be quantified? Despite the fact

that cyclic loading tests have indeed been performed on silty soil samples, it is not yet possible to directly translate these results into actual reductions in bearing capacity due to pile driving. However, the case study demonstrates that both frequency and amplitude can significantly affect dropfalls, and quantifying these effects is essential for understanding when a dropfall will or will not be initiated. This missing link provides a framework for understanding how driving procedures must be adapted to avoid potential hazards. A correlation is established through the plotting of hammer energy and blow count data. In order to provide meaningful insight into the hammer frequency, it is necessary to incorporate blow rates into the analysis, as the current driveability results do not include a time factor. The blow rates provided herein indicate the penetration speed per 25 mm. A comparison can then be drawn between these rates and the blow counts. The issue arises from the absence of this information within the hammer files for the case study in question. The availability of stroke data files has been limited to half of the locations, with the files in question recording both the number of strokes and the timestamp for each stroke. The subsequent issue is that the total number of blows in the stroke data sheet was not corresponding to the blow count sheet, which resulted in the timestamps being unable to be matched with the blow counts.

5.5. Recommendations

To refine SRD predictions and mitigate pile run risk in transitional soils, the following recommendations are made to mitigate the dropfalls and for follow-up studies:

- Perform a new study on a location with dropfalls in transitional contractive soils. Make sure that permeability and the state parameter is measured correctly with lab tests. Test the dropfalls on failure because of shaft friction, failure based on end bearing capacity loss and test the influence of penetration velocity on bearing capacity reduction. Create feasibility of real-time blow count,blow rate and PWP monitoring to detect EPWP accumulation should be investigated, enabling adaptive driving strategies (driving stop or crane master). By making the PWP measured, conclusions can be made on blow count influence. This provide real time insight on fluidisation risks and helps determining the correct failure mechanism together with the accurate soil parameters.
- With the provided theory by this thesis, define new SRD models for silty and stratified soil layers. As discussed in the limitations sector, the state-of-the-art methods are not calibrated on transitional soil layers. Perform parameter sensitivity analysis to fit the SRDs better to driving logs in transitional soils. Focus on the implementation of the contractivity in the base resistance and implement a reduction factor based on permeability of the soil along the shaft. In addition, take pile dimensions into account. Determine for multiple dimensions if the system is dominated by base or shaft resistance. This would help the industry make preciser soil resistance to driving predictions.
- Loading conditions because of impact hammering should be tested in a hollow cylinder apparatus. This is required to obtain a more direct link between soil deformation and impact hammering, with a focus on frequency and amplitude to simulate the the blow rate and hammer energy. More knowledge on this topic could also be useful for vibro hammering and gently pile driving. Interesting is that this understanding can help with easier reaching target penetration depth. This is also the case for the fluidisation principle. As fluidisation is presented in this thesis as a initiator of pile run and thus a risk, it could be used to reach target penetration. The objective of offshore pile installation is to reach target depth as quickly as possible in a safe and stable way.
- To create a new structural modal with a coupled PWP analysis, for example with a FEM that couples shear force to the soil profile and permeability, to simulate EPWP build-up and dissipation between blows. One of the observations in soil-structure interaction is that soil models make rough assumptions on the structural side and vice versa. Coupled soil structure models take a lot of computational effort and are difficult to define as the pile shaft interacts in a elasto-plastic manner. This combined model could link multiple pile-soil interaction questions and could also be useful to determine underwater noise pollution, as well as the interaction with the hammer.

6
Conclusion

The aim of this research was to understand the governing mechanisms that describe pile-soil interaction during impact hammering, and to provide a methodology for predicting dropfalls in transitional soil for future projects. Transitional soils demonstrate mechanical properties that are neither wholly consistent with that of sands nor that of clays, exhibiting characteristics that are intermediate between these two categories. The main characteristics of interest are the permeability and particle sizes. This objective was addressed by answering the main research question:

What is the primary mechanism that initiates a dropfall of an offshore monopile during pile driving in transitional soils?

The main question already emphasises that the focus is on the initiation of a dropfall rather than on behaviour during a dropfall. In order to define what happens in the pile-soil interaction during the initiation of a dropfall, the governing mechanisms must first be described from a fundamental perspective in order to create a theoretical framework that can be used to assess real dropfall cases. Research into pile-soil interaction shows that dynamic impact hammering can cause rearrangement of the soil skeleton, resulting in excess pore water pressure along the shaft and thus loss of shaft friction. To elaborate further, impact driving displaces the pile, exerting a shear force on the soil skeleton along the pile shaft. This causes the particles in the interface layer next to the pile to slide over one another, resulting in dilation of the interface layer. Combined with a contractive far-field layer, this leads to a loss of contact between the particles in the interface layer, creating a mechanical reaction resulting in local PWP changes. If the soil is semi-permeable, water cannot dissipate from the interface layer. This results in fluidisation and loss of shaft friction. This mechanism is triggered under two conditions that govern the theoretical framework:

1. The soil layers providing shaft friction are contractive.
2. The soil layers are partially permeable. It is essential that the EPWP is able to build up, but not quickly dissipate again.

The soil type that suits to this theory is categorised as transitional contractive soil, according to Robertson his SBT_n chart. Examples include silts and clayey sands. This raises the question: How can dropfalls be evaluated against the theoretical criteria for the proposed framework? This study identified three methods of determining whether soil is susceptible to the shaft friction reduction framework, based on CPT correlations and borehole log:

- Plot the CPT data with their correlations on the SBT_n chart. The soil type is obtained based on normalised shaft friction and tip resistance. Please note that significant uncertainty is involved, so further research is necessary.
- Plotting the state parameter over depth can help to identify contractive soil layers. This can again be done using CPT correlations. The findings of this thesis propose that the initial state parameter, denoted by Ψ_0, should be obtained through laboratory tests, as opposed to the CPT-correlated Ψ. The model incorporates an excessive degree of uncertainty and presents significant challenges with regard to scalability.
- In the event of the presence of silty soils being indicated, the laboratory results of the borehole log should be consulted in order to eliminate any uncertainty surrounding the soil type characterisation. The plasticity limit and the particle sizes must be determined through the use of laboratory tests in order to define the soil type.

Based on this methodology, the soil at six pile run locations was assessed for its properties. Five out of six locations met the conditions for shaft friction reduction based on the investigation of soil properties. While this does not prove the theory, the advantage of the presented approach is that the fundamental principals behind the mechanisms are considered, making it generally applicable for risk assessment. The succeeding discussion on the

quantification of shaft friction reduction revealed that the reduction of effective stress does not necessarily result in substantial shaft friction loss, as indicated by the SRD calculation methods. It is also possible that a reduction in the end bearing capacity is due to contractive soil at the pile tip or undrained penetration. It is hypothesised that all three mechanisms could contribute to the total bearing capacity loss. The conclusion of this research is that impact pile driving in transitional soils results in build-up of EPWP, which in turn causes a reduction in shaft friction. It is not yet possible to state with any degree of certainty that this is also the governing mechanism. The proposal of this thesis is that a high dropfall risk is indicated if a greater proportion of the data points are situated within the transitional contractive soil area of the SBTn chart, specifically if more than 50% of the data points fall within this area. For locations exhibiting a substantial quantity of transitional soil (i.e. > 20%), a reduced risk of dropfall persists. In addition, the presence of a high risk of dropfall has been identified in contractive soils. However, further research is required to establish the boundaries of this risk based on for example state parameter values.

The remaining question is: To what extent can static soil resistance to driving be used to predict dropfalls in future projects? In short, the conclusion to this question is that SRD methods cannot accurately predict dropfalls. They describe empirical relationships between CPT data and soil strengths in clay or sand for piles of different dimensions. The boundary conditions on which these methods are based make them unsuitable for predicting dropfalls in silty soils. To apply an SRD method to silty soils, a sensitivity analysis should be performed to obtain more precise calculation coefficients. To specify this more SRD method dependent: The AH and Maynard method are based on primarily shaft friction. The advice is to implement a reduction factor on the shaft resistance in transitional soils for these methods. The UM is base resistance dominated and thus is the advice to reduce the tip resistance for this method based on the contractivity of the soil.

On the contrary, the SRD methods are the easiest implementable tools to quantify soil strength for the industry. The results of the case study demonstrated that certain SRDs are able to come close to predicting the real static equilibrium location, for example the dropfall location or the SWP depth. The results showed that based on SRD predictions, a critical risk zone can be identified for which a soil analysis should be made. If the soil layers in this critical zone meet the theoretical conditions, their is a significant risk on pile run, for which now the right mitigation measures can be taken. The utilisation of CPT correlations, in conjunction with borehole logs when available, is advised. The incorporation of a measure of contractivity and permeability improves the SRD prediction.

To answer the main question, the initiator of pile run in transitional soil can be the built-up of EPWP because of impact driving, resulting in shaft friction reduction. This is based on the level of permeability and contractivity of the soil. In the absence of conclusive evidence from the case study, the hypothesis is considered to be plausible. Further research is needed to explore different failure mechanisms and adjustments to SRDs should be made to pinpoint exact dropfall locations. This thesis establishes a foundational framework that enables early identification of pile run risks, turning uncertainty into actionable insight for future offshore projects.

References

Ahmed, S. S., Alejandro Martinez, and Jason T. DeJong (2024). "Gradation and state effects on the strength and dilatancy of coarse-grained soils". In: *E3S Web of Conferences*. DOI: 10.1051/e3sconf/202454413003.

Alm, T. and L. Hamre (2001). "Soil model for pile driveability predictions based on CPT interpretations". In: *Proceedings of the Offshore Technology Conference*. Houston, TX: Offshore Technology Conference. URL: https://www.issmge.org/publications/online-library.

Alpan, I. (1970). "The geotechnical properties of soils". In: *Earth-Science Reviews* 6, pp. 5–49. DOI: 10.1016/0012-8252(70)90001-2.

American Petroleum Institute (2000). *Recommended Practice for Planning, Designing, and Constructing Fixed Offshore Platforms–Working Stress Design*. Tech. rep. API RP2A-WSD. Washington, DC: American Petroleum Institute.

Ardouz, Ghizlane, K. Baba, Latifa El Bouanani, F. Latifi, and A. Dardouch (2022). "The Influence of the Fundamental Parameters on the Mechanical Behavior of Coarse-Grained Soils". In: *Civil Engineering Journal*. DOI: 10.28991/cej-2022-08-08-012.

Argyroulis, K, J Putteman, K Gavin, and A.A. Roubos (2024). "Pile driveability predictions of open ended tubular piles in sand using the Unified Method". In: *Proceedings of the XVIII ECSMGE 2024*. DOI: 10.1201/9781003431749-391.

Argyroulis, K. (Sept. 2022). "Evaluating pile driveability models and improving driveability predictions of a recent static axial capacity approach". MA thesis. Delft, Netherlands: Delft University of Technology.

Atkinson, J. and P. L. Bransby (1987). "THE MECHANICS OF SOILS, AN INTRODUCTION TO CRITICAL STATE SOIL MECHANICS". In: *Vehicle System Dynamics*.

Ayala, J, A Fourie, and D Reid (2023). "A Unified Approach for the Analysis of CPT Partial Drainage Effects within a Critical State Soil Mechanics Framework in Mine Tailings". In: *Journal of Geotechnical and Geoenvironmental Engineering* 149.6. DOI: 10.1061/JGGEFK.GTENG-10915.

Been, K., J. Obermeyer, J. Parks, and A. Quinonez (Oct. 2012). "Post-liquefaction undrained shear strength of sandy silt and silty sand tailings". In: *Proceedings of the 16th International Conference on Tailings and Mine Waste*. Keystone, Colorado, USA.

Bilgili, Mehmet, Hakan Alphan, and Akin Ilhan (Feb. 2023). "Potential visibility, growth, and technological innovation in offshore wind turbines installed in Europe". In: *Environmental Science and Pollution Research* 30.10, pp. 27208–27226. ISSN: 1614-7499. DOI: 10.1007/s11356-022-24142-x. URL: https://doi.org/10.1007/s11356-022-24142-x.

Bittar, Lehane, Z. LIU, F. NADIM, and S. LACASSE (2022). "Application of the unified CPT method for driven piles to layered deposits". In: *Géotechnique Letters* 12. DOI: 10.1680/jgele.22.00058.

Bolton, M. D. (1986). "The strength and dilatancy of sands". In: *Geotechnique* 36.1, pp. 65–78.

Boulanger, R.W. and J.T DeJong (2018). "Inverse filtering procedure to correct cone penetration data for thin-layer and transition effects." In: *Proceedings of the 4th International Symposium on Cone Penetration Testing (CPT'18)*. Pp. 22–44.

Buckley, Róisín, Yuling Max Chen, Brian Sheil, Stephen Suryasentana, Diarmid Xu, James Doherty, and Mark Randolph (2023). "Bayesian Optimization for CPT-Based Prediction of Impact Pile Drivability". In: *Journal of Geotechnical and Geoenvironmental Engineering* 149.11, p. 04023100. DOI: 10.1061/JGGEFK.GTENG-11385.

Byrne, T., K. Gavin, L.J. Prendergast, P. Cachim, P. Doherty, and S. Chenicheri Pulukul (2018). "Performance of CPT-based methods to assess monopile driveability in North Sea sands". In: *Ocean Engineering* 166, pp. 76–91. ISSN: 0029-8018. DOI: https://doi.org/10.1016/j.oceaneng.2018.08.010. URL: https://www.sciencedirect.com/science/article/pii/S0029801818314926.

CAPE Holland (2024). *Pile Driving Challenge: Pile Run*. Accessed: 2025-03-13.

Carneiro, Daniel, Andrew Rathbone, Kok Siong Soon, and Graham Viecelli (Oct. 2016). "Velocity-Dependent Soil Resistance in Finite Element Analysis of Pipeline Walking". In: *Journal of Offshore Mechanics and Arctic Engineering* 139.2, p. 021701. ISSN: 0892-7219. DOI: 10.1115/1.4034695. eprint: https://asmedigitalcollection.asme.org/offshoremechanics/article-pdf/139/2/021701/6247234/omae_139_02_021701.pdf. URL: https://doi.org/10.1115/1.4034695.

Ceccato, F. and P. Simonini (2017). "Numerical study of partially drained penetration and pore pressure dissipation in piezocone test". In: *Acta Geotechnica* 12, pp. 195–209. DOI: 10.1007/S11440-016-0448-6.

Chai, F., J. Liu B.and Xue, and K. Duffy (2025). "Assessing direct CPT-based methods for predicting pile base resistance using coupled DEM-FDM simulations." In: *Computational Geotech* 183.107230. DOI: 10.1016/j.compgeo.2025.107230.

Chow, S.H., B. Bienen, and M.F. Randolph (2018). "Rapid penetration of piezocones in sand." In: *Cone Penetration Testing 2018*. Delft, the Netherlands, pp. 213–219.

Darcy, Henry (1856). *Les fontaines publiques de la ville de Dijon*. Paris: Dalmont.

Das, Braja M. (2006). *Principles of Geotechnical Engineering*. 6th. Boston: Thomson. ISBN: 0534551440, 9780534551445. URL: https://tudelft.on.worldcat.org/oclc/840394126.

Dayal, U. and J.H. Allen (1975). "The effect of penetration rate on the strength of remolded clay and sand samples." In: *Canadian Geotechnical Journal* 12, pp. 336–348. DOI: 10.1139/t75-038.

Deeks, A. and M. Randolph (May 1993). "Analytical modeling of hammer impact for pile driving". In: *International Journal for Numerical and Analytical Methods in Geomechanics* 17, pp. 279–302. DOI: 10.1002/nag.1610170502.

DeJong, J.T., R.A. Jaeger, R.W. Boulanger, M.F. Randolph, and D.A.J. Wahl (2013). "Variable Penetration Rate Cone Testing for Characterization of Intermediate Soils". In: *Proceedings of the 4th International Conference on Site Characterization (ISC-4)*. Ed. by R. Coutinho and P. Mayne. Porto Galinhas, Brazil, pp. 25–42.

DNV CN-304 Foundations (2016). DNV Classification Notes. Det Norske Veritas (DNV). URL: https://rules.dnv.com/docs/pdf/DNV/cn/2016-04/DNV-CN-304.pdf.

Du, Jun, Zhiming Xiong, Xinggang Shen, and Chenchen Li (2023). "Experimental Study on the Effect of Coarse Grain Content on the Dilatancy and Particle Breakage Characteristics of Coarse-Grained Soils". In: *Geofluids*. DOI: 10.1155/2023/2307881.

Duffy, K (2023). *CPyT package*. https://github.com/triaduct/cpyt/blob/main/README.md. GNU General Public License v3.0.

Duffy, K, C Reale, and K Gavin (2025). "Analytical approach to predicting pile self-weight penetration, considering penetration rate effects". In: *Ocean Engineering* 338. DOI: 10.1016/j.oceaneng.2025.121949.

Erbrich, C and M. F. Randolph (June 2025). "Modelling and Avoiding Pile Free-Fall in Offshore Design". In: *Proceedings of the 5th International symposium on frontiers in offshore geotechnics*. Nantes, France, pp. 224–237.

EU (Feb. 2025). URL: https://oceans-and-fisheries.ec.europa.eu/ocean/blue-economy/marine-renewable-energy_en.

Finnie, I. M. S. and M. F. Randolph (1994). "Punch-through and liquefaction induced failure of shallow foundations on calcareous sediments". In: *Proceedings of the International Conference on Behavior of Offshore Structures (BOSS '94)*. Boston, USA, pp. 217–230.

Fredlund, M., D. Fredlund, and G. Wilson (2000). "An equation to represent grain-size distribution". In: *Canadian Geotechnical Journal* 37, pp. 817–827. DOI: 10.1139/T00-015.

Fugro (2018). *Changhua OWF Factual Data Report*. Tech. rep. 18007S-5(02. Leidschendam, The Netherlands: Fugro.

— (2021). *Cone Penetration Test Interpretation*. Tech. rep. FNLM-GEO-APP-012. Leidschendam, The Netherlands: Fugro.

García Martínez, M.F., L. Tonni, G. Gottardi, and I. Rocchi (2016). "Influence of Penetration Rate on CPTU Measurements in Saturated Silty Soils". In: *Geotechnical and Geophysical Site Characterisation 5*. Ed. by Acosta-Martínez Lehane and Kelly. Sydney, Australia: Australian Geomechanics Society, pp. 473–478. ISBN: 978-0-9946261-1-0.

Huang, Shu-li, Shuying Wang, Changjie Xu, Yu-feng Shi, and Fei Ye (2019). "Effect of Grain Gradation on the Permeability Characteristics of Coarse-grained Soil Conditioned with Foam for EPB Shield Tunneling". In: *KSCE Journal of Civil Engineering* 23, pp. 4662–4674. DOI: 10.1007/s12205-019-0717-7.

International Energy Agency (2019). *Offshore Wind Outlook 2019*. Tech. rep. Accessed: 2021-10-07. International Energy Agency. URL: https://www.iea.org/reports/offshore-wind-outlook-2019.

Jardine, Richard, Andrew Merritt, and Felix Schroeder (Mar. 2015). "The ICP Design Method and Application to a North Sea Offshore Wind Farm". In: *Geotechnical Special Publication*, pp. 247–256. DOI: 10.1061/9780784479087.025.

Jefferis, M and K Been (2016). *Soil liquefaction; A Critical State Approach*. CRC Press, p. 73.

Kaliakin, V. N. (2017). *Chapter 2 - Example Problems Related to Soil Identification and Classification*. Butterworth-Heinemann, pp. 51–92. ISBN: 978-0-12-804491-9. DOI: 10.1016/B978-0-12-804491-9.00002-1. URL: https://www.sciencedirect.com/science/article/pii/B9780128044919000021.

Karakan, E. (2022). "Comparative Analysis of Atterberg Limits, Liquidity Index, Flow Index and Undrained Shear Strength Behavior in Binary Clay Mixtures". In: *Applied Sciences*. DOI: 10.3390/app12178616.

Kashichenula, K, K Sudhakaran, and S Maghsoodi (2025). "Performance of different soil resistance models to assess the pile runs during offshore pile driving". In: *Proceedings of ISFOG 2025*. Nantes, France, pp. 1239–1244.

Kementzetzidis, Evangelos (2024). *Fundamentals of Soil Behaviour*. Presentation, CIEM4000 - Soil Structure Interaction. URL: https://brightspace.tudelft.nl/d2l/le/content/594917/viewContent/3614737/View.

Lambe, T. W. and R. V. Whitman (1969). *Soil Mechanics*. New York: John Wiley & Sons.

Lee, J. and F. Zhao (Feb. 2021). *Global Offshore Wind Report 2021*. Tech. rep. Global Wind Energy Council, pp. 1–80. URL: https://gwec.net/global-offshore-wind-report-2021/.

Lehane, B (2025). *Unified CPT method calculation tool*. URL: https://pile-capacity-uwa.com/about?pile=driven (visited on 08/01/2025).

Lehane, B.M., J.K. Lim, P. Carotenuto, F. Nadim, S. Lacasse, R.J. Jardine, and B.F.J. van Dijk (2017). "Characteristics of Unified Databases for Driven Piles". In: *Proceedings of the 8th International Conference on Offshore Investigation and Geotechnics: Smarter Solutions for Offshore Developments*. Vol. 1. Society for Underwater Technology, pp. 162–194.

Lehane, Z. Liu, E. Bittar, F. Nadim, S. Lacasse, R. J. Jardine, P. Carotenuto, M. Jeanjean P.and Rattley, K. Gavin, and J. Haavik (2020). "A new 'unified' CPT-based axial pile capacity design method for driven piles in sand." In: *Proceedings of the 4th International symposium on frontiers in offshore geotechnics*. Reston, VA, USA, pp. 463–477.

Liu, Ke, Dong Wang, and Jingbin Zheng (2022). "Numerical investigation of spudcan penetration under partially drained conditions". In: *Ocean Engineering*. DOI: 10.1016/j.oceaneng.2021.110425.

Masch, F. and Kleber J. Denny (1966). "Grain size distribution and its effect on the permeability of unconsolidated sands". In: *Water Resources Research* 2, pp. 665–677. DOI: 10.1029/WR002I004P00665.

Maynard, A. W., L. Hamre, D. Butterworth, and F. Davison (2019). "Improved Pile Installation Predictions for Monopiles". In: *Stress Wave Theory and Testing Methods for Deep Foundations: 10th International Conference*. Ed. by P. Bullock, G. Verbeek, S. Paikowsky, and D. Tara. West Conshohocken, PA: ASTM International, pp. 426–449. DOI: 10.1520/STP1611201701644. URL: http://dx.doi.org/10.1520/STP1611201701644.

McCoy, Angel, Walter Musial, Rob Hammond, Daniel Mulas Hernando, Patrick Duffy, Philipp Beiter, Paula Pérez, Ruth Baranowski, Gage Reber, and Paul Spitsen (2024). *Offshore Wind Market Report: 2024 Edition*. Technical Report NREL/TP-5000-90525. Golden, CO: National Renewable Energy Laboratory. URL: https://www.nrel.gov/docs/fy24osti/90525.pdf.

Meijers, P., A. Tsouvalas, and A. Metrikine (2017). "The Effect of Stress Wave Dispersion on the Drivability Analysis of Large-Diameter Monopiles". In: *Procedia Engineering* 199, pp. 2390–2395. DOI: 10.1016/J.PROENG.2017.09.272.

Negro, Vicente, José-Santos López-Gutiérrez, M. Dolores Esteban, Pablo Alberdi, Mario Imaz, and José-María Serraclara (2017). "Monopiles in offshore wind: Preliminary estimate of main dimensions". In: *Ocean Engineering* 133, pp. 253–261. ISSN: 0029-8018. DOI: https://doi.org/10.1016/j.oceaneng.2017.02.011. URL: https://www.sciencedirect.com/science/article/pii/S0029801817300690.

Netherlands Enterprise Agency (Apr. 2023). *Offshore Wind Market Report*. Tech. rep. The Hague, Netherlands: Netherlands Enterprise Agency. URL: https://www.rvo.nl/sites/default/files/2023-04/Offshore-Wind-Market-Report.pdf.

NGI (2024). *PIGS - Piling in Glauconitic Sand Joint Industry Project (JIP)*. URL: https://www.ngi.no/en/projects/pigs/ (visited on 07/14/2025).

Osborne, Alistair (Sept. 4, 2024). "Putting more energy into offshore energy". In: *The Times*. URL: https://www.thetimes.com/business-money/economics/article/putting-more-energy-into-offshore-energy-fg8wm9vzt?region=global.

Paik, K. and R. Salgado (2003). "Estimation of active earth pressure against rigid retaining walls considering arching effects". In: *Geotechnique* 53.7, pp. 643–653. DOI: 10.1680/geot.2003.53.7.643.

Patnaik, Surya N., Rula M. Coroneos, and Dale A. Hopkins (1999). *Compatibility Conditions of Structural Mechanics*. Tech. rep. NASA/TM-1999-209175. Cleveland, Ohio: NASA Glenn Research Center. URL: https://ntrs.nasa.gov/archive/nasa/casi.ntrs.nasa.gov/19990083068.pdf.

Prendergast, Luke J., Putri Gandina, and Kenneth Gavin (2020). "Factors Influencing the Prediction of Pile Driveability Using CPT-Based Approaches". In: *Energies* 13.12. ISSN: 1996-1073. DOI: 10.3390/en13123128. URL: https://www.mdpi.com/1996-1073/13/12/3128.

Randolph, J. Dolwin, and R. Beck (1994). "Design of driven piles in sand". In: *Geotechnique* 44.3, pp. 427–448.

Randolph, M.F. (2003). "Science and empiricism in pile foundation design". In: *Geotechnique* 53.10, pp. 847–875. DOI: 10.1680/geot.2003.53.10.847.

Randolph, Mark and Susan Gourvenec (2011). *Offshore Geotechnical Engineering*. 1st. Taylor & Francis Group.

Robertson (2022). "Evaluation of flow liquefaction and liquefied strength using the cone penetration test: an update". In: *Canadian Geotechnical Journal* 59.4, pp. 620–624. DOI: 10.1139/cgj-2020-0657. URL: https://doi.org/10.1139/cgj-2020-0657.

Robertson, P (1990). "Soil classification using the cone penetration test." In: *Canadian Geotechnical Journal* 27.1, pp. 151–158. DOI: 10.1139/t90-014.

— (2010). "Soil Behaviour Type from the CPT: An Update". In: *Proceedings of the 2nd International Symposium on Cone Penetration Testing*. Vol. 2. Huntington Beach, California, pp. 575–583. URL: http://www.cpt10.com/PDF_Files/2-56RobSBT.pdf.

Robertson, P (2016). "Cone penetration test (CPT)-based soil behaviour type (SBT) classification system — an update". In: *Canadian Geotechnical Journal* 53, pp. 1910–1927. DOI: 10.1139/CGJ-2016-0044.

Rocscience Inc. (2021). *CPT Data Interpretation Theory Manual*. Tech. rep. Rocscience Inc. URL: https://www.rocscience.com.

Rosati, A., D. Gaudio, H. Falepin, W. Ovalle-Villamil, S. Muraro, and M. Cabrera (June 2025). "Centrifuge tests to investigate pile run risk in transitional soils". In: *Proceedings of the 5th International symposium on frontiers in offshore geotechnics*. Nantes, France.

Salgado, R., D. Loukidis, G. Abou-Jaoude, and Y. Zhang (2002). "Interface shear strength and coefficient of lateral earth pressure for inclined soil-structure interfaces". In: *Journal of Geotechnical and Geoenvironmental Engineering* 128.6, pp. 484–494. DOI: 10.1061/(ASCE)1090-0241(2002)128:6(484).

Shepherd, R. (1989). "Correlations of Permeability and Grain Size". In: *Ground Water* 27, pp. 633–638. DOI: 10.1111/J.1745-6584.1989.TB00476.X.

SIF (2025). URL: https://sif-group.com/en/monopiles-and-transition-pieces/.

Singh, Sasha (2021). *How to drill a borehole*. URL: https://www.umvoto.com/how-to-drill-a-borehole/#:~:text=What%20is%20a%20borehole?,any%20type%20of%20geological%20material. (visited on 07/25/2025).

Smith, E.A.L. (1960). "Pile-Driving Analysis by the Wave Equation". In: *Journal of the Soil Mechanics and Foundations Division, ASCE* 86.4, pp. 35–64. URL: https://ascelibrary.org/doi/10.1061/JSFEAQ.0000281.

Stevens, R., E. Wiltsie, and T. Turton (1982). "Evaluating Pile Drivability for Hard Clay, Very Dense Sand and Rock". In: *Proceedings of the Offshore Technology Conference*. Vol. OTC 4205. Houston, TX: Offshore Technology Conference, pp. 465–481.

Sun, D., D. Sheng, L. Xiang, and S. Sloan (2008). "Elastoplastic prediction of hydro-mechanical behaviour of unsaturated soils under undrained conditions". In: *Computers and Geotechnics* 35, pp. 845–852. DOI: 10.1016/J.COMPGEO.2008.08.002.

Sun, L, T Jia, S. Yan, W. Guo, Y. Ren, and Z. Lei (2016). "Prediction of Pile Running during the Driving Process of Large-Diameter Pipe Piles". In: *Ocean Engineering* 128, pp. 48–57. DOI: 10.1016/j.oceaneng.2016.10.023. URL: https://www.sciencedirect.com/science/article/pii/S0029801816304619.

Sun, L., J. Shi, Y. Zhang, X. Feng, Y. Tian, and R. Wang (2022). "Analytical method for predicting pile running during driving". In: *Applied Ocean Research* 125, p. 103234. DOI: https://doi.org/10.1016/j.apor.2022.103234. URL: https://www.sciencedirect.com/science/article/pii/S0141118722001729.

Take, W.A, A.J Valsangkar, and M.F Randolph (1999). "Analytical solution for pile hammer impact". In: *Computers and Geotechnics* 25.2, pp. 57–74. ISSN: 0266-352X. DOI: https://doi.org/10.1016/S0266-352X(99)00018-X. URL: https://www.sciencedirect.com/science/article/pii/S0266352X9900018X.

Thijssen, R. and S. Roelen (May 2024). "Prediction of Pile Run During Pile Driving: Analytical Model and Field Observations". In: *Proceedings of the Offshore Technology Conference*. Copyright 2024, Offshore Technology Conference. Houston, TX, USA: Offshore Technology Conference. DOI: 10.4043/35471-MS.

Thooft, K., T. S. Lu, and W. F. Van Impe (1997). "Cavity expansion theory applied to CPT- and model pile test simulations". In: *Proceedings of the 14th International Conference on Soil Mechanics and Foundation Engineering*. International Society for Soil Mechanics and Geotechnical Engineering. Hamburg, Germany.

Tomic, Bartolomej (June 2020). *Heerema's Aegir Heavy Lifter in Drop Fall Incident Offshore Taiwan*. URL: https://www.oedigital.com/news/479464-heerema-s-aegir-heavy-lifter-in-drop-fall-incident-offshore-taiwan.

Toolan, F.E. and D.A. Fox (1977). "Geotechnical planning of piled foundations for offshore platforms." In: *Proc. Inst. Civ. Eng. 62*, pp. 221–224.

Tsetas, Athanasios, Apostolos Tsouvalas, and Andrei V. Metrikine (2021). "Installation of Large-Diameter Monopiles: Introducing Wave Dispersion and Non-Local Soil Reaction". In: *Journal of Marine Science and Engineering* 9.3. ISSN: 2077-1312. DOI: 10.3390/jmse9030313. URL: https://www.mdpi.com/2077-1312/9/3/313.

Ural, N. and B. Görgün (2019). "Effect of Different Sands on One-Dimensional and Hydraulic Consolidation (Radial) Tests of Clay". In: *Iranian Journal of Science and Technology, Transactions of Civil Engineering* 43.Suppl 1, pp. 331–341. DOI: 10.1007/s40996-018-0168-2. URL: https://doi.org/10.1007/s40996-018-0168-2.

Verruijt, Arnold (2001). *Grondmechanica*. 2nd ed. Delft, Netherlands: Delftse Uitgevers Maatschappij, p. 296. ISBN: 9065620451, 9789065620453.

Whitaker, Stephen (1986). "Flow in porous media I: A theoretical derivation of Darcy's law". In: *Transport in Porous Media* 1, pp. 3–25. URL: https://api.semanticscholar.org/CorpusID:121904058.

White, D. J. and M. D. Bolton (2004). "Displacement and strain paths during plane-strain model pile installation in sand". In: *Géotechnique* 54.6, pp. 375–397. DOI: 10.1680/geot.2004.54.6.375. URL: https://doi.org/10.1680/geot.2004.54.6.375.

Wu, Shengshen, Annan Zhou, Jie Li, J. Kodikara, and W. Cheng (2019). "Hydromechanical behaviour of overconsolidated unsaturated soil in undrained conditions". In: *Canadian Geotechnical Journal*. DOI: 10.1139/CGJ-2018-0323.

An Improved Pile Driveability Theory for Gulf of Mexico Soils (May 1983). Vol. All Days. OTC Offshore Technology Conference, OTC-4503–MS. DOI: 10.4043/4503-MS. URL: https://doi.org/10.4043/4503-MS.

Zhang, G, P.K. Robertson, and R.W.I. Brachman (2002). "Estimating liquefaction induced ground settlements from CPT for level ground." In: *Canadian Geotechnical Journal* 39.5, pp. 1168–1180. DOI: 10.1139/t02-047.

Zhao, Z. Liu, P. Shi, Jian Li, G. Cai, and Changfu Wei (2016). "Average Soil Skeleton Stress for Unsaturated Soils and Discussion on Effective Stress". In: *International Journal of Geomechanics* 16. DOI: 10.1061/(ASCE)GM.1943-5622.0000610.

A

Pore Water Pressures CPT

Figures A.1 to A.6 display the measured PWP for all six locations. The colours orange, gray and green in the background represent the soil layers clay, sand and silt, resulting from lab tests.

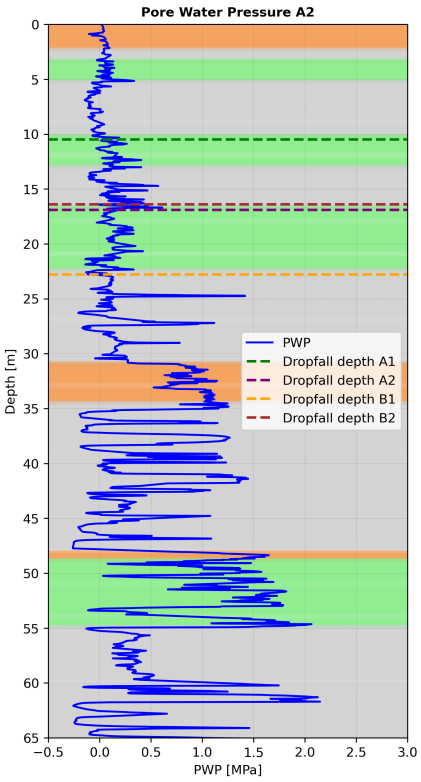

Figure A.1: Pore Water Pressure over depth for location A2 before installation, measured with CPT

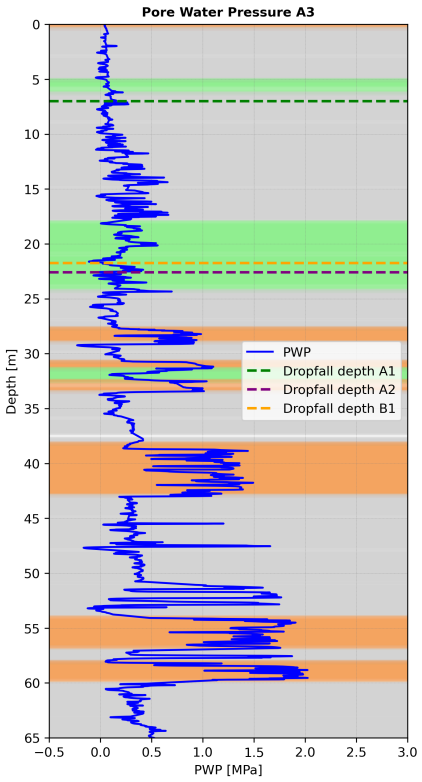

Figure A.2: Pore Water Pressure over depth for location A3 before installation, measured with CPT

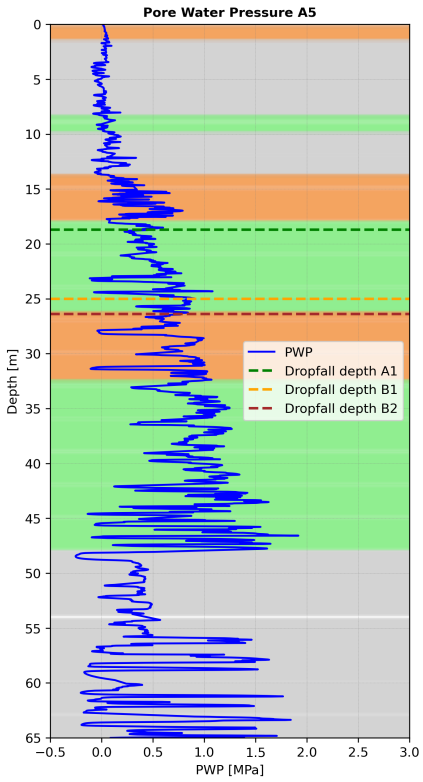

Figure A.3: Pore Water Pressure over depth for location A5 before installation, measured with CPT

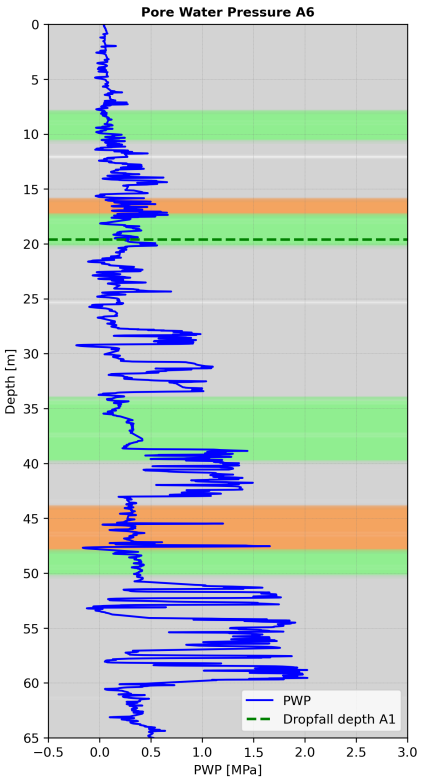

Figure A.4: Pore Water Pressure over depth for location A6 before installation, measured with CPT

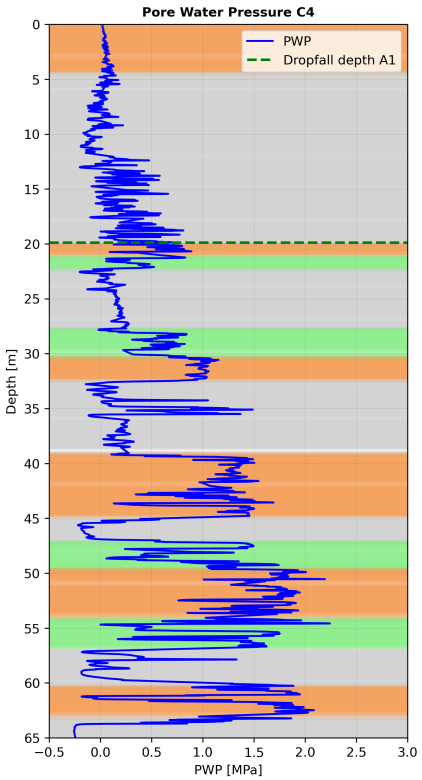

Figure A.5: Pore Water Pressure over depth for location C4 before installation, measured with CPT

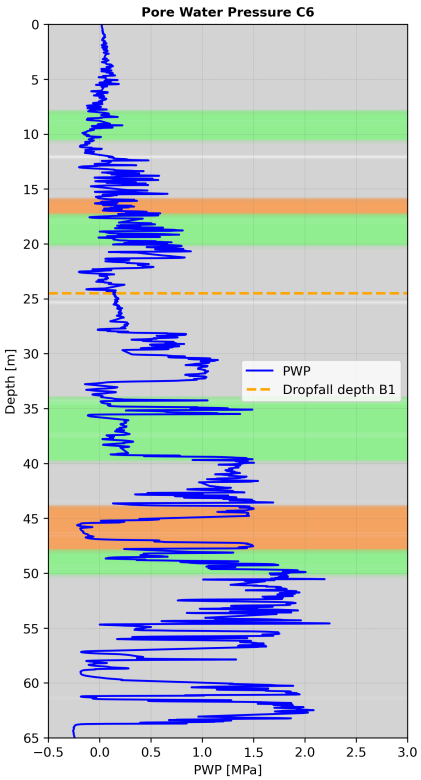

Figure A.6: Pore Water Pressure over depth for location C6 before installation, measured with CPT

B

SRD Performance

This appendix contains the performance of the in this thesis used SRD methods. It supports the outcomes presented in Table 5.1. Plots B.1 to B12 visualise the error and deviation of the methods. The diagonal line in the figures represents a perfect prediction by the models. The greater the distance between this line and the points, the greater the error and standard deviation.

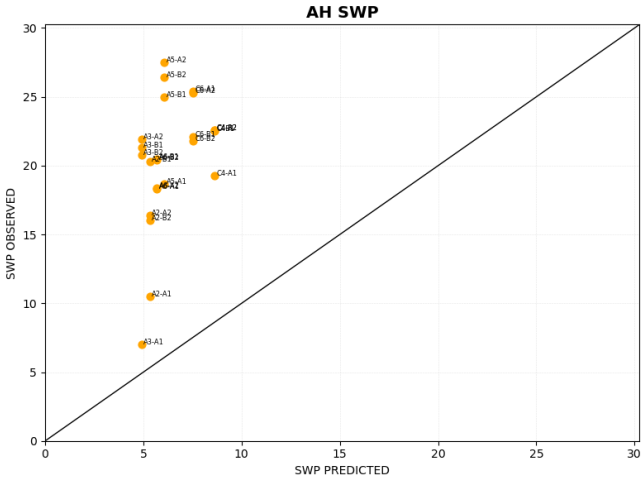

Figure B.1: Observed versus predicted self weight penetration following the Alm and Hamre SRD method for multiple Changhua locations.

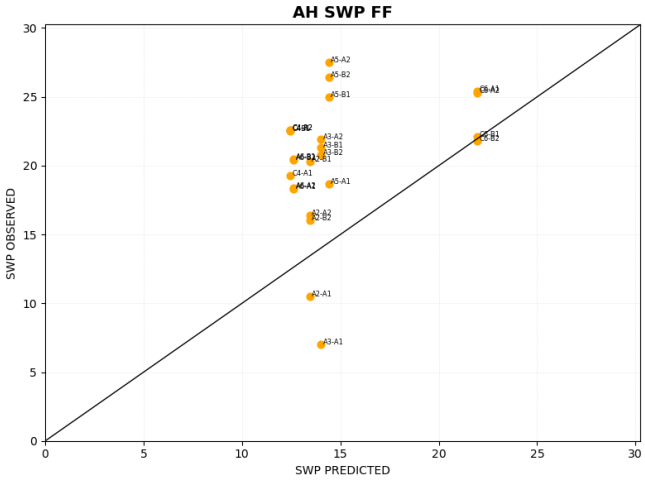

Figure B.2: Observed versus predicted self weight penetration following the Alm and Hamre SRD method (friction fatigue included) for multiple Changhua locations.

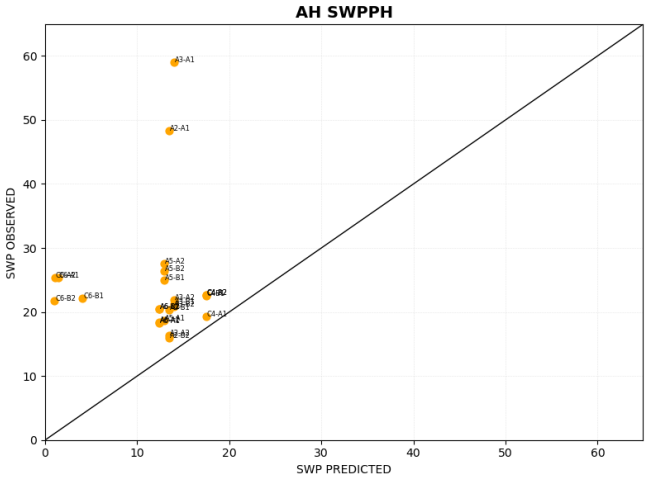

Figure B.3: Observed versus predicted self weight penetration pile plus hammer following the Alm and Hamre SRD method for all Changhua locations.

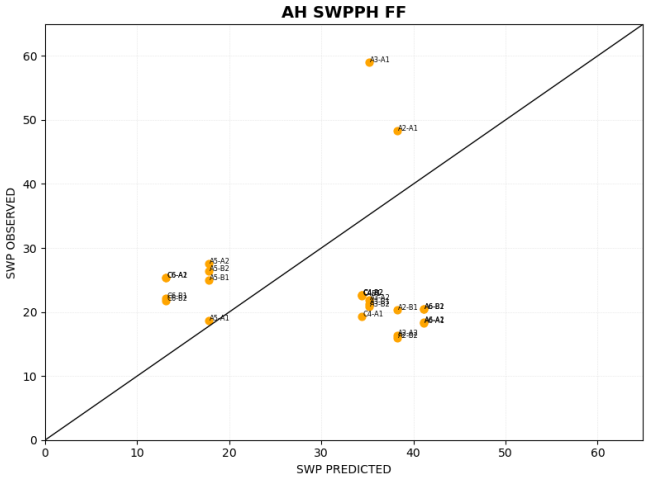

Figure B.4: Observed versus predicted self weight penetration pile plus hammer following the Alm and Hamre SRD method (friction fatigue included) for multiple Changhua locations.

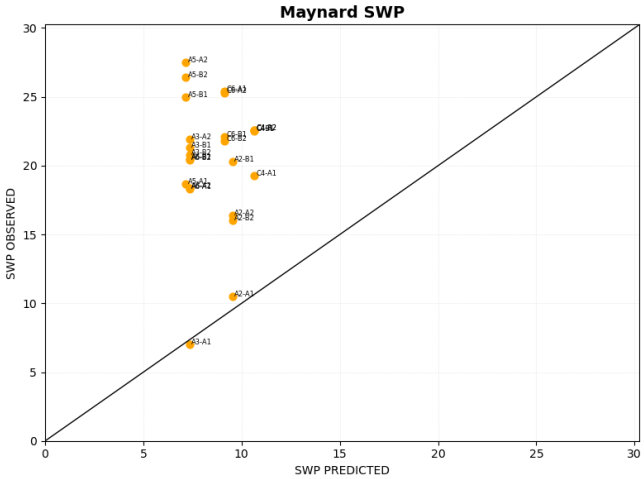

Figure B.5: Observed versus predicted self weight penetration following the Maynard SRD method for multiple Changhua locations.

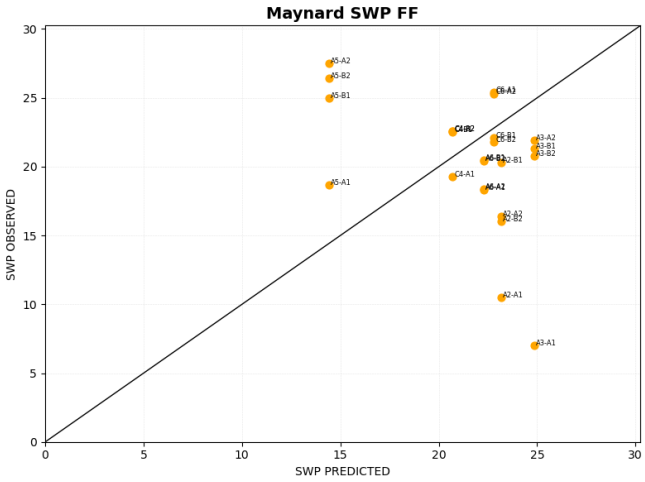

Figure B.6: Observed versus predicted self weight penetration following the Maynard SRD method (friction fatigue included) for multiple Changhua locations.

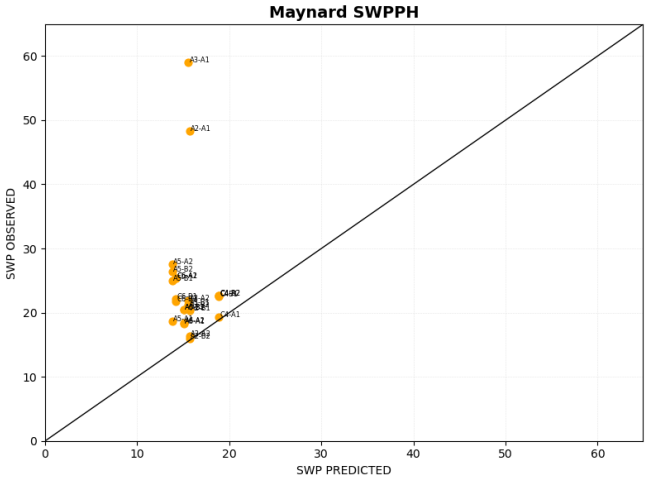

Figure B.7: Observed versus predicted self weight penetration pile plus hammer following the Maynard SRD method for multiple Changhua locations.

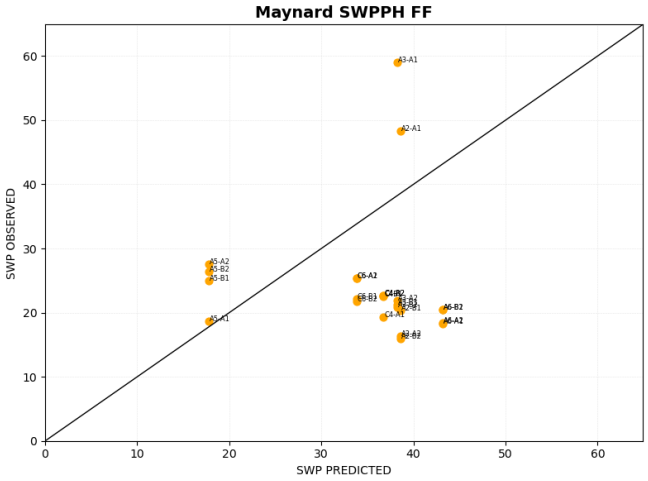

Figure B.8: Observed versus predicted self weight penetration pile plus hammer following the Maynard SRD method (friction fatigue included) for multiple Changhua locations.

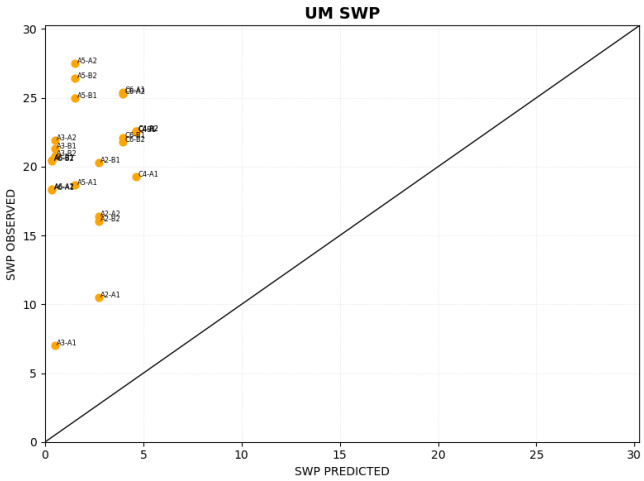

Figure B.9: Observed versus predicted self weight penetration following the Unified SRD method for multiple Changhua locations.

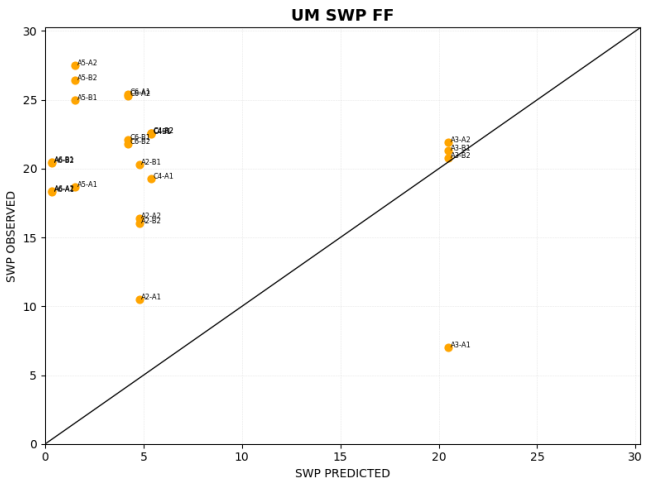

Figure B.10: Observed versus predicted self weight penetration following the Unified SRD method (friction fatigue included) for multiple Changhua locations.

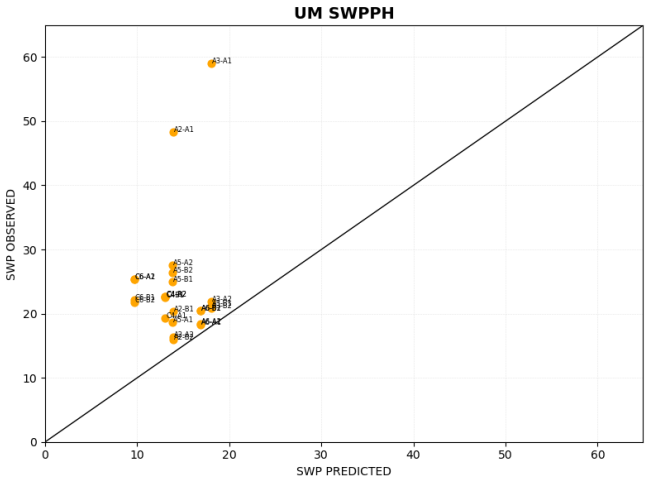

Figure B.11: Observed versus predicted self weight penetration pile plus hammer following the Unified SRD method for multiple Changhua locations.

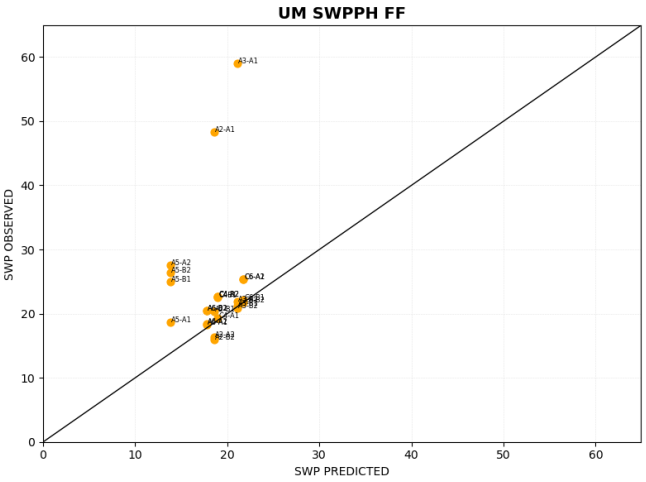

Figure B.12: Observed versus predicted self weight penetration pile plus hammer following the Unified SRD method (friction fatigue included) for multiple Changhua locations.

C

Other SRD and axial capacity methods

The axial strength, or capacity, of a pile V_{ult} represents the ultimate bearing capacity of a foundation pile. When the weight of the pile and hammer system exceed the bearing capacity, so giving a negative V_{ult}, the pile will accelerate downwards uncontrolled, called pile run. As described in Offshore geotechnical engineering (Mark Randolph and Gourvenec 2011), from vertical equilibrium, it is equal to the sum of the total ultimate shaft resistance Q_{sf} and ultimate base resistance Q_{bf} minus the submerged weight of the pile W'_{pile} (which must also be supported by the soil resistance) giving:

$$V_{\text{ult}} = Q_{\text{sf}} + Q_{\text{bf}} - W'_{\text{pile}} \tag{C.1}$$

$$Q_{\text{sf}} = \pi D \int_0^L f_{\text{s}}\, dz \tag{C.2}$$

$$Q_{\text{bf}} = \frac{\pi D^2}{4} q_b \tag{C.3}$$

The rest of this section highlights the DNV method, widely used by the industry. It also explains the ICP and UWA method, as the used Unified Method is build on those older methods. The state-of-the-art methods used in this thesis are described in section 3.3. Methods like Toolan and Fox (1977) and Stevens et al. (1982) are not considered.

C.1. DNV Skirt Foundation Method (1992)

The DNV Skirt Foundation Method (1992) is a partly CPT-based SRD model that improves upon previous methods by incorporating soil displacement effects. The design of offshore piles in cohesive soils is based largely on the experience with onshore piles. The methods developed are empirical and subject to the limitations and uncertainties in the database. (*DNV CN-304 Foundations* 2016). To conclude, DNV is an old method which uses the general not CPT based API input (American Petroleum Institute 2000). Only tested CPT method on North Sea sand for small piles. The DNV standard does have a method for skirted foundations and suction caissons.

Cohesive soils
Cohesive soils do not depend on CPT data, but are calculated according to Stevens et al. (1982). The unit end resistance, q_b, of piles in mainly cohesive soils may as an average be taken equal to 9 times the undrained shear strength of the soil at the level of the pile tip, provided that the installation process has not reduced the shear strength. Experience indicates that size effects may be of importance also in cohesive soils, i.e. that large diameter piles develop a smaller unit end resistance than do small diameter piles in the same soil. The displacement required to mobilize the unit end resistance will be an order of magnitude greater than that required to mobilize the skin resistance, which should be considered in the pile capacity predictions, especially where the pile end resistance represents a substantial part of the total axial pile resistance. An upper limit of 200 kPa is recommended for the unit skin friction on the basis of previous North Sea experience. End bearing is not CPT based for cohesive soils.

Unit skin friction:

$$f_s = \alpha \cdot \bar{c_u} \cdot F_c \cdot F_L \tag{1}$$

Unit end resistance:

$$q_b = 9 \cdot s_u \tag{C.4}$$

Where:

- f_s = Shaft friction
- α = Adhesion factor
- $\bar{c_u}$ = Average undrained shear strength over the embedded pile length
- F_c = Soil strength correction factor
- F_L = Pile penetration correction factor
- q_b = End bearing
- s_u = Undrained shear strength of the soil

Cohesionless soils
Prediction of the axial capacity of driven offshore piles in cohesionless soils often requires extrapolations beyond the boundaries of the database with respect to pile size, pile penetration, pile load and soil conditions. This is especially the case with piles designed for many North Sea locations, where the soils may be dense to very dense and often overconsolidated. Interesting for this research is that silt is considered as cohesionless. Due to the uncertainties in the database, the pile design parameters should be conservatively assessed. Limiting values are normally defined for the unit skin friction and the unit end resistance.

Unit skin friction: Minimum of:

$$f_{s1} = 120 \text{ kPa} \tag{a}$$

$$f_{s2} = \text{CPT sleeve friction} \tag{b}$$

Unit end resistance:

$$q_b = 0.7 q_c \text{ (OCR} = 2 - 4), \; q_p \leq 15 \text{ MPa} \tag{d}$$

$$q_b = 0.5 q_c \text{ (OCR} = 6 - 10), \; q_p \leq 15 \text{ MPa} \tag{e}$$

Where:

- f_{s1} = Minimum unit skin friction, given as 120 kPa
- f_{s2} = CPT sleeve friction
- q_b = Bearing end resistance
- q_c = Cone tip resistance
- OCR = Overconsolidation ratio, with different formulas for different OCR ranges

C.2. UWA-05 Method

The SRD methods from Alm and Hamre (2001) and earlier on are considered as the traditional SRD methods(Byrne et al. 2018). In 2005 was the UWA method developed based on North Sea sand and was assessed against the API-00 (not CPT based), Fugro-04, ICP-05 and NGI-04, which are also sand based methods. These methods are relevant because they where later on combined to the Unified Method, used in this thesis. The UWA-05:

- is a significant improvement on existing API recommendations.
- provides better predictions for a new extended database of load tests than the ICP-05, Fugro-04 and NGI-04 CPT based design approaches.
- provided new insights into the mechanisms controlling the development of shaft friction for open-ended displacement piles in sand.

The UWA-05 method simplifies to the following form for full scale offshore piles, as IFR=1 and the dilation term $\Delta\sigma'_r$ can be ignored.

End Bearing Capacity:

$$q_b = q_c \times (0.15 + 0.45 A_r) \tag{C.5}$$

Where:

- q_b = End bearing capacity
- q_c = Cone resistance from CPT
- A_r = Area ratio

Radial Shear Stress:

$$f_s = 0.03 \cdot q_c \cdot A_r^{0.3} \left[\max \left(\frac{h}{D} - 2 \right) \right]^{-0.5} \tan \delta$$

Where:

- f_s = Shaft friction
- q_c = Cone resistance from CPT
- A_r = Area ratio
- h = Pile penetration depth
- D = Pile diameter
- δ = Friction angle

Effective Area Ratio:

$$A_r = 1 - \left(\frac{D_i^2}{D^2} \right) \tag{C.6}$$

C.3. ICP approach

The Imperial College Pile (ICP) consists of multiple methods based on hundred of driven large steel tubular piles in the North and Baltic sea and is an improvement of the ICP-05 method. The ICP field tests confirmed that the Coulomb criterion $\tau_{\text{local}} = \sigma'_{rf} \cdot \tan(\delta)$ governs local shaft shear failure in both sands and clays. The governing effective angle of interface shearing resistance δ can be found reliably from ring-shear interface tests (Jardine et al. 2015). The shaft radial effective stress at failure σ'_{rf} is the sum of σ'_{rc}, the local radial effective stress set up by installation, and $\Delta\sigma'_{rd}$, the dilatant increase in σ'_r that develops during loading. In sands, $\Delta\sigma'_{rd}$ is given by:

$$\Delta\sigma'_{rd} = \frac{G\Delta R}{R} \tag{C.7}$$

Where:

- G = Local shear stiffness (related to the CPT resistances q_c)
- ΔR = The pile's surface roughness
- R = The pile radius

As the pile radius is in the numerator, this term is neglected for large diameter monopiles. The local radial effective stresses set up by installation are strongly affected by the soils' local in-situ state, and in sands, the ICP makes direct use of the CPT tip resistance q_c profiles to predict design profiles of both σ'_{rc} and $\Delta\sigma'_{rd}$. This gives the following equation for the radial effective stress σ'_{rc} in sands:

$$\sigma'_{rc} = 0.029 \cdot q_c \left(\frac{\sigma'_{v0}}{P_a} \right)^{0.13} \left(\frac{h}{R^*} \right)^{0.38} \tag{C.8}$$

Where:

- σ'_{rc} = Radial effective stress set up by installation
- q_c = Cone tip resistance
- σ'_{v0} = Initial vertical effective stress
- P_a = Atmospheric pressure
- h = Pile embedment depth
- R^* = Effective pile radius

The shaft radial effective stress at failure in **clays** can be defined as:

$$\sigma'_{rf} = \left(\frac{K_f}{K_c}\right)\sigma'_{rc} \tag{C.9}$$

where the loading factor $\frac{K_f}{K_c}$ is constant and may be assumed equal to 0.8. The field research in clays showed that pile installation and equalization leads to local radial effective stress profiles that can be expressed as:

$$\sigma'_{rc} = K_c\sigma'_{v0} \tag{C.10}$$

where:

- σ'_{rf} = Shaft radial effective stress at failure in clays
- K_f = Loading factor for shaft friction
- K_c = Constant coefficient for radial effective stress in clays

Note that K_c is not constant, but depends on the clay's local Yield Stress Ratio (YSR) and sensitivity.